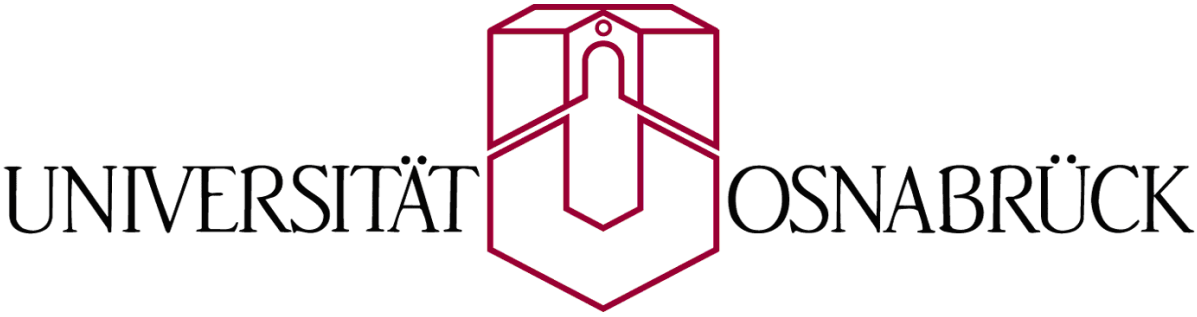

Spatiotemporal Dynamics of Assembly and Activation of Class II Cytokine Receptors

Dissertation

Presented to the department of Biology/Chemistry, University of Osnabrück in partial fulfillment of the requirements for the degree of '*Doctor Rerum Naturalium*'

by

Junel Sotolongo Bellón

Osnabrück

February 2022

Summary

Class II cytokine receptors are important pleiotropic regulators of the immune system that play a central role in pathogen defense, tumor surveillance and immune system homeostasis. Most of these activities are very promising for biomedical applications, which, however, have so far failed to succeed due to severe undesired side effects resulting from the pleiotropic nature of these cytokine receptors. Controlling the functional plasticity of class I/II cytokine receptor signaling by engineered cytokines has recently emerged as a promising approach to selectively reduce such side effects. In this context, systematic studies on the IFNα/β receptor and other systems have identified that the binding kinetics of the ligand-receptor interaction play an important role in defining signaling specificity. This has been explained by altered equilibrium and dynamics of the signaling complex in the plasma membrane.

In this work, I have investigated how the spatiotemporal organization and dynamics of signaling complexes regulate activation and signaling specificity of other members of the class II cytokine receptors. I focused on the type II IFN and IL-10 systems that supposedly form hexameric ligand-receptor signaling complexes in the plasma membrane. To this end, we developed an orthogonal multicolor anti-GFP nanobody-based labeling strategy, that allowed imaging of up to four different class II cytokine receptor subunits simultaneously. Using this labeling strategy, I investigated the spatiotemporal dynamics of IFNGR and IL-10R complex assembly by co-localization and co-tracking of single receptor subunits. Thereby, I did show that unliganded receptor subunits of IFNGR and IL-10R remain monomeric at the cell surface, whereas binding of the ligand led to fast and efficient receptor homo- and hetero-dimerization, verifying a ligand-induced receptor complex assembly model for both cytokine receptors. Moreover, I verified the hexameric ligand-receptor complex structure *in cellulo*. Analysis of single molecule trajectories and co-trajectories revealed a decrease in mobility and diffusion of IFNGR and IL-10R subunits upon ligand stimulation indicating receptor confinement and endocytosis. In this context, I identified an abnormal diffusion behavior of IL-10R2 that was dependent on the length of its transmembrane helix. We used partial agonists for both receptor complexes to systematically alter receptor binding stoichiometry and complex stability in the plasma membrane and correlated these with downstream signaling responses. Our analysis revealed a minor contribution of the second low affinity receptor subunit and its associated kinase to the overall signaling activity. However, the second high affinity binding subunit was indispensable to acquire full signaling potential. We managed to obtained decoupling of gene expression for both hexameric class II cytokine receptors by utilizing engineered ligands with altered receptor binding affinities. Our findings could pave the way for new biomedical approaches with engineered IFNγ and IL-10 in the future. Furthermore, we uncovered pathogenic mechanisms behind the IFNGR2-T168N mutant and auto-IFNγ antibodies, both of which

prominently cause the Mendelian Susceptibility to Mycobacteria Disease (MSMD) syndrome, showing that both interfere with IFNGR activation by preventing recruitment of IFNGR2 into receptor complexes.

Table of contents

1 Introduction 1

1.1 Immune system 1

1.2 Cytokines are the communicators of the hematopoietic system 5

1.3 Structure and function of class II cytokine receptors 7

1.3.1 Cellular responses initiated by IFNGR and IL-10R signaling 10

1.3.2 Viral escape strategies for class II cytokine signaling 13

1.4 Mechanism of class II cytokine receptor activation and signaling 14

1.4.1 Key player of the JAK/STAT signaling pathway 15

1.4.2 Mechanism and regulation of JAK/STAT signal transduction 16

1.4.3 Mechanism of receptor assembly and activation 17

2 Objectives 21

3 Strategies 22

3.1.1 Single molecule fluorescence microscopy 22

3.1.2 Orthogonal GFP-tag based labeling strategy 22

4 Results and Discussion 24

4.1 Part I: The interferon-γ receptor complex 24

4.1.1 Endogenous receptor complexes at single molecule level 24

4.1.2 Spatiotemporal dynamics of type II interferon receptor assembly 26

4.1.2.1 Anti-GFP nanobody-based orthogonal labeling technique 27

4.1.2.2 Homo- and hetero-dimerization of IFNGR subunits 29

4.1.2.3 Mobility and diffusion properties of IFNGR 33

4.1.2.4 Stoichiometry and model of IFNGR complex assembly 34

4.1.3 Pleiotropy of IFNGR signaling 37

4.1.3.1 Crystal structure of complete IFNγ receptor complex 38

4.1.3.2 Structure-guided design of partial agonists 41

4.1.3.3 Decoupling of IFNγ induced gene expression 43

4.1.4 Pathophysiology of IFNGR signaling 45

4.1.4.1 Pathogenic mechanism of the gain of N-glycosylation mutation IFNGR2-T168N 46

4.1.4.2 Pathogenic mechanism of anti-IFNγ autoantibodies 47

4.1.5 Contributions and publications 53

4.2 Part II: The interleukin-10 receptor complex 55

4.2.1 Spatiotemporal dynamics of interleukin-10 receptor assembly 55

4.2.1.1 Homo- and hetero-dimerization of IL-10R subunits 55

4.2.1.2 Mobility and diffusion properties of IL-10R 56

4.2.2 Abnormal diffusion properties of IL-10R2 59

4.2.3 Pleiotropy of IL-10R signaling 61

4.2.3.1 Viral IL-10 homologous hijack human immune system 62

4.2.3.2 Engineering of an affinity maturated IL-10 variant 64

4.2.3.3 Affinity maturated IL-10 variant enhances IL-10R complex assembly at the plasma membrane 66

4.2.3.4 Effect of engineered ligands on immunosuppressive IL-10 signaling response 67

4.2.3.5 Effect of engineered ligands on immunostimulatory IL-10 signaling response 71

4.2.4 Contributions and publications 75

5 Conclusion 77

5.1 Mechanism of class II cytokine receptor assembly and activation 77

5.2 Role of hexameric receptor complexes in IFNGR and IL-10R signaling 79

5.3 Implications of receptor mobility and diffusion for signaling 79

5.4 Mechanism of controlling class II cytokine receptor signaling pleiotropy 81

5.5 Limitations and future perspectives 82

6 Materials and Methods 84

6.1 Molecular biology 84

6.2 Protein purification and labeling 87

6.3 Cell culture 88

6.4 Microscopy 88

6.5 Data Evaluation and Statistical Analysis 90

7 References 92
8 List of Abbreviations 108
9 Acknowledgements 110
10 Declaration 111

1 Introduction

1.1 Immune system

All cellular life is exposed to the threat of pathogenic intruders, which have evolved to take advantage of the host's organism. As an example, viruses hijack the replication machinery of the host in order to reproduce, whereas bacteria that adopted an intracellular lifestyle exploit the metabolism of the host cell. With the development of multicellular organisms, this threat was even further expanded, as new pathogenic lifestyles emerged. These pathogens may be categorized by their size and target location: (i) intracellular pathogens, that invade cells and thereby cause damage to single cells, such as viruses and some bacteria; (ii) extracellular pathogens, that remain in the extracellular space and may inflict damage to tissues, such as bacteria, archaea and fungi; (iii) eukaryotic parasites, that are too large to invade cells and can move through the body in a complex life cycle [1].

In response to these diverse pathogens, mammals have developed a complex immune system in the course of evolution. Its main purpose is to detect and repel any foreign intruder, but also maintain the integrity of the body such as in fighting cancer. In achieving this task, the immune system faces different challenges. One important challenge being that it must have access to the entire body to appropriately react to any new threat in time and place. Therefore, it seems reasonable that the immune system and the blood system are closely related and originate from the same pluripotent hematopoietic stem cells [2]. In the bone marrow, the central lymphoid organs and the thymus, production, and differentiation of cells of the hematopoietic system takes place. In contrast, the peripheral lymphoid organs, the spleen, lymph nodes and lymphatics, form a dense mesh that connects all tissues with dedicated centers, where the immune response can develop efficiently. Looking at the whole picture the immune system forms a delocalized and constantly changing organ. All its components depend heavily on a dynamic and robust communication to make sure, that each part of the immune system fulfills his task precisely. This is important, as defense against pathogens is always a balance between life and death. Too weak or too potent measures will often lead to failure of the system resulting in severe diseases or even death of the organism.

Another challenge is given by the large variety of previously mentioned pathogens. Therefore, the immune system builds on a broad arsenal of defense mechanisms, each tailored to specific types of pathogens and the damage they may inflict on the body, and it is not surprising that it comes along with a large variety of specialized cell types to serve this purpose (**Figure 1**). All different cell types of the hematopoietic system originate from pluripotent hematopoietic stem cells (HTC) that reside in the bone marrow. Differentiation and maturation of specialized cells from HTCs is tightly regulated by the interplay of many mediator proteins named cytokines. In general, the immune

system can be categorized into the innate immunity and the adaptive immunity, which both depend on each other for the host to achieve efficient and effective defense against pathogens [3].

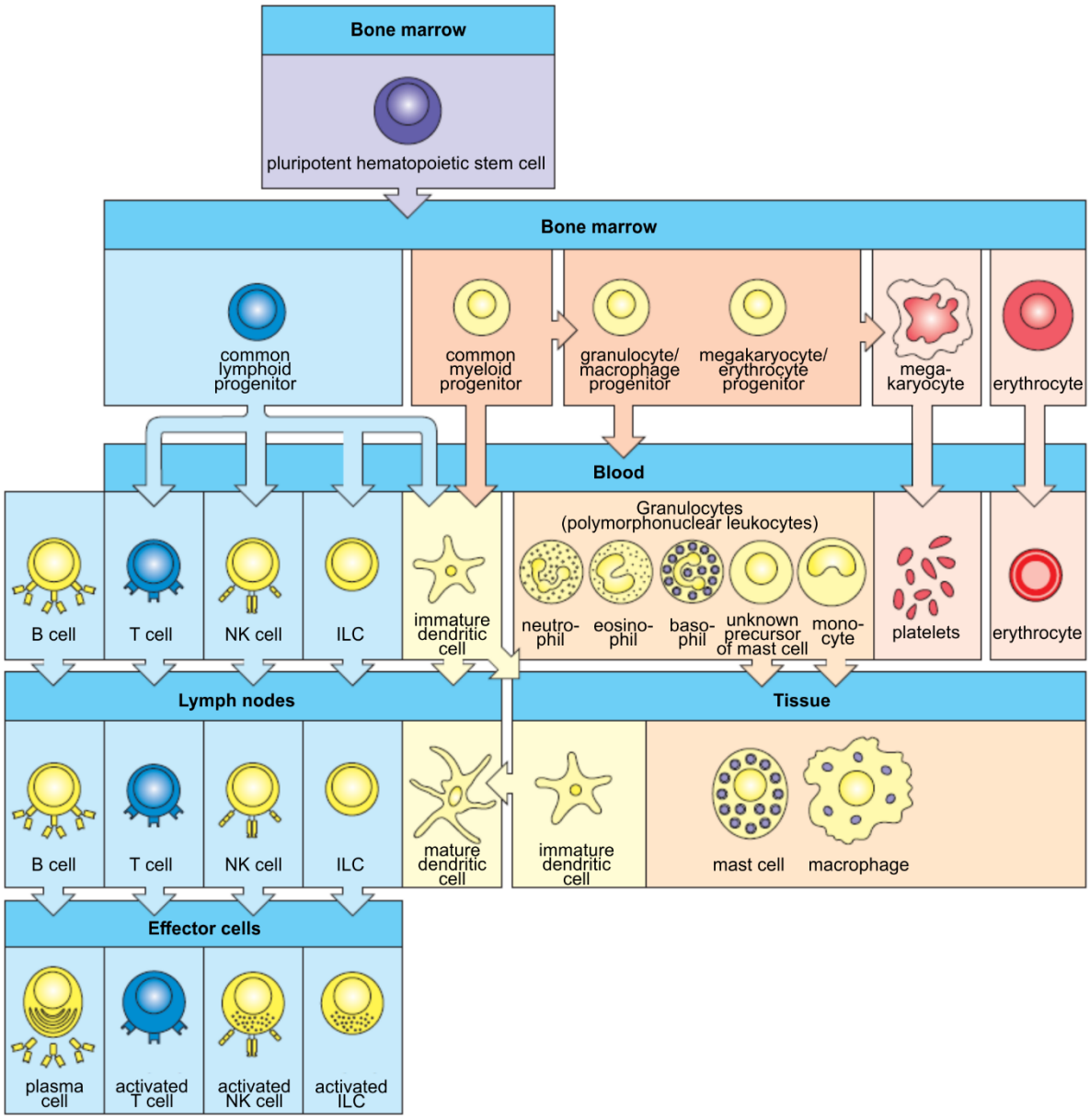

Figure 1: Cell type differentiation in the blood and immune system. Taken and modified from [1].

The innate immune system is an immediate and pathogen-unspecific immune response. It is initiated by sensory cells upon detection of inflammatory inducers, which include structures that are typical for pathogens, e.g. fungi specific polysaccharides, unique components of the bacterial cell wall and different viral oligonucleotides [4-6]. These sensory cells include phagocytic cells of the immune system, such as macrophages, neutrophils and dendritic cells, whose main task is to recognize and phagocytose pathogenic cells and molecules. Macrophages reside in almost all tissues and differentiate from monocytes that have migrated into the tissue. In addition to destroying pathogens via phagocytosis, they fulfill an important task by orchestrating immune responses. They

induce inflammation and activation of other immune cells by releasing inflammatory mediators as communication signals. Lastly, macrophages act as general scavenger cells of the body by clearing dead cells and cellular debris. Granulocytes are named after characteristic staining granules in their cytoplasm, which contain degrading enzymes and other antimicrobial substances. The most abundant granulocyte, neutrophils, fulfill a similar task as macrophages by destroying pathogens using phagocytosis. The far less abundant eosinophils and basophils release the content of their granules after encountering pathogens that are too large to be taken up by phagocytosis. Together with mast cells, they play a predominant role in defending against parasites. Finally, the dendritic cells have a unique role, as they constantly perform phagocytosis, as well as macropinocytosis of large volumes of extracellular fluid. After detecting foreign molecules, they migrate via lymphatics to the lymph nodes where they kick off the adaptive immune response by a process called antigen presentation that will be addressed later in this chapter [7]. While most cells possess the ability to present antigens, dendritic cells, macrophages, and B cells are specialized in doing so and thus are also named professional antigen presenting cells (APC). Another important group of immune system cells are lymphocytes, which differentiate from the common lymphoid progenitor cells. Among them, natural killer (NK) cells and innate lymphoid cells (ILC) belong to the innate immune system, too. NK cells can directly kill other cells, such as cells infected with viruses, by releasing messengers upon contact that initiate lysis or apoptosis of the target cell [3]. They differentiate and mature in the bone marrow and later circulate through the blood system. On the contrast, ILCs reside in peripheral tissues and are important sources of mediators of inflammatory response.

All other lymphocytes belong to the adaptive immune system and have in common that each cell expresses antigen receptors at its cell surface. In contrast to the innate immunity, the adaptive immunity is acquired by an organism throughout its lifetime. The principle underlying the adaptive immunity is based on each lymphocyte, except for NK cells or ILCs, recognizing a single specific antigen. This is achieved during the development of each individual cell through a complex gene rearrangement that is called V(D)J recombination [8]. After this process each cell has its unique antigen receptor, leading to a huge diversity in antigens that are recognized by the pool of lymphocytes. In theory, any possible antigen is recognized by at least one lymphocyte of the body. Any lymphocyte that binds to its specific antigen is activated and creates many identical progenies thereby building up a defense against this specific antigen. Once the pathogen is defeated, most lymphocytes die and only a few remain as memory cells, thus allowing a faster and more specific defense the next time the body encounters the same pathogen. In addition to NK cell and ILC, there are two main types of lymphocytes that are distinguished by the structure of their antigen receptor. B lymphocytes (B cells) complete their development in the bone marrow and have antigen receptors resembling an antibody (immunoglobulin) [9]. Upon activation, B cell differentiate into plasma cells and start producing a huge number of immunoglobulins with the same specificity as their

antigen receptor. T lymphocytes (T cells) by contrast originate from the bone marrow but fully mature in the thymus. They can be further distinguished into different cell types based on specific markers on their cell surface, which also define their function. Almost each cell of the body has cell-surface glycoproteins called major histocompatibility complexes (MHC) that help the adaptive immunity by presenting peptides from degraded proteins. For example, during a viral infection, the infected cell will degrade viral proteins and present peptides derived from these viral proteins as antigen at their surface. T cells can recognize these antigens and subsequently trigger different effects on the target cell. Cytotoxic T cells will kill cells presenting the antigen they are specific to. They express the marker and co-receptor CD8, which binds MHC class I proteins expressed by almost all cells of the body and hence are usually named CD8+ T cells. Another important group of T cell represent the different helper T cells. They express CD4, which binds to MHC class II proteins that are expressed by the professional APCs of the immune system. They develop into a variety of different effector subsets and help the immune system by producing many different messengers, which in turn help driving the immune system in different directions. Likewise, helper T cells are termed CD4+ T cells. Two important subtypes of CD4+ T cells are T helper type 1 (T_h1), which propagate phagocytosis and cell-mediated immunity (type 1 immunity), and T helper type II (T_h2), which primarily initiate the antibody production by B-cells, also termed humoral immune response (type 2 immunity) [10].

The success of the immune system depends on the ongoing vital interplay of this great diversity of cells as well as tissues and organs. To drive such a delicate and diverse system, a robust but also dynamic and versatile communication is needed. This communication must meet important requirements. As the blood and immune system are closely related and emerge from the same hematopoietic stem cells in the bone marrow, it must coordinate the production, differentiation, and activity of all kinds of cells of both systems simultaneously. This also includes that each cell finds its way to and remains at its corresponding destination. In the case of infection, the communication must ensure that only the components involved in the defense mechanism matching the invading pathogen are activated. Consequently, it must guarantee that each cell fulfills its corresponding task just at the right time. Lastly, communication must carefully balance the immune response to succeed in pathogen defense while maintaining the lowest possible host-damage. Especially in the case of intracellular pathogens, such as viruses, stopping cell replication and differentiation, as well as programmed cell death, can be powerful tools or even the ultimate way to stop pathogen spreading. But if these cellular mechanisms, as well as defense mechanisms at tissue and organism level, such as fever and inflammation, get out of control, they will induce more damage to the host than the pathogen. Therefore, defects in the balancing mechanisms often lead to severe autoimmune and chronic inflammation diseases, but also immunosuppression and cancer. Such a complex communication system is realized in animals through messengers termed ‘cytokines’.

1.2 Cytokines are the communicators of the hematopoietic system

Cytokines are small messenger proteins that are produced and secreted by cells in a hormone-like fashion to act on other cells [11, 12]. They recognize and activate dedicated cytokine receptors on the plasma membrane of cells. Thereby they induce downstream signaling pathways, thereby initiating gene expression programs in the target cell. Yet, unlike hormones, cytokines are mostly limited to autocrine or paracrine signaling. Consequently, cytokines are not produced by only a specific kind of cell in some centralized organ, as it would be usually the case for hormones. Instead, most cells are capable of producing a set of cytokines under specific circumstances and likewise most cells are responsive to a specific set of cytokines. In general, whether a specific cell is responsive to a certain cytokine is dictated by the ability of this cell to express the corresponding cytokine receptor. This limited range of cytokines allows local immune responses and prevents systemic inflammations, such as found in a septic shock [13]. Cytokine signaling frequently leads to the secretion of other cytokines and a cascade of signaling pathways. The resulting network of an overwhelming number of cytokines and their signaling pathways creates a fine-grained communication system to precisely adjust the immune and blood system.

Cytokines and their receptors are quite diverse, both, structurally and mechanistically. Thus, several attempts have been undertaken to categorize them in the past. Consequently, different classifications based on various criteria, such as immune response and cytokine protein structure, co-exist. Nevertheless, a classification based on the protein structure of the cytokine receptors has stood out as it turned out to be the most useful in the clinical and experimental field. This classification defines six families of cytokine receptors: the immunoglobulin superfamily (IgSF), the transforming growth factor beta (TGF-β) receptor family, the chemokine receptors, the tumor necrosis factor receptor superfamily (TNFRSF), and the class I and class II cytokine receptors. The IgSF is characterized by structural homology to immunoglobulins and contains – among a large variety of soluble and membrane bound proteins other than cytokine receptors – the interleukin-1 receptor family and colony stimulatory factor 1 (CSF1) receptor. Members of the interleukin-1 receptor family are extremely potent modulators of inflammation activating the nuclear factor kappa B (NF-κB) pathway [14, 15], whereas CSF1 mediates the differentiation of target cells to macrophages and related cell types via PI3K/AKT/mTOR signaling pathway [16, 17]. The members of the TGF-β receptor family are serine/threonine kinase receptors that take an important part in embryonic stem cell maintenance and differentiation [18], as well as in cell growth, differentiation and cellular homeostasis of adult organisms through signaling pathways that involve phosphorylation of transcription factors named SMADs [19]. Chemokines, or chemotactic cytokines, interact with a large group of G protein-coupled receptors (GPCR) that coordinate leukocyte recruitment and activation by chemotaxis [20]. As GPCRs, they conventionally transduce signaling via cyclic AMP and inositol 1,4,5-triphosphate/diacylglycerol as second messengers [21].

Members of the TNFRSF bind their cognate agonists, the tumor necrosis factor proteins (TNFs), via an extracellular cysteine-rich domain [22]. In contrast to most other cytokines, TNFs are often not expressed as soluble protein, but as single spanning membrane proteins, that can be proteolytically cleaved on some occasions [23]. Most of the time, though, TNFs are expressed at the surface of cells and interact with neighboring cells that express the corresponding TNF receptor at their surface [24]. TNFs and their receptors are primarily expressed by cells of the immune system and contribute to a wide range of biological and immunological activities [22], such as morphogenesis of secondary lymphoid organs [25, 26], contribute the function of cytotoxic T cells and maintaining homeostasis of the lymphoid compartment by stimulating activation and death of effector cells [22, 27]. The death signal is transduced through JUN kinase and caspase activity, whereas the survival signals are mediated via activation of the NF-κB signaling pathway [28].

The remaining two families of cytokine receptors, the class I and class II cytokine receptors, share more structural similarities than the other cytokine receptor groups mentioned previously. Receptors of these two families all activate downstream signaling pathways via non-covalently associated Janus family tyrosine kinases (JAKs). The most important effector proteins of these receptors are the members of the signal transducer and activator of transcription (STAT) family. JAK/STAT signaling by class I/II cytokine receptors plays a key role in regulating proliferation, differentiation, and activation of all types of immune cells. Characteristic features of these pathways are high pleiotropy and redundancy [12, 29] and the determinants defining specific cellular decisions have remained unclear. This pleiotropy and redundancy can be evoked by multiple cytokines binding to the same cell surface receptor, but also by several often closely related cell surface receptors using overlapping downstream effector molecules [12]. Class I receptors can be distinguished by a conserved juxtamembrane “WSXWS” amino acid motif at the extracellular region that is absent in class II cytokine receptors [30]. Besides that, receptor subunits of both classes share a largely disordered intracellular domain, that serve as binding site for tyrosine kinases and effector molecules, a single membrane spanning α-helical transmembrane domain, and an extracellular domain comprising several fibronectin type III domains, that are involved in cytokine binding [31]. The stoichiometry of the receptor complexes ranges from homodimers and heterodimers up to higher oligomeric receptor complexes [32, 33]. Due to high diversity in the group of class I cytokine receptors, as well as high pleiotropy and redundancy in signaling responses, it is rather difficult to narrow down the physiological function of class I cytokine receptor signaling. Instead, class I cytokine receptors do take part in a broad spectrum of important tasks including controlling hematopoiesis, mediating proliferation and differentiation of various cell types of the immune system, triggering and regulation of immune responses. The remaining group of class II cytokine receptor, which this work will focus on, includes three distinct interferon receptors and the interleukin-10 (IL-10) receptor family. They are predominantly involved in anti-

viral defense [34, 35] and regulation of the immune system, but also in fighting tumors and some other non-viral pathogens [36], and thereby they have aroused great interest in medical applications [37].

1.3 Structure and function of class II cytokine receptors

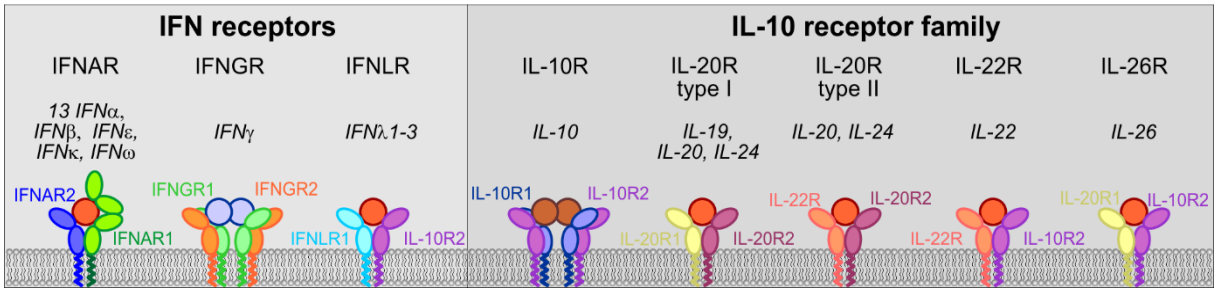

Figure 2: Class II cytokine receptor complexes with their respective cytokines. [38]

The interferons (IFN) originally got their name from their defining property of interfering with viral replication [36, 39] by evoking an antiviral state in target cells. They can be further classified based on the specific receptor complex that they recognize at the cell surface (**Figure 2**): The type I IFNs comprises 13 subtypes of IFNα in humans, along with IFNβ, IFNε, IFNκ and IFNω, which solely bind to the IFN-α/β receptor (IFNAR) [40]. The IFNAR complex consist of a ligand-binding subunit that binds type I IFNs with high affinity (IFNAR2) and an accessory subunit (IFNAR1) that possesses a markedly lower binding affinity for its ligands [41]. In contrast, IFNγ is the only known member of the type II IFNs and binds to the IFNγ receptor (IFNGR) [40], which consist of the binding subunit IFNGR1 and the accessory subunit IFNGR2. While all type I IFNs are monomeric and engage a ternary receptor complex consisting of a ligand and one copy of each receptor subunit (**Figure 3**), IFNγ is a constitutive ligand dimer and thus the IFNGR forms a hexameric complex consisting of a dimeric ligand and two copies of each receptor subunit [42].

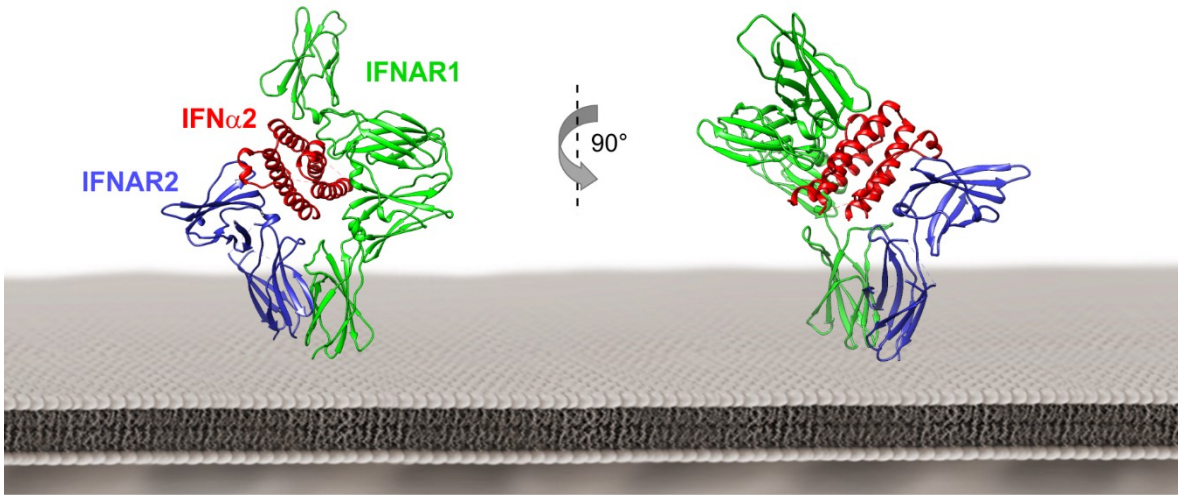

Figure 3: Crystal structure of the extra cellular domains of the ternary interferon α/β receptor complex. PDB: IFNAR2 (blue), IFNα2 (red) – 3SE3; IFNAR1 (green) – AF-P17181-F1.

Mouse studies have shown that both type I and type II IFNs are essential for promoting a complete antiviral response in the host, but the effects they induce and activation time during infection are quite different [35]. Type I IFNs are among the first cytokines secreted by pathogen sensor cells, such as dendritic cells, during a viral infection, as a response of pattern-recognition receptors to virus-specific stimuli, such as double-stranded RNA [43, 44]. Secretion of type I IFNs not only kicks off potent innate antiviral defense mechanisms at cellular level, but also induces fundamental responses of the adaptive immune system [30]. Type II IFN, by contrast, is secreted at a later stage during the immune response by lymphocytes [45-48] and is an important modulator of both, innate and adaptive immunity, too [46, 49]. Both receptors of the type I and type II IFNs are ubiquitously expressed on all nucleated cells of the body [50], which matches their ability to evoke antiviral defense in each cell that could potentially replicate viruses.

The type III IFNs comprise IFNλ1, IFNλ2 and IFNλ3, which were previously named IL-29, IL-28A and IL-28B, respectively, as well as IFNλ4. They all bind to the IFNλ receptor (IFNLR) [40], which consist of the binding subunit IFNLR1 and the accessory subunit IL-10R2. The latter is a shared receptor subunit that is also part of the IL-10, IL-22, and IL-26 receptor complexes (**Figure 2**) [51, 52]. In contrast to the receptors of type I and type II IFNs, as well as IL-10R2, the expression of IFNLR1 is restricted to cells of epithelial origin, kidney, liver, lungs, and gastrointestinal tract [50, 53]. Other than that, type I, and type III IFNs share common characteristics. They both can induce an antiviral state in host cells, activate largely overlapping signaling pathways and effector molecules, and alter the expression of a very similar set of genes [54].

Furthermore, the IL-10 receptor family does belong to the class II cytokine receptors (**Figure 2**). Among them, the IL-10 receptor is the best studied member. The only known ligand IL-10 does form a constitutive dimer with striking similarities in tertiary structure to IFNγ (**Figure 4**) [55, 56]. Likewise, the dimeric IL-10 engages two binding subunits IL-10R1 and two accessory subunits IL-10R2 in a hexameric receptor complex [51, 57]. The expression of IL-10R1 is mainly restricted to leukocytes and dendritic cells, unlike the ubiquitous expression of IL-10R2 [52]. As opposed to IFNs, IL-10 does not convey antiviral activity, but represents a central immune regulator with both immune stimulating and immune suppressing abilities [58].

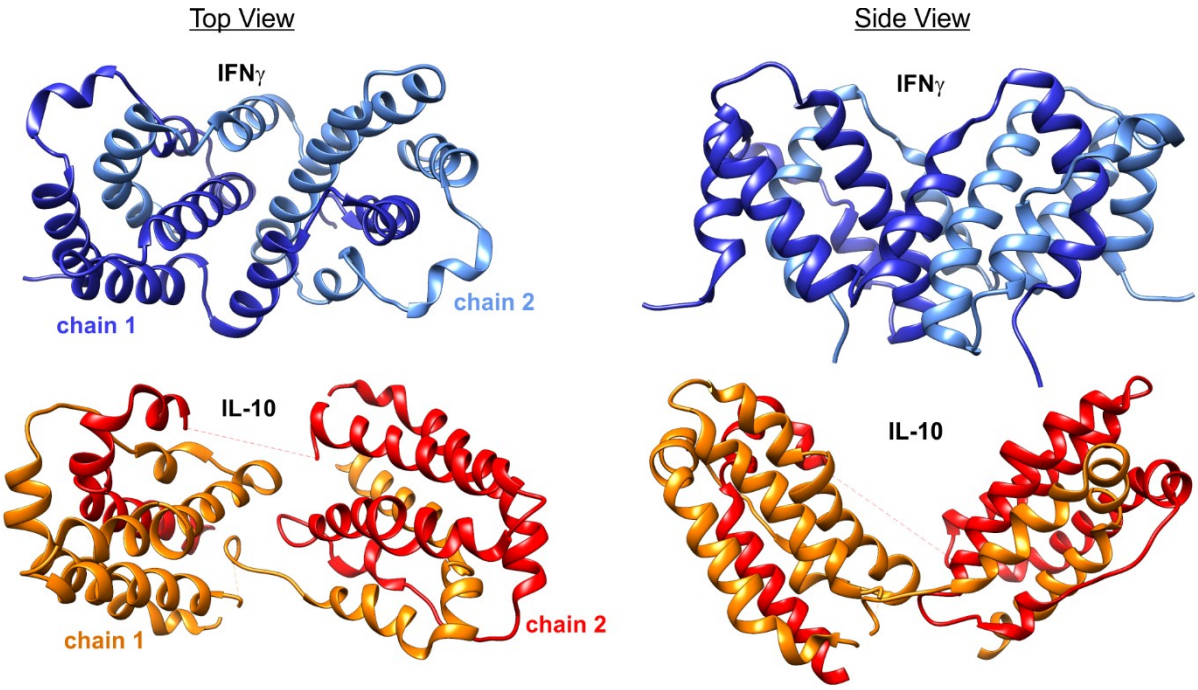

Figure 4: Crystal structure of IFNγ and IL-10 dimers. Two chains of IFNγ (light blue, blue) and IL-10 (orange, red) are intertwined with each other that both are required to form a stable quaternary structure. PDB: IFNγ – 6E3K; IL-10 – 6X93.

Due to its central role in antiviral defense, IFNs have received a lot of attention in biomedical research during the last decades. This has led to a profound understanding of the signaling mechanism and cellular responses of type I IFN. Thereby, diverse pleiotropic cellular responses have been identified for type I IFN signaling, which can be summarized by antiviral, antitumor and immunoregulatory activities [36]. While all type I IFNs can induce an antiviral state in the target cell with similar potencies, some of them can evoke additional cellular effects, e.g. IFNβ can regulate cell proliferation and differentiation more potently [59]. These findings have given rise to one of the most interesting questions regarding the type I IFN signaling: How can a variety of type I IFNs encode this functional plasticity, despite binding to a single receptor complex and relying on the same limited number of downstream signaling components. Early mutational studies on ligand-receptor interactions [60-65] in combination with structural analysis of parts and complete IFNAR complexes [65-70] revealed, that different binding affinities of the ligands to the IFNAR subunits rather than differences in the complex structure control pleiotropy in type I IFN signaling [59, 71-75]. Moreover, engineered IFNα variants that mimic the binding affinities of IFNβ, were shown to have an almost identical signaling pattern [76, 77]. The derived model that signaling response is regulated by receptor recruitment and activation dynamic, which is governed by the receptor binding affinities of the type I IFNs, could eventually be confirmed in living cells by single molecules imaging and biophysical analysis [59].

A comparable detailed mechanism was not shown for other class II cytokine receptors so far. In fact, distinct differences in receptor complex and ligand-receptor interaction suspect a different signaling mechanism for IFNGR. Strikingly, IL-10R shares remarkable similarities with the IFNGR regarding ligand-binding properties and subunit orientation in the complex, as well as the overall complex protein structure [42, 57, 78]. The corresponding ligands share a homo-dimeric structure [55, 56], that is unique among other class II cytokines and are related to the hexameric structure of the receptor complex. Within the biological principle "function follows form" these similarities suggest a common mechanism for both hexameric class II cytokine receptors IFNGR and IL-10R that is distinct from that of IFNAR. Above all, both hexameric class II cytokine receptors are lacking different ligands with varying binding affinities to encode signaling pleiotropy. Instead, both ligands IFNγ and IL-10 induce pleiotropic signaling responses on various cells via their specific receptor complex. Understanding the regulatory mechanism, by which hexameric class II cytokine receptors control which genes are activated, and which are not, could open new possibilities for exploiting some of their biological effects in a medical context.

1.3.1 Cellular responses initiated by IFNGR and IL-10R signaling

IFNγ and IL-10, as well as their receptors, are not only structurally but also functionally related, as they play antagonistic roles in modulation of the immune response. This is reflected in their affiliation to type 1/type 2 immunity (**Figure 5**) [10]. Upon activation by inflammatory inducers, professional APCs, such as macrophages and dendritic cells, begin to secrete IL-10 and IL-12 [79, 80], the balance of which is critical for immunoregulation during infection [80]. Secreted IL-12 activates naïve T_h0 cells and promote their differentiation into mature T_h1 cells [79, 81], which produce primarily IFNγ among IL-2 [82]. Eventually, secreted IFNγ acts on professional APCs and stabilize the production of IL-12 in a positive feedback loop [83, 84]. This branch of helper T cell differentiation is also termed IFNγ/IL-12 axis [85] and promotes cell-mediated immunity by activating macrophages (type 1 immunity) [10]. However, already the absence of IL-12 leads to IL-4 secretion by helper T cells, which in turn induce their differentiation to T_h2 cells [81, 86]. Mature T_h2 cells secrete IL-10 alongside IL-4, IL-5 IL-9 and IL-13 [82] and promote humoral immunity and inhibition of inflammation (type 2 immunity) [10, 80]. IL-4 and IL-10 inhibit the production of IFNγ and IL-12 [87] and prevent IFNγ signaling [88, 89], thus blocking maturation of naïve T_h0 cells into T_h1 cells and further promoting T_h2 cell differentiation. Likewise, IFNγ inhibits the production of IL-4 by T_h0 cells during polarization and thus the maturation of naïve T_h0 cells into T_h2 cells [10, 90-92]. In addition to their mutually exclusive roles in type 1/type 2 immunity, IFNγ and IL-10 fulfill numerous other immunoregulatory functions during immune response. To avoid getting lost in detail, only the most prominent effects of IFNγ and IL-10 signaling will be addressed in the following part.

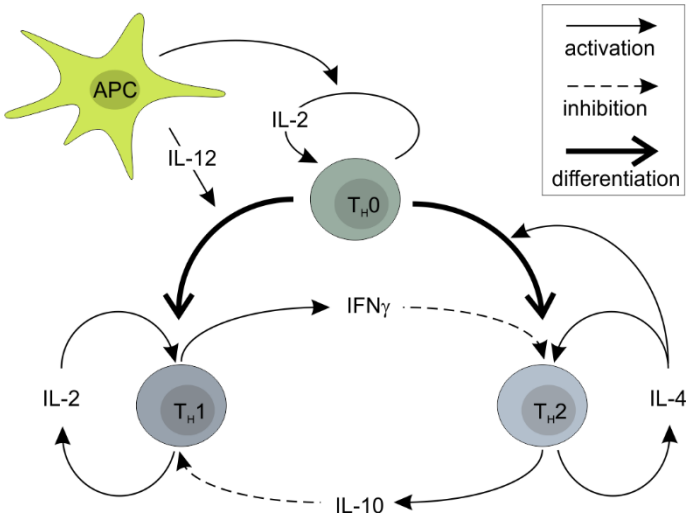

Figure 5: Regulation of helper T cell differentiation by IL-10 and IFNγ. Modified from [93]

Although, IFNγ mainly regulates the transition between innate and adaptive immunity [94], it fulfills essential tasks in innate immunity through regulation and activation of macrophages [95]. IFNγ signaling exerts an antiproliferative and growth inhibitory effect on macrophages by arresting their cell cycle in the G1-phase [95-97]. Moreover, IFNγ treatment of macrophages may inhibit apoptosis [96] hence providing a survival signal and ensuring high biosynthetic activity. Nevertheless, apoptosis is an essential mechanism for macrophages to ensure functionality and prevent colonization by intracellular pathogens [95, 98]. IRF-1 tumor-suppressor gene is a deciding factor for apoptosis, the expression of which is reported to be controlled by IFNγ signaling and has been linked to the tightly regulated expression of IFNGR2 at the cell surface [99-101]. In this sense, IFNγ have been observed to induce apoptosis in myeloid cells more efficiently as these cells do generally express high numbers of IFNGR at their cell surface [95, 99]. Furthermore, IFNγ signaling activates microbicidal effector functions in macrophages, such as increasing pinocytosis and receptor-mediated phagocytosis and enhancing microbial killing abilities [95, 102, 103]. IFNγ-mediated microbial killing abilities include up-regulation of reactive nitrogen and oxygen species production in macrophages through transcriptional induction of substrates, cofactors, catalysts and enzymes [95, 104-107], as well as tryptophan depletion as antiparasitic mechanism [108]. In addition to macrophage activation, IFNγ does regulate the transition from innate to adaptive immunity mainly by the previously mentioned T lymphocyte regulation, antibody production through B cell isotype switching to IgG2a [109] and driving inflammation through local upregulation of adhesion molecule and chemokine expression [95]. Furthermore, IFNγ does increase the expression of both Class I and Class II MHC at the cell surface [110, 111]. Moreover, several other IFNγ-induced effects, including changes in composition and expression of proteasome complexes [112] as well as chaperons and transport proteins [113, 114], aim to improve the quality, quantity and repertoire of peptides used in MHC antigen presentation [95]. Together these changes

increase the potential for T cell recognition of foreign peptides and thus stimulate both cell-mediated and humoral immunity [95]. Finally, IFNγ exerts a number of direct antiviral effects, often specifically tailored to certain viruses, targeting each individual step in the viral life cycle from entry and replication up to release and reactivation [46]. However, these IFNγ-mediated antiviral effects can be hard to discriminate from those mediated by type I IFNs because of redundancy in downstream signaling pathway and activated set of genes [46, 115, 116]. This is further complicated as IFNγ may induce the expression of type I IFNs, which then can contribute to the observed antiviral effects of IFNγ [46, 116]. Taking these effects together, IFNγ is an important proinflammatory immunomodulator that also induces a set of antiviral effects. Defects in IFNγ signaling usually lead to Mendelian Susceptibility to Mycobacterial Disease (MSMD) syndrome, which is characterized by recurrent disseminated infections with environmental mycobacteria or Salmonella [85] and emphasizes the importance of IFNγ in controlling pathogens and preventing infections.

Conversely, IL-10 is a central regulator of the immune system that primarily induces immune suppressive activities and also some immune stimulating activities to delicately adjust the vital balance between pathogen control and tissue damage [58]. This regulatory function is achieved by IL-10 primarily through the inhibition of cytokine and chemokine production in target cells [117], thus intervening in the communication structure and determining the course for new directions in the immune system. In monocytes, macrophages, and DC IL-10 signaling inhibits the production of the pivotal proinflammatory cytokines IL-1 and TNF, but also IL-6, IL-12, and IL-18 [87, 118, 119], thereby evoking its main anti-inflammatory activities. IL-10 may also inhibit the production of numerous chemokines by activated monocytes [117, 120, 121], which likewise does contribute to the anti-inflammatory effect of IL-10 through termination of leukocyte recruitment. In addition, IL-10 downregulates the presentation of antigen loaded class II MHC [122, 123], as well as the expression of T cell function related factors, such as ICAM-1 and B7, in monocytes, hence dampening the T cell-activating capacity of monocyte APC [117, 124]. Furthermore, IL-10 signaling inhibits the production of GM-CSF, G-CSF and M-CSF in these cells hence controlling the survival and differentiation of monocytes [117, 125]. Together these changes downregulate the population and activity of macrophages, which further emphasizes the opposing role of IL-10 in respect to IFNγ signaling. In contrast, IL-10 fulfills distinct regulatory functions in B cell activation, proliferation, and differentiation, having implications for humoral immunity. Dependent on the activation state of B cells, IL-10 seems to induce or prevent apoptosis of these cells [126]. Nevertheless, autocrine IL-10 signaling induces B cell differentiation into IgG- ad IgM-secreting plasma cells [127]. Furthermore, IL-10 does increase the expression of Class II MHC but not Class I MHC in B cells [128] which is in line with their stimulatory effect on B cells. To a similar extent, IL-10 does have conflicting effects on different T cell subsets [129]. IL-10 is expressed by different

kinds of regulatory T cells, which play an important role in restricting immunopathology and induction of peripheral self- and foreign antigen tolerance [58]. Accordingly, IL-10 signaling does inhibit cytokine production and proliferation of active CD4+ T cells as mentioned earlier. Moreover, IL-10 signaling has both, stimulatory and inhibitory effects, on recruitment, cytotoxic activity, and proliferation of CD8+ T cells [117, 129, 130]. The immunoregulatory function of IL-10 becomes evident as it is produced by T cells in response to many proinflammatory cytokines as a negative feedback loop [58, 117], thus restricting their effects and providing a self-regulating mechanism to the immune system. Additionally, the regulatory function of IL-10 acts as a main switch on most pro-inflammatory cytokines such as IL-4, TNF, IL-12 and IFNγ, as IL-10 signaling is capable of directly reversing active effects of these cytokines [117]. The importance of these regulatory effects for a functional immune system is emphasized as defects in IL-10 signaling typically lead to inflammatory bowel disease or other exaggerated inflammatory disorders [117].

1.3.2 Viral escape strategies for class II cytokine signaling

The importance of IFN signaling for antiviral immune response is further emphasized by diverse strategies developed by viruses targeting IFN signaling to escape the host's immune response [50]. Multiple viruses can downregulate the expression and surface presentation of IFNAR and thereby render the cell less responsive to type I IFNs. Herpes simplex virus and Vesicular stomatitis Indiana virus have shown to induce a ligand-independent but serine phosphorylation and ubiquitination-dependent downregulation of IFNAR1 from the cell surface via a P38 kinase pathway in response to pattern-recognition receptor stimulation [131, 132]. While this feature is necessary for the regulation of type I IFN signaling in dendritic cells, which plays a central role in homeostasis of dendritic cells [132-134], the Severe Acute Respirator Syndrome Coronavirus (SARS-CoV) seems to exploit it to its advantage. The SARS-CoV induced accessory 3a protein causes stress in the ER and modulates the unfolded protein response, which leads to downregulation of IFNAR1 and eventually to apoptosis in infected cells [50, 135]. Also, the SARS-CoV-2 does impair the secretion of type I IFNs to overcome the immune system of severe COVID-19 patients [136, 137]. The West Nile virus has developed another way to inhibit type I IFN signaling in infected cells, by preventing the accumulation of IFNAR1 on the cell surface. Nonstructural proteins of the West Nile virus activate proteolytic degradation of IFNAR1 – but not IFNAR2 – independent of serine phosphorylation [138]. The resulting depletion of IFNAR1 leads to reduced responsiveness to type I IFNs of the target cell. Likewise, type II IFN signaling has been found to be targeted by the Kaposi's sarcoma-associated herpesvirus in order to escape the host's immune system [50]. The Kaposi's sarcoma-associated herpesvirus encoded proteins K3 and K5 has been shown to induce ubiquitination, endocytosis and degradation of IFNGR1 and thereby reduce the responsiveness of the target cells to IFNγ [139].

In addition to regulation of the surface expression of IFN receptors, various viruses, such as myxoma virus, vaccinia virus, cowpox virus and camelpox virus, encode and secrete IFN receptor mimetics, that can directly bind and neutralize IFNs [50, 140-143]. Despite not directly evoking cellular antiviral states, IL-10 signaling plays an important role in regulating the host's antiviral defense. This is evident in the fact, that several large DNA viruses, including the Epstein-Barr virus (EBV), the cytomegalovirus (CMV) and some poxviruses [30, 144, 145], have evolved IL-10 homologs to escape immune system detection. These homologs use the human IL-10 receptor and signaling to determine the course for immune suppression. The EBV induced IL-10 homolog (ebvIL-10) shares ~83% sequence identity with the human IL-10 [117] but has a 1,000-fold reduced binding affinity for the IL-10 receptor complex on cells [146, 147]. It is only expressed during the lytic phase of virus infection and selectively induces only a subset of IL-10 response genes [148-150]. As both molecules activate the same receptor complex on the same cell types, this implies that there is a mechanism involved in ligand binding, which controls the pleiotropy in signaling responses of IL-10 signaling [117]. Furthermore, this mechanism is centered on the binding affinity of the ligand to IL-10R1, as ebvIL-10 signaling was sensitive to cell surface IL-10R1 expression and impaired signaling response after ebvIL-10 stimulation could be recovered by overexpression of IL-10R1 [147]. Like EBV, the β-herpes virus CMV encodes an IL-10 homolog (cmvIL-10) that recognizes and signals through human IL-10R1 [151, 152]. However, cmvIL-10 shares only 27% sequence similarity with the human IL-10 [151] and yet possess a comparable binding affinity for IL-10R1 [152]. Structural comparison of liganded IL-10R1 revealed a ~40° larger interdomain angle between both cmvIL-10 subunits compared to the human variant [152]. The increased interdomain angle of cmvIL-10 is hypothesized to result in an altered IL-10R1 re-organization in cell surface IL-10R complexes [152]. In contrast to ebvIL-10, cmvIL-10 induces a similar signal pattern as human IL-10 [153]. These prominent differences in the mechanism by which the viral IL-10 homologs exploit the IL-10 signaling pathway suggest that both viruses captured cellular IL-10 at some time point and later independently evolved different molecular mechanisms that suit the requirement of viruses for evasion of the host defense [117, 152]. The conspicuous connection between receptor binding affinity and signaling pattern might have implications for the underlying mechanism of IL-10 signaling pleiotropy. Understanding the regulatory mechanism of signaling pleiotropy in the IL-10 signaling pathway potentially provides valuable insight into the signaling mechanism of IFNGR and vice versa, given the remarkable similarity in protein structure and binding affinities of both cytokine receptor complexes.

1.4 Mechanism of class II cytokine receptor activation and signaling

Class I/II cytokine receptors have in common that they primarily rely on the JAK/STAT signaling pathway to convey their information to the cell [154, 155]. This is also true for both hexameric class II cytokine receptors, IFNGR and IL-10R. Although activation and crosstalk with signaling

pathways other than the JAK/STAT pathway have been observed for these receptors in some occasions [155, 156], disruption of central components of the JAK/STAT pathway have led to abrogation of IFNGR and IL-10R-specific cellular responses [157, 158]. This indicates that JAK/STAT signaling is the principal signaling pathway for IL-10 and IFNγ and is necessary to evoke their hallmark effects. According to the indispensable role of JAK/STAT signaling pathway for hexameric class II cytokine receptor signaling, this work will henceforth focus on JAK/STAT signaling and neglect other signaling pathways.

1.4.1 Key player of the JAK/STAT signaling pathway

The JAK/STAT signaling pathway is an example for direct and uncomplicated signal transduction. Members of the eponymous tyrosine **Ja**nus **k**inase (JAK) family and the **s**ignal **t**ransducer and **a**ctivator of **t**ranscription (STAT) protein family are the only components known to be indispensable for signal transduction. Members of both JAK and STAT families share strong structural homology inside their protein family (**Figure 6A**) [159]. The JAK family contains four members JAK1, JAK2, JAK3, and TYK2 [159]. Class I/II cytokine receptors themselves do not bear an intrinsic kinase activity, that would be required for activation of downstream signaling components. Instead, one member of the JAK family is constitutively bound via its FERM-SH2 domains to the box motifs in the intracellular domain of the receptor subunit [160, 161]. In addition to the FERM-SH2 domains, JAKs contain a kinase domain, that promotes tyrosine phosphorylation, and a pseudo kinase domain, that lacks kinase activity but plays a substantial role in regulation of kinase activity [162]. In hexameric class II cytokine receptor complexes the binding receptor subunits, IFNGR1 and IL-10R1, are associated with JAK1 [160, 163], whereas the accessory receptor subunits IFNGR2 and IL-10R2 are associated with JAK2 and TYK2, respectively [164, 165].

The STAT protein family contains seven members STAT1, STAT2, STAT3, STAT4, STAT5a, STAT5b and STAT6 [166], all of which possess a DNA binding domain that assists in their function as transcription factors [167]. Additionally, they contain an N-terminal and coiled-coil domain, that are involved in nuclear translocation [168], as well as an SH2 domain that allow for dimerization of phosphorylated STAT proteins [169] and C-terminal transactivation domain. IFNGR is known to activate solely STAT1 under normal conditions [170], whereas IL-10R may activate primarily STAT3 and to a lesser extend STAT1 [171, 172], as well as STAT5 in non-macrophage cell lines (**Figure 6B**) [171]. However, in absence of STAT3 or excess of STAT1, such as after priming with IFNs, IL-10R activated more STAT1 proteins and consequently induces a pro-inflammatory response [173, 174]. Likewise, IFNGR has been shown to activate STAT3 in absence of STAT1 [175]. Accordingly, which STAT protein is phosphorylated and to which extent upon cytokine receptor activation is not only governed by the specificity of the STAT recruitment sites, but also

by availability and concentration of cellular STAT proteins. Moreover, signaling pleiotropy seems to be a product of several intertwined factors.

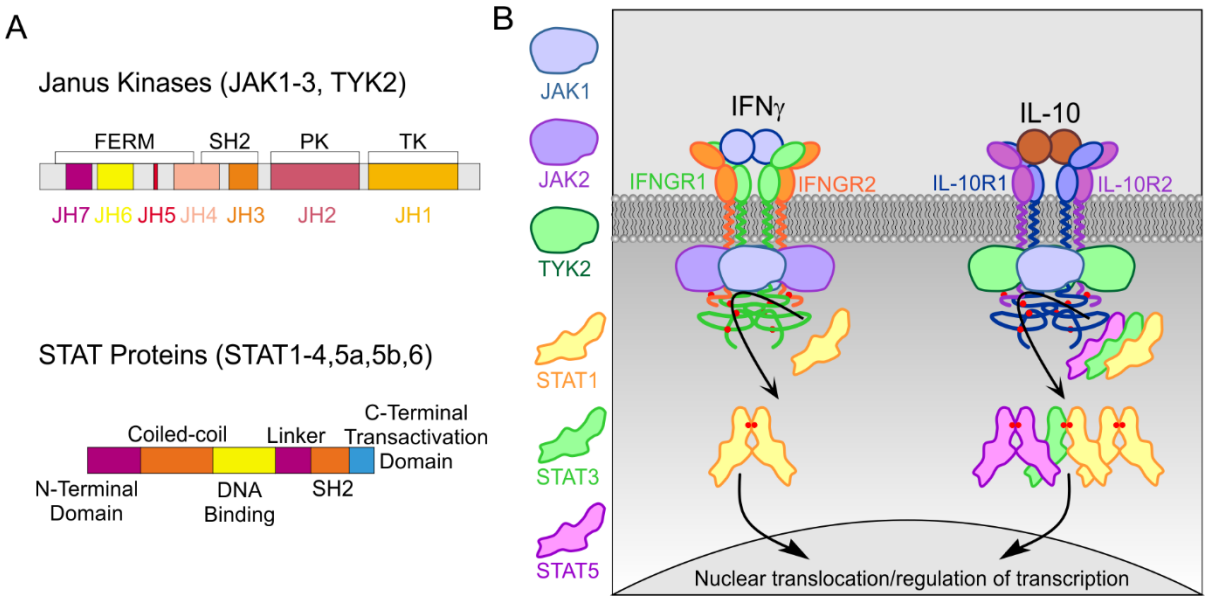

Figure 6: JAK/STAT signaling pathway of hexameric class II cytokine receptors. A) Domain structures of Janus kinases und STAT proteins. JH = JAK homology domains. Taken and modified from [33]. B) Depiction of JAK and STAT members involved in IFNGR and IL-10R signaling.

1.4.2 Mechanism and regulation of JAK/STAT signal transduction

In principle, the JAK/STAT signaling pathway is initialized through the binding of cytokines to the extracellular domain of their specific cytokine receptor at the cell surface (**Figure 7**). Ligand-receptor interaction is thought to induce dimerization that bring the associated JAKs into close proximity where they subsequently activate each other via transphosphorylation [166]. The activated JAKs continue to phosphorylate specific tyrosine residues in the intracellular domain of the binding subunit (IFNGR1 → Y444; IL-10 → Y427, Y477), thereby creating recruitment sites for the SH2 domains of STAT proteins [170, 171]. The accessory receptor subunit, however, is not phosphorylated in response to ligand binding [164] and therefore likely contribute to signaling primarily by providing a second JAK protein. After recruitment to the receptor, STAT proteins are activated by JAKs through phosphorylation of a specific tyrosine residue near the C-terminus [170] that is conserved among all STAT proteins [166]. Phosphorylated STATs are released from the receptor and translocate into the nucleus to bind dedicated DNA sequences in the promoter regions of genes [176]. This conserved phospho-tyrosine residue enables the STAT proteins to bind SH2 domains of other STAT proteins to form homo- and heterodimers thus forming a transcription factor complex [169]. In the case of type II IFN signaling, only STAT1 homodimers are formed, which promote transcription of specific genes by binding to Interferon-**G**amma **A**ctivated **S**equence (GAS) in their promoter region. Other STAT dimers might bind additional co-factors, such as type I IFN stimulated STAT1:STAT2 heterodimers that bind **I**nterferon **R**esponse **F**actor 9 (IRF9),

thereby forming **I**nterferon **S**timulated **G**ene **F**actor 3 (ISGF3) and facilitating gene transcription by binding to **I**nterferon-**S**timulated **R**esponse **E**lements (ISRE) [50, 95].

While JAKs, and STATs are required to perform signal transduction, several other regulator and effector proteins interact with and modulate the JAK/STAT signaling pathway (**Figure 7**) [166]. These effector proteins include signal-transducing adapter molecules (STAM) [177] and the SH-2B/LNK/APS family of adapter proteins [178, 179]. Both are known to interact with JAKs or STATs and thus through a yet unknown mechanism differentially regulate the JAK/STAT signaling pathway. Additionally, protein tyrosine phosphatases (PTPs), such as SHP-1 and CD45, have been observed to negatively regulate JAK/STAT signaling [180-183]. SHP-1 contains two SH2 domains which assist in targeting of tyrosine phosphorylated cytokine receptors and JAKs before mediating dephosphorylation of those tyrosine residues [181, 182], whereas CD45 is membrane-bound and has been shown to directly dephosphorylate JAK2 [183]. Furthermore, negative feedback regulators, such as the suppressor of cytokine signaling protein (SOCS) family, have been identified in the context of JAK/STAT signaling pathway [166, 180]. SOCS are expressed and activated in response to several cytokines and inhibit JAK/STAT signaling by seemingly different mechanisms – however, the mechanism of most SOCS has not been resolved yet [180]. Lastly, members of the protein inhibitors of STATs (PIAS) family interact with phosphorylated STAT dimers and prevent them from binding to DNA [184, 185].

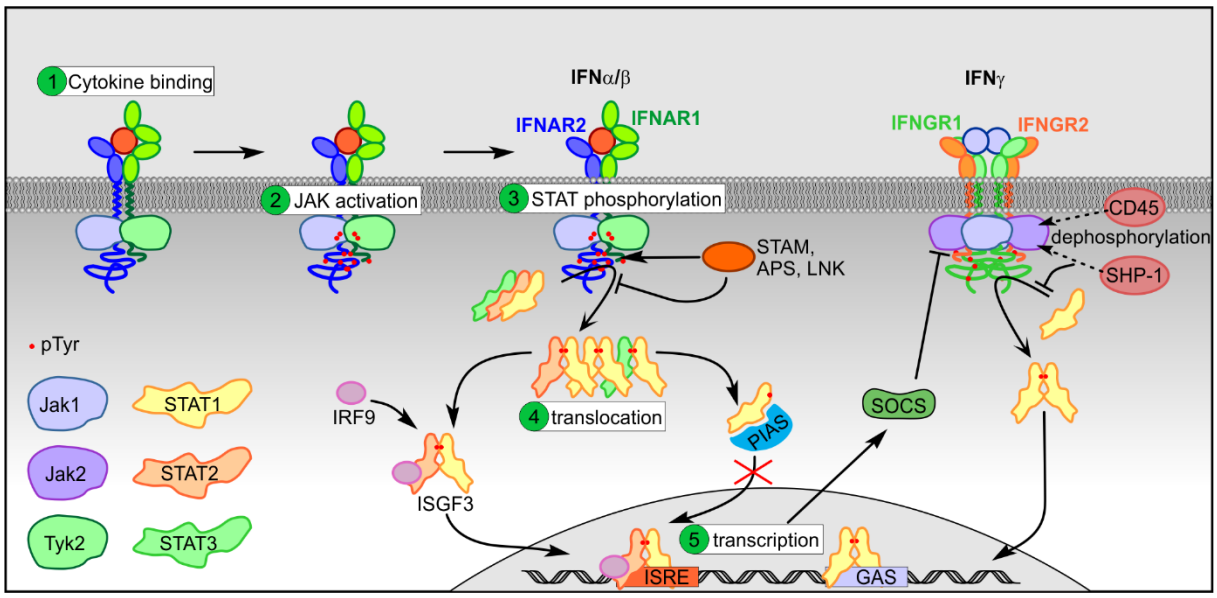

Figure 7: Sketch of the canonical JAK/STAT signalling pathway induced by type I and type II IFNs. The sketch illustrates the process of signal transduction as well as the general interplay of representative regulators and effector molecules with the JAK/STAT signalling pathway. Image adapted from [40, 155]

1.4.3 Mechanism of receptor assembly and activation

Although components and regulators of the JAK/STAT signaling pathway, as well as the principle of signal transduction, are well characterized, the mechanism of cytokine receptor assembly and

activation remains unclear. Especially the mechanism of class I/II cytokine receptor assembly has been controversially discussed and a consensus has not been reached yet. Different models have emerged from this time. Early on, in vitro studies on purified IFNGR1 ECDs and on-cell chemical crosslinking could show dimerization of two IFNGR1 subunits induced by IFNγ [186]. Shortly after, receptor co-precipitation studies by the same group revealed that, while JAK1 co-precipitates with IFNGR1 and JAK2 with IFNGR2 in absence of IFNγ, both receptor subunits only co-precipitates after ligand stimulation [187]. These observations defined a multi-step ligand-induced receptor dimerization model, in which unliganded IFNGR subunits exist as monomers on the plasma membrane (**Figure 8**) and only after ligand stimulation receptor subunits dimerize, bringing associated JAKs into close proximity and thus driving transphosphorylation. Such model enabled a biophysical description of complex formation, in which the interplay of binding affinities of cytokines to the binding subunit (K_D^{3D}) and to the accessory subunit (K_D^{2D}) control receptor complex assembly and consequently receptor activation [188]. In the past protein engineering has been successfully used to modify ligand-receptor binding affinities thereby altering cytokine receptor signaling [76, 189, 190] and could potentially be used to further investigate IFNGR signaling activation and pleiotropy. Similar models were also developed for numerous class I/II cytokine receptors [191], including IFNAR, human growth hormone, and IL-4/13 receptor [59, 192, 193]. A rather contrary model evolved from Förster resonance energy transfer (FRET) studies that suggested the IFNGR complex to be pre-assembled in absence of its ligand (**Figure 8**) [194]. This observation founded the basis of models which propose that the IFNGR complex is activated by ligand-induced conformational changes [195]. Comparable results were obtained for the IL-10R complex, thereby also proposing a pre-assembled receptor complex model for IL-10R and claiming this model to be an inherent feature of class II cytokine receptors [196]. An alternative model suggested that IFNGR1 and IFNGR2 are pre-associated and confined in lipid nanodomains, which supposedly play an essential role in ligand-induced conformational changes [197]. Likewise, previous work had shown that other class I cytokine receptors, such as the erythropoietin receptor and the human growth hormone receptor, would also follow a pre-assembled receptor complex model [198-200].

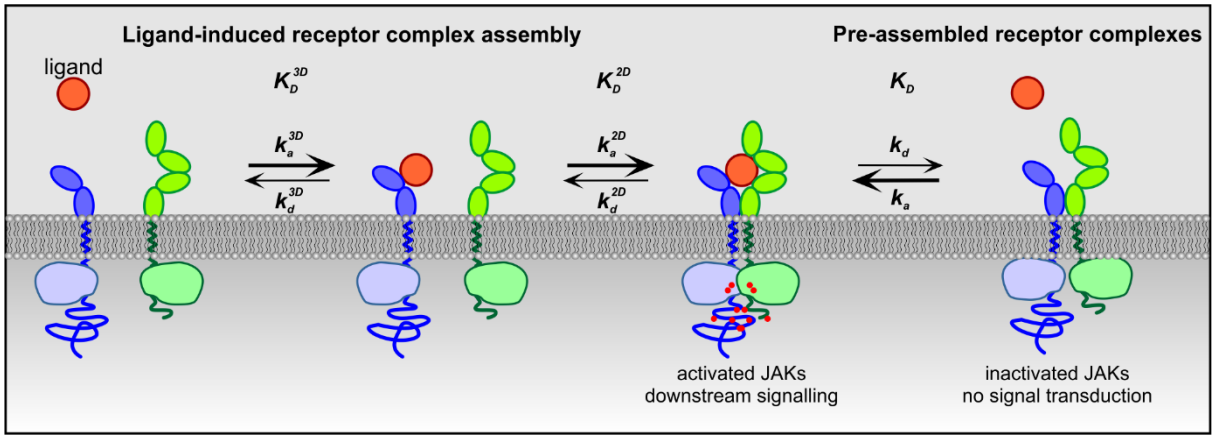

Figure 8: Opposing models describing class I/II cytokine receptor assembly and activation.

Despite disagreeing on the mechanism of class I/II cytokine receptor assembly, different models agree that activation of associated JAKs and downstream signaling is inevitably triggered by ligand-receptor interaction. Lately, this simple hypothesis has become increasingly controversial as it is insufficient to address a growing number of open questions. For hexameric class II cytokine receptors one pivotal question is particularly striking: How are pleiotropic effects induced on different cells using a single ligand and receptor complex? This is especially interesting for IFNGR, as it induces solely phosphorylation of STAT1 [170] and therefore apparently relies on a single molecular regulator to exert pleiotropic responses. Solving this puzzle for IFNGR and IL-10R is urgently required as both signaling pathways offer promising benefits in medical applications but have been hampered so far owing to its pleiotropy and counterbalancing immunostimulatory and immunomodulatory activities [201, 202]. Going into a similar direction, various other aspects of hexameric class II cytokine receptor signaling remain unresolved. Why do IFNGR and IL-10R require a hexameric receptor stoichiometry – and consequently up to four associated JAKs – to conduct signaling, while for other class I/II cytokine receptors, even including hexameric class I cytokine receptors IL-6R and IL-11R, two associated JAKs are sufficient? According to the predominant model on JAK activation and JAK/STAT signal transduction, a ternary complex consisting of one of each binding receptor subunit, accessory receptor subunit and a monomeric ligand, should provide all features which are necessary and sufficient to enable IFNGR and IL-10R signaling. In fact, in the past IFNγ and IL-10 have been engineered to form ligand monomers and thus induce ternary complex formation [203, 204]. In one approach, a 6 amino acid linker was introduced between helix D and E, which provided more flexibility for helices E and F and thus enabled formation of a stable monomer (**Figure 9A**). In another approach, two IFNγ subunits were fused by a linker and thus expressed as a single-chain variant (**Figure 9B**). This allowed disrupting one IFNGR1 binding interface by a single point mutation [205] and thereby creating a “monovalent ligand dimer” [206]. Although both monomers provoked cellular responses nonetheless, their efficiency and ability to induce STAT phosphorylation was reduced [204, 206], indicating that

receptor hexamers are not required to activate associated JAKs, however, they are necessary to arouse full signaling potential.

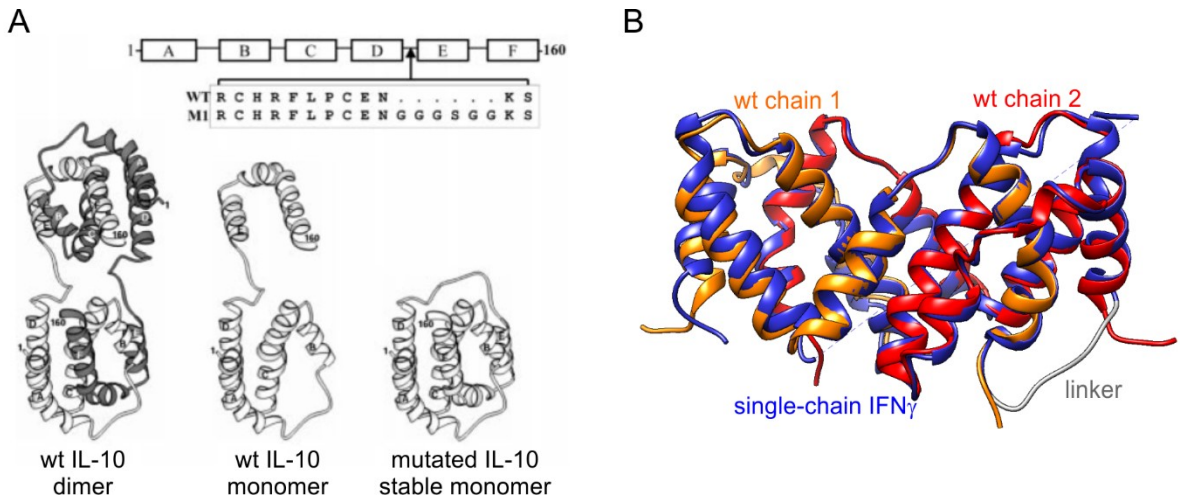

Figure 9: Monomeric variants of IFNγ and IL-10 that induce ternary complexes. A) A linker is introduced between helix D and E of IL-10. Thereby, helix E and F can adapt the same orientation as helix E and F of the second subunit in the wild-type dimer structure and thus allow formation of a stable IL-10 monomer. Taken from [203]. **B)** Superimposed structure of wild type IFNγ dimer (orange, red) and the single-chain variant (blue), which was created by fusing two IFNγ subunits via a linker (grey). PDB: 1EKU (single chain), 6E3K (wild type).

Lately, increasing understanding of complexity and function of central cellular processes, such as membrane confinement and endosomal trafficking, has broadened the view on the mechanism of cytokine receptor activation. Originally, receptor trafficking leading to lysosomal degradation was seen as a simple yet effective way to switch off cytokine signaling by eventually excluding activated receptors from the cytoplasm. Studies on the role of endocytosis in controlling cytokine receptor activation have shown, that inhibition of clathrin-mediated endocytosis (CME) likewise inhibits type I IFN receptor activation [207] indicating endocytosis to play a more active role in cytokine receptor activation than previously assumed. These findings suggested that at least for type I IFN receptor, despite receptor-ligand interaction at the plasma membrane receptor activation is not triggered prior to endocytosis. Interestingly, inhibition of CME did not affect type II IFN signaling, even though in the same study IFNGR was shown to similarly depend on CME for internalization [207]. Also following aspects of receptor trafficking, such as retromer sorting and endosomal signaling, have been shown to impact cytokine signaling in various ways [208-210]. Whether and how these aspects of endosomal trafficking affect hexameric class II cytokine receptor signaling remains obscure. In contrast, a major role in regulation of signal transduction and internalization of receptors has been ascribed to plasma membrane organization recently. For an instance, the T168N mutation in IFNGR2, which is known to promote MSMD in homozygous patients [211], has been recently proposed to hinder IFNGR association with lipid nanodomains [197].

2 Objectives

Class II cytokine receptors are important pleiotropic regulators of the immune system that play a central role in pathogen defense, tumor surveillance and immune system homeostasis. Most of these activities are very promising for biomedical application, which, however, have so far failed to succeed due to severe undesired side effects resulting from the pleiotropic nature of these cytokine receptors. Controlling the functional plasticity of class I/II cytokine receptor signaling by engineered cytokines has recently emerged as a promising approach to selectively reduce such side effects. In this context, systematic studies on the IFNα/β receptor and other systems have identified that the binding kinetics of the ligand-receptor interaction play an important role in defining signaling specificity. This has been explained by altered equilibrium and dynamics of the signaling complex in the plasma membrane.

In this work, I have investigated how the spatiotemporal organization and dynamics of signaling complexes regulate activation and signaling specificity of other members of the class II cytokine receptors. I focused on the type II IFN and IL-10 systems that supposedly form hexameric ligand-receptor signaling complexes in the plasma membrane. To this end, we developed an orthogonal multicolor anti-GFP nanobody-based labeling strategy, that allowed imaging of up to four different class II cytokine receptor subunits simultaneously. Using this labeling strategy, I investigated the spatiotemporal dynamics of IFNGR and IL-10R complex assembly by co-localization and co-tracking of single receptor subunits. Analysis of single molecule trajectories and co-trajectories was utilized to examine mobility and diffusion behavior of IFNGR and IL-10R subunits and their changes upon stimulation. We used partial agonists for both receptor complexes to systematically alter receptor binding stoichiometry and complex stability in the plasma membrane and correlated these with downstream signaling responses. Using our receptor dimerization approach, we furthermore uncovered pathogenic mechanisms behind the IFNGR2-T168N mutant and auto-IFNγ antibodies, both of which interfere with receptor activity and prominently cause the Mendelian Susceptibility to Mycobacteria Disease (MSMD) syndrome.

3 Strategies

3.1.1 Single molecule fluorescence microscopy

Investigating the spatiotemporal dynamics of cytokine receptor assembly in living cells required an imaging technique that can resolve the dynamic and interaction of single receptor subunits with reasonable time resolution. In this work, this was achieved by multicolor single molecule localization and tracking microscopy. Conveniently, many cytokine receptors have been reported to be expressed in low copy numbers at the cell surface [59, 188, 193, 212] making this approach a promising method to investigate their spatiotemporal dynamics. Single molecule localization microscopy (SMLM) can overcome the diffraction limit by fitting the point spread function of an isolated single emitter with a Gaussian function to determine its centroid with nanometer precision [213]. In order to follow complex formation of diffusing receptors in the plasma membrane at real time, we combined multicolor total internal reflection fluorescence (TIRF) excitation with simultaneous multi-channel detection using a four-color image splitter in front of a highly sensitive EMCCD camera. The evanescence field generated in TIRF microscopy at the glass-medium interface penetrates only 100-200 nm into the sample with decaying intensity hence only fluorophores within that range of the glass cover slip get excited. Thereby, fluorescently labeled single receptor subunits in the basal plasma membrane of the cell are excited and background fluorescence from cellular auto-fluorescence or out-of-focus fluorophores is drastically suppressed. This results in highest signal-to noise ratios required for robust single molecule localization and tracking. Furthermore, the imaging speed of TIRF microscopy is only limited by the camera read-out speed which typically allows for frame rates of 10-100 Hz at full resolution depending on camera technology. Single molecule tracking of transmembrane receptors in living cells with high-fidelity requires acquisition speeds of 30-50 Hz based on typical diffusion constants of ca. 0.1 $\mu m^2/s$ and receptor densities of 0.1-0.5 receptors per μm^2. Our approach not only enable spatial correlation by co-localization analysis, but also paved the way for temporal correlation of different molecules in subsequent tracking analysis. The thereby observed co-diffusion of different receptor subunits was used to rule out unspecific single molecule co-localization governed by receptor density-dependent transient overlap of localizations. Moreover, tracking analysis enabled investigation of receptor mobility and diffusion.

3.1.2 Orthogonal GFP-tag based labeling strategy

In single molecule fluorescence microscopy, bright fluorophores with optimized photophysical properties are required to achieve high SNR while maintaining reduced photobleaching and phototoxicity. Especially, spatiotemporal correlation analysis of receptor-complex formation demands a degree of labeling (DOL) close to unity to successfully detect as many single molecule interactions as possible. This is even more important for hexameric complex with four receptor

subunits. Each non-labeled protein further reduces the apparent interaction rate and the dynamic range of this method. Unfortunately, fluorescent proteins perform poorly in single molecule localization and tracking microscopy owing to their fast photobleaching because of an increase in laser power needed to compensate for their low quantum yield and brightness. Furthermore, maturation time of fluorescent proteins is rather slow and hence limits the DOL of cell surface receptors in a way that is hard to quantify. Likewise, conventional enzymatic covalent labeling strategies involving SNAP-tags or halo-tags impress by high labeling specificity but disappoint with DOL of 0.3-0.4 [59, 214]. In addition, the underlying enzymatic reactions may take considerable time prior to the experiments and the receptor's DOL does decline throughout the experiment as receptor subunits are internalized and new, unlabeled receptor subunits translocate to the cell surface. In this work, we developed and applied a new orthogonal labeling strategy based on non-fluorescent GFP-tags and highly specific dye-conjugated anti-GFP nanobodies (NB), to combine various advantages of the aforementioned labeling strategies. In 2010 Kirchofer *et al.* presented two distinct monoclonal camelid NBs termed Enhancer and Minimizer that modulate GFP fluorescence by recognizing overlapping epitopes with sub-nanomolar binding affinity [215]. We exploited their overlapping epitopes to make sure that only one NB can bind at a time. Additionally, we engineered two GFP derivatives using site-specific mutagenesis to bind exclusively either Enhancer (mXFPe) or Minimizer (mXFPm) while maintaining their high binding affinity. Owing to this high binding affinity we achieved fast and substantial binding of NBs to cell surface cytokine receptors N-terminally tagged with GFP derivatives while using a relatively low concentration of 5 nM labeled NBs. This low concentration requirement allowed us to keep the NBs in solution throughout the experiment and thereby avoid the decline of DOL due to receptor turnover, as new receptors appearing at the cell surface will be labeled quickly.

Using our orthogonal labeling strategy, we can investigate protein-protein interaction between two different receptor subunits by tagging one subunit with mXFPm and the other with mXFPe and labeling the receptors simultaneously with Enhancer and Minimizer conjugated with spectrally distinguishable organic fluorescent dyes. In the following, we will refer to such kind of experiment as receptor hetero-dimerization analysis. Alternatively, we can investigate the interaction of two copies of the same receptor subunits by performing receptor homo-dimerization analysis. Here, we express a receptor subunit N-terminally tagged with mXFPe for instance, and subsequently label it by simultaneous incubation with equimolar concentrations of two Enhancer NBs conjugated to different fluorescent dyes. Finally, we could combine both labeling strategies, hetero- and homo-dimerization, in a 4-color experiment on hexameric class II cytokine receptor to visualize full complexes.

4 Results and Discussion

4.1 Part I: The interferon-γ receptor complex

4.1.1 Endogenous receptor complexes at single molecule level

Interferon signaling represents mammalian cells' first line of defense against viral infections. Its cellular response interferes with viral replication, potentially slowing down or even stopping viral propagation. To ensure fast and effective response to viral infections, most cell types endogenously produce type I (IFNAR) and type II (IFNGR) interferon receptors. We used recombinantly produced cytokines site-specifically conjugated with photostable fluorescent dyes to experimentally assess density and properties of cytokine receptor complexes on the surface of living cells. To elucidate these aspects of IFNAR and IFNGR, endogenous cell surface receptors were labeled with fluorescent dye conjugated IFNα2 and IFNγ and subsequently subjected to single molecule total internal reflection fluorescence (TIRF) microscopy. Fast and efficient binding of IFNα2-DY647 and IFNγ-DY647 to the surface of HeLa cells could be detected within the first minutes of the experiment (**Figure 10**). Most single molecule events within the area covered by cells moved randomly in a Brownian-like manner and most likely represented single receptor complexes on the cell surface. Whereas a small portion of the single molecule events did not show any movement at all. Single molecule events in the areas not covered by cells were generally not mobile. Strikingly, when saturating cell surfaces with unlabeled IFNα2 or IFNγ (500 nM) prior to addition of IFNα2-DY647 or IFNγ-DY647 (5 nM) negligible amounts of mobile receptor complexes could be detected. This indicated that the observed binding of labeled cytokines is highly specific for IFNα2 or IFNγ respectively. Furthermore, these observations lead to the assumption that immobile particles represent unspecific binding of labeled ligand to the glass cover slip rather than on the cell surface. Consequently, immobile particles were excluded in future analysis.

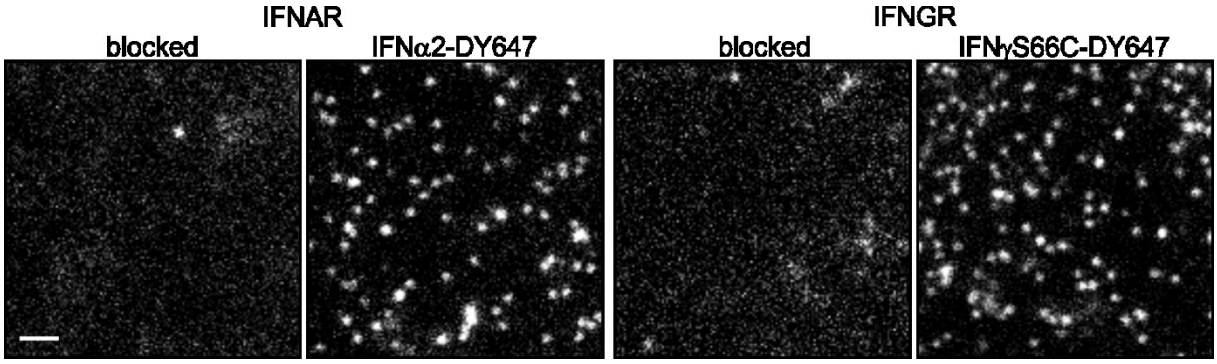

Figure 10: Binding of DY647-conjugated IFNα2 or IFNγ to the surface of wild-type HeLa cells. Binding specificity was shown in control cells by pre-incubation with high concentrations of unlabeled cytokines. TIRF microscopy images. Scale bar: 2 μm.

To get an overview of IFNAR and IFNGR complexes under physiological conditions the previously described experiments were expanded from HeLa cells to frequently used human tissue cell lines, including A549, Hap1 and RPE1. All observations made for HeLa cells were also true for the other cell lines, yet differences in cytokine receptor density and mobility were noticed between all cell lines. Subsequently, the acquired image data was subjected to single molecule localization and tracking analysis. Mean square displacement (MSD) analysis of the resulting single molecule trajectories revealed that the average diffusion constant of IFNAR was in general slightly higher than that of IFNGR under the same condition (**Figure 11** B). This could be attributed to IFNAR forming ternary complexes including two transmembrane receptor subunits [59], whereas IFNGR has been reported to form hexameric complexes containing up to four transmembrane receptor subunits [42, 216]. Interestingly, the changes in diffusion constants of a specific receptor complex between different cell lines was more significant than the changes between IFNAR and IFNGR in the same cell line. Strikingly, the profile of diffusion constants including the examined cell lines was similar for both IFNAR and IFNGR, with receptors showing the fastest diffusion in Hap1 and the slowest in RPE1. These observations strongly suggested that the overall diffusion of type I and type II interferon receptors is rather defined by the cell's properties than by the receptor itself. Differences in cytoskeleton, such as the size of the meshes of cortical actin [217], or membrane confinement could be responsible for altered receptor diffusion in different cell lines. However, to pinpoint these assumptions further experiments were needed.

Using the single molecule localization data, we could precisely determine the average density, given by the number of receptors in a defined area, of IFNAR and IFNGR on the surface of single living cells. This approach was particularly powerful, because it enabled direct quantification of cytokine receptors exclusively at the cell surfaces in real-time. As expected, IFNAR and IFNGR were expressed on the surface of all tested cell lines, even though the density of IFNGR was in general slightly higher compared to IFNAR (**Figure 11** C). The average receptor density at the plasma membrane was ~0.45 μm^{-2} for IFNAR and ~0.65 μm^{-2} for IFNGR. However, A549 cells did show an increased IFNAR surface density to an extend comparable to IFNGR surface expression. Whereas the surface density of IFNGR was reduced in RPE1 cell to the level of IFNAR surface expression.

In conclusion, the surface density of IFNAR and IFNGR observed on all cells in this experiment was within a suitable range for single molecule fluorescence microscopy (SMFM). This emphasized SMFM to be the method of choice for investigating the spatiotemporal dynamics of interferon receptor complex assembly on living cells as close as possible to physiological conditions.

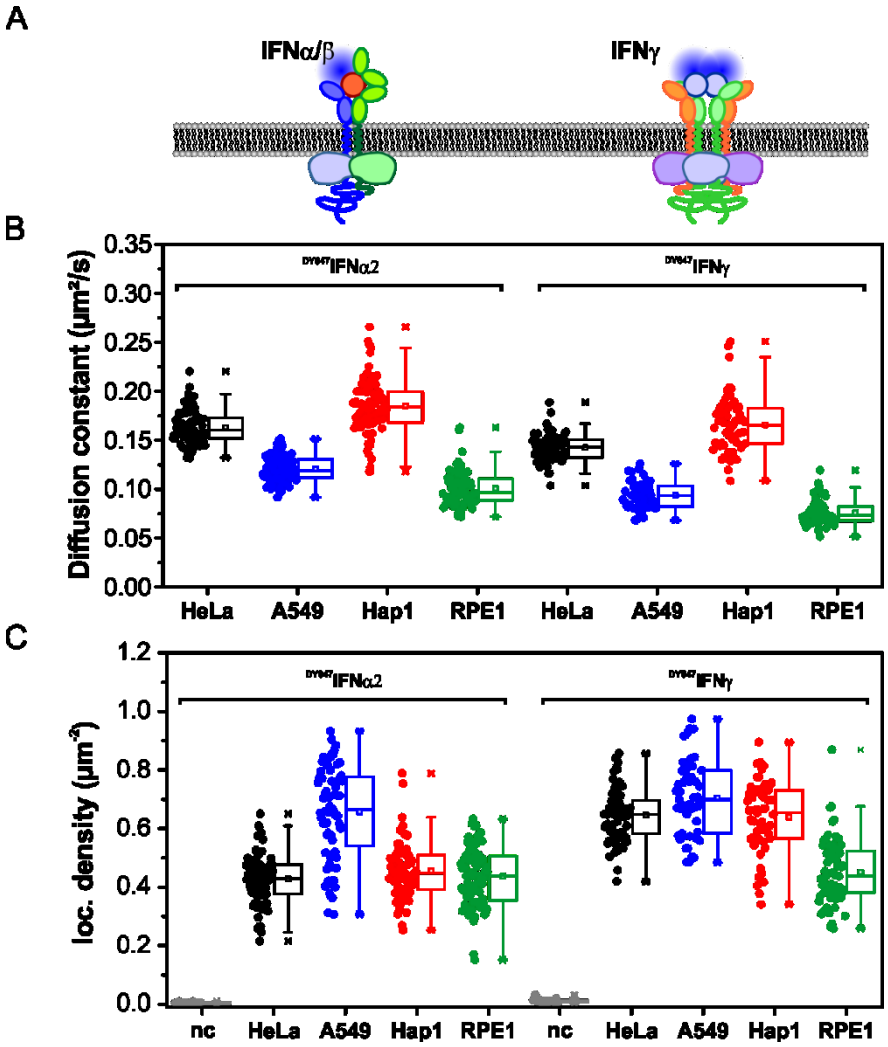

Figure 11: Type I and II interferon receptor expression and mobility on the surface of different tissue cell lines. **(A)** Cartoon portraying models of type I (left) and II (right) interferon receptor complexes. **(B)** Diffusion constants of surface bound IFNα2 and IFNγ in otherwise untreated HeLa, A549, Hap1 or RPE1 cell lines. Experiments were done at room temperature (~22 °C). Each data point represents averaged diffusion constants of a single cell. **(C)** Initial localization density of surface bound IFNα2 and IFNγ. Nc, negative control: HeLa cells were pre-incubated with high concentrations of unlabeled IFNα2 or IFNγ for 10 minutes.

4.1.2 Spatiotemporal dynamics of type II interferon receptor assembly

Despite being discovered more than half a century ago and ever since playing a central role in cytokine science, interferon receptor's mechanism of oligomerization and activation remains highly controversial. Mainly, two opposing models could be distilled from research of the past decades: (1) binding of the ligand to already preformed receptor complexes on the cell surface leads to internal conformational changes and thus to receptor activation and (2) binding of the ligand to monomeric receptor subunits at the cell surface initiates receptor complex assembly and eventually signaling. These opposing models could not be addressed properly without looking at the behavior of single receptor subunits on the surface of living cells. Furthermore, chapter 4.1.1 did show that type II interferon receptors are expressed at ~0.6 receptors per µm² on the cell surface – a property

that must be carefully considered when experimentally assessing the chemical equilibrium of receptor oligomerization.

4.1.2.1 Anti-GFP nanobody-based orthogonal labeling technique

To do the latter, it was not sufficient to visualize receptor complexes by labeled cytokines. While we could achieve efficient labeling of the high affinity binding receptor chain by increasing cytokine concentration, it did not yield any information about whether the low affinity accessory receptor chain was present in the receptor complex. Additionally, this experimental setup did not bear information about the resting state of cytokine receptor's oligomerization, as labeling consequently led to signaling activation by ligand binding.

To overcome these challenges, we developed an orthogonal labeling technique based on green fluorescent protein (GFP) derivatives and cameloid anti-GFP nanobodies (NB) Enhancer (EN) and Minimizer (MI) [215]. These NBs engaged partially overlapping topologies on GFP, so that only one of both NBs could potentially bind to a single GFP at a time (**Figure 12** A). By introducing two point mutations in mEGFP (N198D, Y200F → mEGFPe, **Figure 12** B) binding of MI was weakened. Vice versa, by introducing two point mutations in mECFP (E142K, H164N → mECFPm, **Figure 12** B) binding of MI was strengthened, while simultaneously weakening binding of EN. We expected to accomplish through these genetical modifications orthogonal binding of MI to mECFPm and EN to mEGFPe respectively. To test the orthogonality of our NB labeling system we performed a competitive binding assay on living cells using the very well characterized type I interferon receptor model [59]. To this end, either mEGFPe or mECFPm were N-terminally fused to type I interferon receptor subunit 1 (IFNAR1) and individually expressed on the surface of HeLa cells at a single molecule level. All IFNAR1 constructs were labeled by simultaneous incubation with 10 nM of EN-Rho11 and MI-DY647 before probing labeling specificity by dual-color TIRF imaging (**Figure 12** C). Throughout the experiment EN-Rho11 and MI-DY647 were both kept in solution at 2nM concentration to ensure a high degree of labeling by immediate labeling of receptors newly trafficked to the cell surface. Additionally, an "anti-oxygen cocktail", consisting of an enzymatic oxygen scavenging system (glucose, glucose oxidase and catalase) in combination with a redox system (Methyl Viologene and ascorbic acid), was utilized to enhance the photostability of both fluorescent dyes [218]. Simultaneously, unspecific binding of labeled NBs to the cover slip was prevented by culturing HeLa cells on substrates coated with poly-L-lysine-graft-polyethylene glycol (PLL-PEG), which was additionally functionalized with RGD peptides to support cell adhesion [219]. Single receptors were localized and tracked using SLIMfast software. As expected, both NB variants could bind to mEGFP-IFNAR1 on the surface of HeLa cells. In contrast, mEGFPe-IFNAR1 was almost exclusively bound by EN, whereas mECFPm-IFNAR1 was

exclusively bound by MI (**Figure 12** D). In vitro characterization of the interaction of NBs and mEGFPe by label-free and fluorescence real-time solid phase detection revealed a similar association rate constant k_a for the interaction of both NBs to mEGFPe, but a more than 50-fold faster dissociation rate constant k_d for MI compared to EN (data not shown). We took advantage of this feature to further minimize binding of MI to mEGFPe by incubating with EN for 5 minutes before addition of MI. Additionally, the amino acid residue at position 66 was mutated to phenylalanine for mEGFPe (Y66F → mXFPe) and mECFPm (W66F → mXFPm) to render both proteins non-fluorescent. This opened the opportunity to use especially GFP and spectrally comparable dyes as a third color if needed. As we aimed to spatiotemporally correlate two different receptor subunits on the surface of living cells an effective degree of labeling (DOL) of at least 1 for each receptor subunit was desirable. In a dimeric receptor complex the DOL of each receptor subunits could be considered as probability of being labeled. Hence, single DOLs multiplied to an overall probability of observing dimers in a complex. Related to our labeling technique this would mean the lower the single DOLs are, the lower the apparent dimerization would be, thus substantially decreasing the dynamic range of the readout. Therefore, it was necessary to determine the effective DOL of mXFPm and mXFPe labeled with MI and EN, respectively. For this purpose, the previously described anti-GFP NB-based labeling technique was combined with N-terminal SNAPf-tag labeling in a single molecule Förster resonance energy transfer (smFRET) experiment (**Figure 12** E). HeLa cells were transfected with mEGFPe-IFNAR1, mECFPm-IFNAR1 or their non-fluorescent versions with N-terminally fused SNAPf-tag. After labeling with SNAP-Surface647 as FRET-acceptor, NBs labeled with Rho11 were added as FRET-donor. Subsequently, smFRET was quantified by alternating laser excitation. The DOL was determined from the number of acceptor molecules detected upon donor excitation compared to the number of acceptor molecules observed after direct acceptor excitation. Remarkably high DOL of ~1.0 for EN/mEGFPe and ~0.8 for MI/mECFPm were detected (**Figure 12** F). The DOL of EN/mXFPe and MI/mXFPm was comparably high. Therefore, the effective DOL of our NB labeling technique was much more competitive, than conventional post-translational labeling techniques, such as SNAPf-tag labeling. Additionally, as we kept NBs in solution throughout the experiment, new receptors were labeled as they were trafficked to the cell surface. This feature in combination with convincingly high DOL made our labeling strategy suitable to tackle the spatiotemporal dynamic and correlation of cytokine receptor subunits.

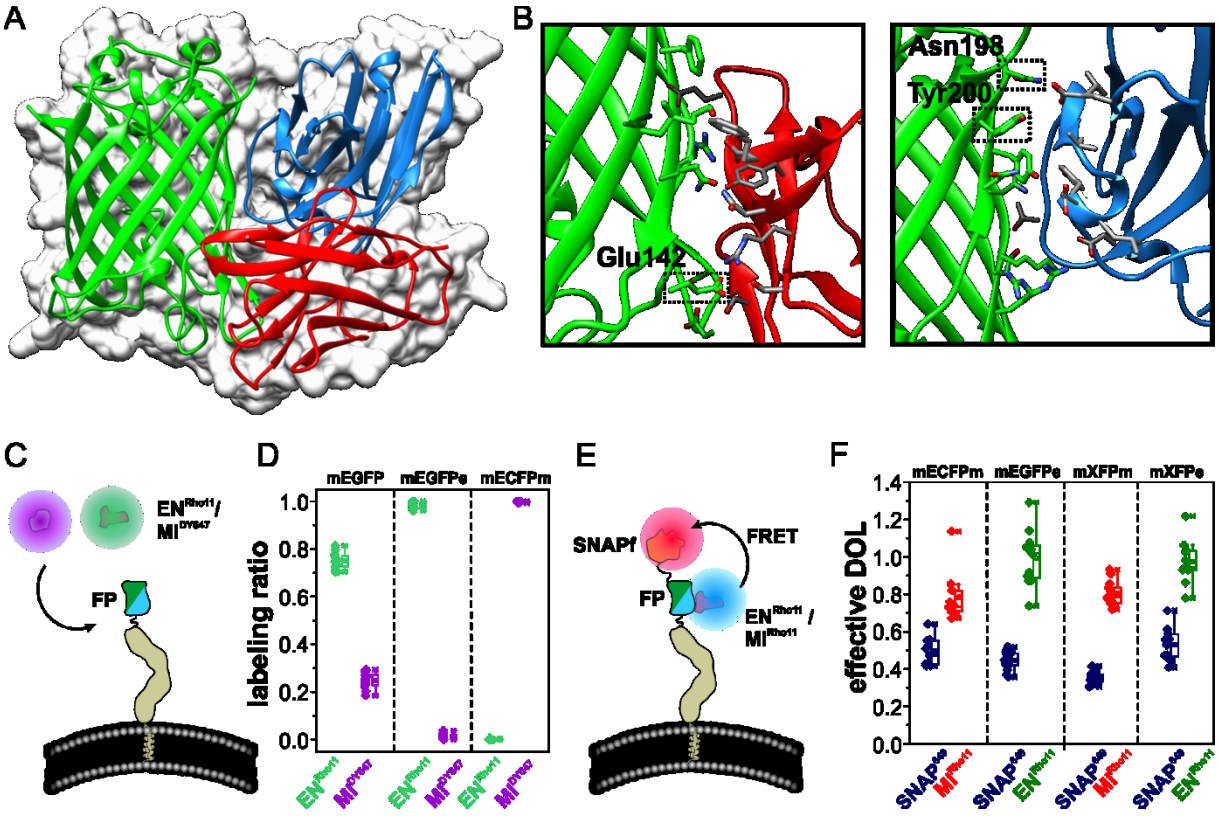

Figure 12: Orthogonal labeling based on engineerd GFP-tags and cameloid α-GFP nanobodies. (A) Overlay of the crystal structure of GFP (green) with overlapping binding of Enhancer (EN, red) or Minimizer (MI, blue) (PDB entries: 3K1K and 3G9A, respectively). **(B)** Enlarged view of the binding interfaces. Residues mutated for selectively destabilizing recognition by EN (left) and MI (right) are highlighted by dotted rectangles. **(C, D)** Competitive binding of EN and MI on different engineered GFP variants. Labeling ratio was calculated from localization densities. **(E, F)** Effective degree of labeling (DOL) estimated by single molecule FRET.

4.1.2.2 Homo- and hetero-dimerization of IFNGR subunits

With this powerful labeling technique in hand, we could probe single IFNγ receptor (IFNGR) subunits on the surface of living cells. This would allow us to investigate the mode of receptor complex formation of the IFNGR. The type II interferon receptor complex comprises two different receptor subunits, the high affinity binding receptor chain, IFNGR1, which is constitutively expressed on all nucleated cells, and the accessory receptor chain, IFNGR2, the expression of which is tightly regulated. The only known agonist IFNγ is a homodimer. Each subunit of IFNγ supposedly engages one copy of IFNGR1 and IFNGR2, eventually resulting in a hetero hexameric receptor complex. Hence, to fully assess the receptor complex stoichiometry of IFNGR during its resting state and after signaling activation by IFNγ, it was necessary to probe not only the interaction between two different receptor subunits (hetero-dimerization), but also between two identical subunits (homo-dimerization).

First, we probed hetero-dimerization of IFNGR1 and IFNGR2 by performing dual-color single molecule TIRF microscopy on HeLa cells co-transfected with mXFPm-IFNGR1 and mXFPe-IFNGR2. Cell surface IFNGR1 and IFNGR2 were labeled by incubating the cells with 5 nM of MI-

Rho11 and EN-A643 (**Figure 13** A) as previously described shortly before imaging. As before the experiments were conducted in presence of anti-oxygen cocktail and on PLL-PEG-RGD coated cover slips to minimize unspecific binding of the dye to the glass surface. After imaging, TIRF microscopy images were subjected to a dual-color co-tracking analysis based on our custom made SLIMfast software. Different spectral channels were aligned using a transformation matrix, that was calculated from TetraSpeck beads emitting in both channels. This allowed for spatial correlation of individual IFNGR1 and IFNGR2 after being temporally correlated into single trajectories (**Figure 13** B, red and blue). Receptor subunits that showed correlated movement (detained in a proximity of 150 nm) for a minimum of 320 ms – which we refer to as co-tracked receptor subunits – were identified as heterodimers (**Figure 13** B, magenta). These co-localization/ co-tracking thresholds allowed reliable elimination of density-dependent random co-tracking [188]. In its resting state (absence of IFNγ), which was confirmed by flow cytometry analysis of phosphorylated Signal Transducer and Activator of Transcription 1 (STAT1) effector proteins in non-transfected HeLa cells (**Figure 13** E), uncorrelated and random diffusion of individual IFNGR1 was observed as confirmed by single molecule photobleaching (**Figure 13** C) and dual-color co-tracking analysis (**Figure 13** B, D). After addition of 10 nM IFNγ substantial hetero-dimerization of IFNGR1 and IFNGR2 could be observed, as indicated by receptor co-tracking (**Figure 13** D). After stimulation with 40 nM of a functional monomeric IFNγ (mIFNγ) [204], which possessed only one IFNGR1 binding site, hetero-dimerization of IFNGR1 and IFNGR2 was roughly halved. At first glance this was surprising, as the overall density of IFNGR1 and thus the IFNGR2 recruitment sites at the cell surface did not change between the experiment. However, as we have learned in chapter 4.1.1 there is a substantial amount of unlabeled endogenous IFNGR at the plasma membrane of HeLa cells. As in contrast to mIFNγ, the wild type IFNγ should be capable of recruiting two of each subunit, yet only one of each is needed to be labeled to detect heterodimers. Therefore, IFNγ could potentially show higher apparent dimerization at lower effective degree of labeling due to endogenous receptors.

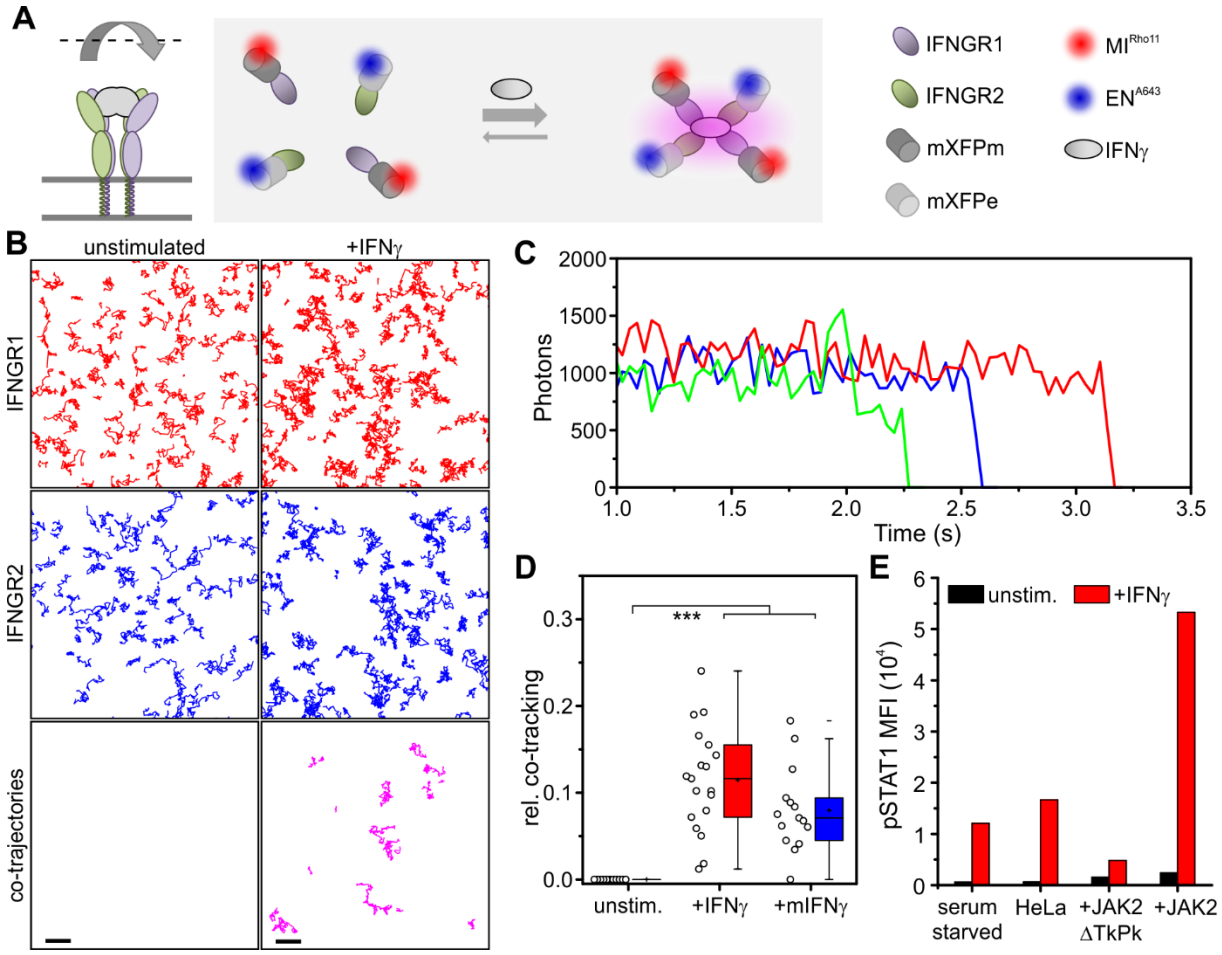

Figure 13: Hetero-dimerization of IFNGR1 and IFNGR2 after stimulation with IFNγ. (A) Cartoon portraying labeling of individual IFNGR subunits with anti-GFP nanobodies minimizer (MI) and enhancer (EN), which are labeled with Rho11 or AT643, respectively. **(B)** Trajectories of single receptors, IFNGR1 (red) and IFNGR2 (blue), or receptor dimers (magenta) of a representative cell in absence (left) or presence (right) of IFNγ. **(C)** Single-step bleaching of representative IFNGR1 subunits plotted as photons over time. **(D)** Relative co-tracking of single IFNGR1 and IFNGR2 molecules in HeLa cells unstimulated or incubated with IFNγ (red) or mIFNγ (blue). Each data point represent a single cell. Co-tracking was averaged over 5 seconds relative to IFNGR1. Statistical analysis was done in an unpaired students t-test: ***, $P \leq 0.001$. **(E)** Phosphoflow cytometry of HeLa cells unstimulated or incubated with IFNγ. Control cells were additionally transfected with either wild-type JAK2 or an inactive JAK2 mutant lacking its tyrosine kinase domain (ΔTkPk).

Next, we tested homo-dimerization of IFNGR1 in HeLa cells transfected with mXFPm-IFNGR1. Stochastic labeling was utilized to achieve dual-color labeling of a total mXFPm-IFNGR1 population. By simultaneous incubation with 5nM of MI-Rho11 and MI-A643, we made sure that ideally one half of IFNGR1 population was labeled with Rho11 and the other with A643 (**Figure 14** A). Afterwards we could use the actual dye ratio bound to IFNGR1 to correct the apparent dimerization for stochastic dye distribution. As observed for hetero-dimerization, IFNGR1 remained monomeric in absence of IFNγ. Only after addition of 10 nM IFNγ a substantial fraction of IFNGR1 homodimers appeared (**Figure 14** C). Similar homo-dimerization of IFNGR1 could be observed in cells over-expressing mXFPe-IFNGR2, which was confirmed on a single cell level by labeling with EN-ATTO488. As expected, after stimulation with 40 nM mIFNγ which possessed only one IFNGR1 binding site no co-tracking of IFNGR1 could be observed. Analogously, IFNGR2

homo-dimerization was probed by labeling with EN-Rho11 and EN-ATTO643 (**Figure 14** B), whereas IFNGR1 was labeled with MI-A488 if required. Similar results were obtained for IFNGR2 homo-dimerization, but with substantially lower receptor co-tracking levels (**Figure 14** D), which were in line with the drastically lower binding affinity of IFNγ for IFNGR2 compared to IFNGR1 [220]. Additionally, IFNGR2 binding to IFNγ strictly requires preceding binding of IFNGR1 [220]. Hence, IFNGR2 homodimers could only occur at IFNGR receptor complexes containing two IFNGR1, the fraction of which was previously calculated as IFNGR1 homodimers (**Figure 14** C).

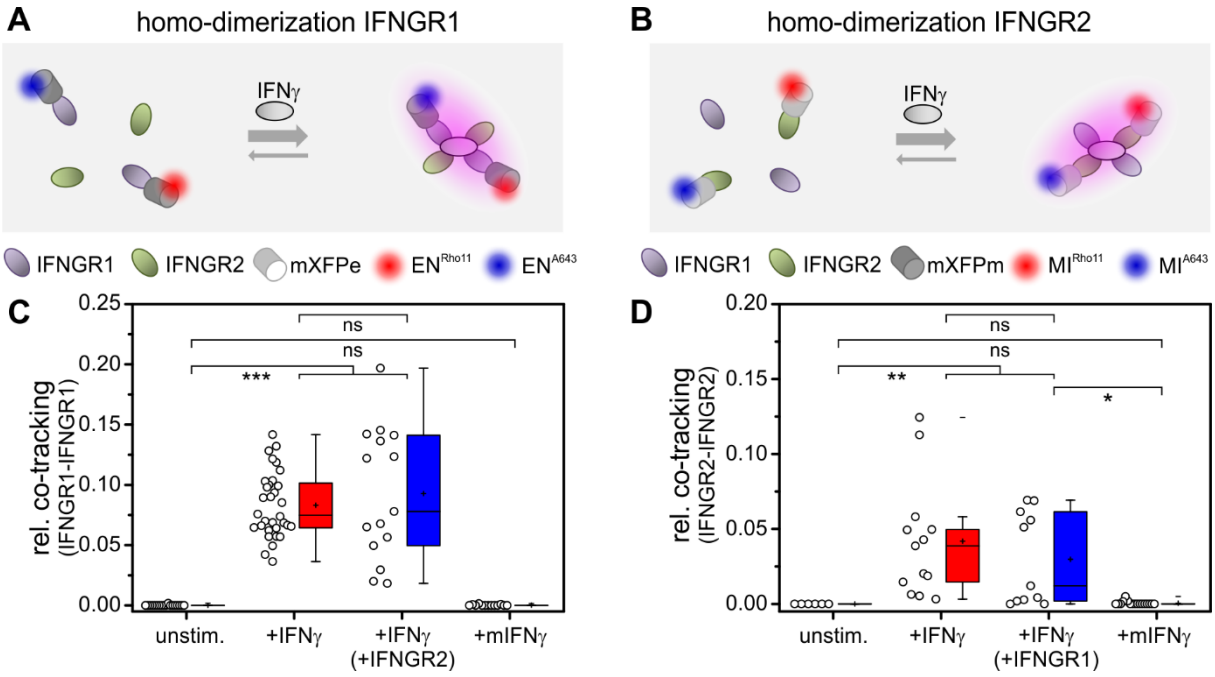

Figure 14: Homo-dimerization of IFNGR1 and IFNGR2 after ligand stimulation. (A, B) Cartoon portraying the labeling strategy used to detect IFNGR1 (A) or IFNGR2 (B) homodimers. Magenta circle represents receptor complexes recognized as homodimers. **(C, D)** Relative co-tracking of two IFNGR1 (C) or two IFNGR2 (D) subunits in HeLa cells treated with IFNγ or mIFNγ. As a control for requirement of the respective other subunit the missing receptor subunit was overexpressed by transient transfection (+IFNGR2 in C, +IFNGR1 in D). Statistical analysis was done in an unpaired students t-test: ns, non-significant; *, $P \leq 0.05$; **, $P \leq 0.01$; ***, $P \leq 0.001$.

These results suggest IFNγ-induced formation of receptor homo- and heterodimers according to the structural model shown in **Figure 15** C with efficiencies governed by the differential binding affinities of the receptor subunits. To further explore the structural organization of IFNGR1 and IFNGR2 in the homo- and heterodimers formed at the plasma membrane, we estimated the distances between receptor subunits by single molecule FRET. In case of IFNGR1/IFNGR2 heterodimers, significant increase in the donor signal was observed upon acceptor photobleaching (**Figure 15** A). An average FRET efficiency of ~25% was obtained from this analysis (**Figure 15** B). Given the theoretical Förster radius of 6.9 nm for the Rho11/ATTO643 pair, this FRET efficiency corresponds to an approximated distance of 8.3 nm. A similar FRET efficiency was obtained for IFNGR1/IFNGR2 heterodimers formed by mIFNγ (**Figure 15** B). These results are in line with the distance of approximately 7 nm between the N-termini in the cis- and the trans-

heterodimers predicted by the crystal structure [78] (**Figure 15** C) when taking into account the additional 1-1.5 nm distance caused by the mXFP-tags and the NBs. By contrast, FRET was not detectable for homo-dimeric IFNGR1 complexes, for which substantially larger distance of 9.2 nm between the N-termini are expected from the crystal structure (**Figure 15** C). All together these findings indicate a short distance interaction between two co-tracked receptor subunits IFNGR1 and IFNGR2, which is in line with the proposed structural model.

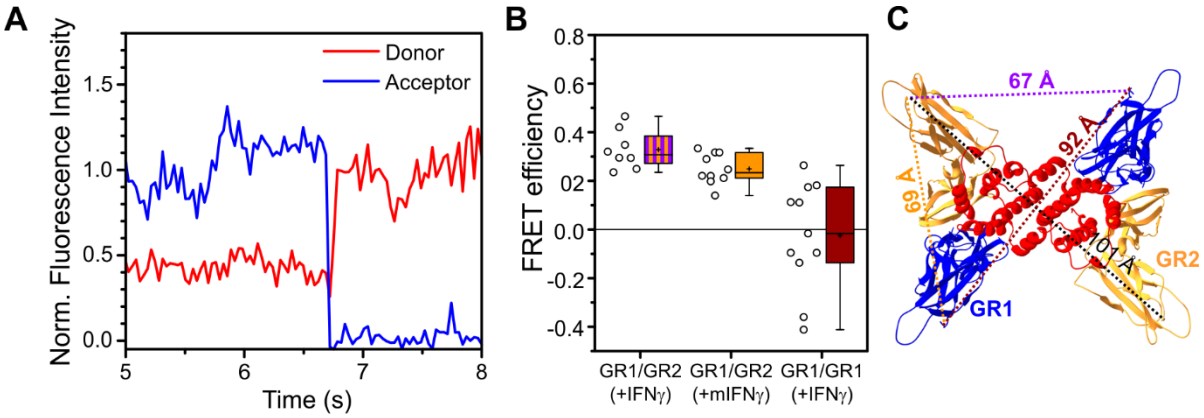

Figure 15: Recovery of intensity after acceptor bleaching shows short distance of hetero-dimeric IFNGR subunits. **(A)** Normalized fluorescence intensity of a representative Donor and Acceptor pair plotted over time. **(B)** FRET efficiencies for heterodimers (orange and magenta) or IFNGR1 homodimers (dark red). Each data point represents a single Rho11/AT643 FRET pair. **(C)** Vertical view on the structural model of the extracellular IFNGR complex. Distances between N-terminus of different subunits are marked by dotted lines.

4.1.2.3 Mobility and diffusion properties of IFNGR

Beside receptor co-tracking additional valuable information about receptor mobility could be drawn from single receptor subunit trajectories. This allowed us to examine the effect of receptor oligomerization on its mobility. To this end, single-molecule trajectories from previous data of IFNγ receptor hetero and homo-dimerization were subjected to mean square displacement (MSD) and step size distribution analysis (**Figure 16**). Receptor subunits dwelling on a narrow area (80 nm radius) for at least one second (30 frames) were classified as immobile receptor subunits. In absence of ligand, most of the receptors (~95%) were mobile (**Figure 16** D). A linear mean square displacement (MSD) with increasing lag time was observed, which yielded similar diffusion constants for both receptor subunits (**Figure 16** A, C). A substantial decrease of the diffusion constant by ~50% was observed upon addition of IFNγ, which was most pronounced when restricting the analysis to receptor dimers. In comparison, only a slight reduction of diffusion constant could be observed for both receptor subunits including dimers upon stimulation with mIFNγ (**Figure 16** B, C). Furthermore, the fraction of immobile particles significantly increased in presence of IFNγ, but not mIFNγ (**Figure 16** D). This effect was particularly stronger for IFNGR1 compared to IFNGR2, which was in line with a higher fraction of IFNGR1 being in a complex as observed with our co-tracking analysis. Taken together, a stringent correlation of diffusion properties with the stoichiometry of receptor subunits was found by our analysis, supporting a

simple model of ligand-induced tetramerization and heterodimerization by IFNγ and mIFNγ, respectively.

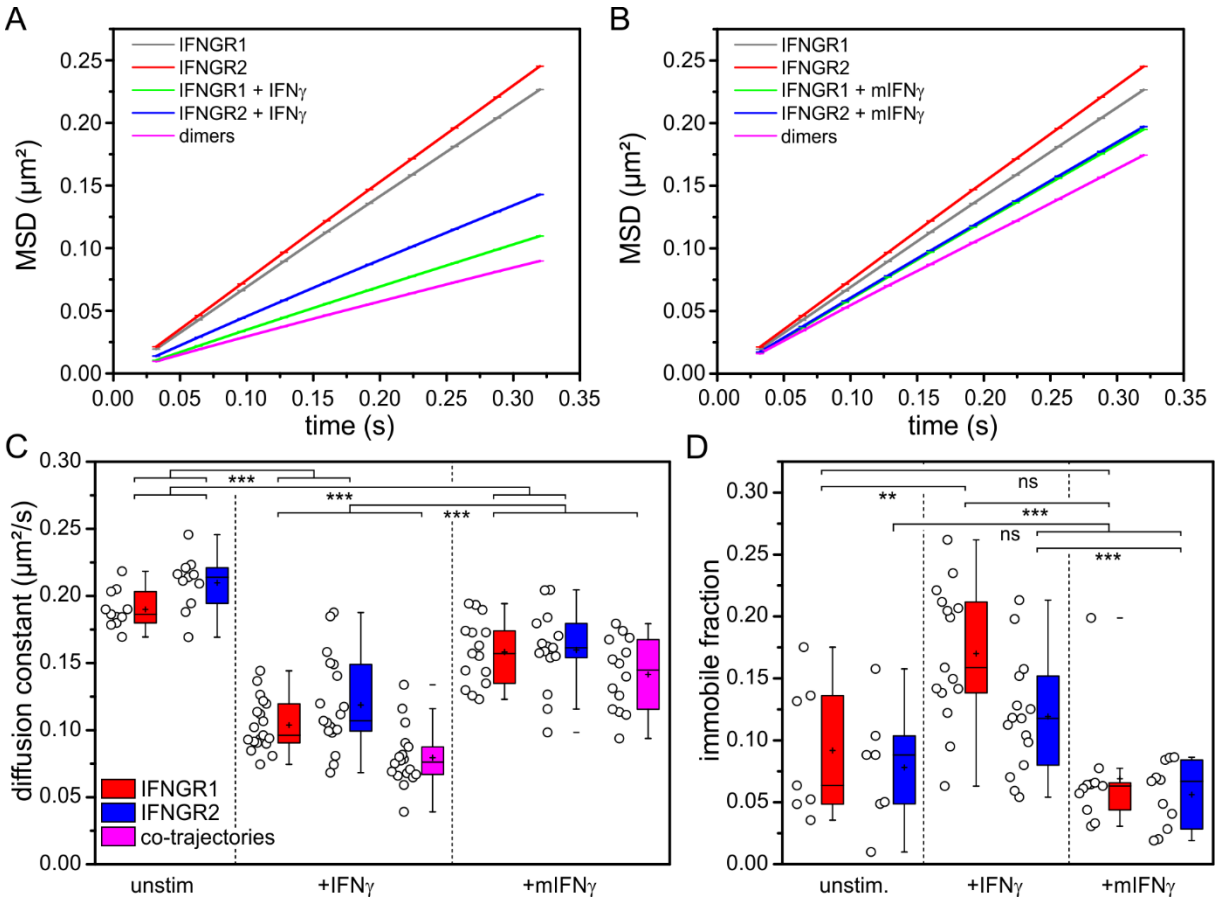

Figure 16: Diffusion properties of IFNGR subunits. (A) Mean square displacement (MSD) curves of IFNGR1 and IFNGR2 in absence and presence of IFNγ. Trajectories are pooled from a single representative cell. Dimers are co-trajectories of both subunits. Error bars represent CI95%. **(B)** MSD curves of IFNGR1 and IFNGR2 as shown in (A) but stimulated with mIFNγ. **(C)** Diffusion constants of single IFNGR subunits and receptor dimers in absence and presence of IFNγ or mIFNγ. Each data point represents averaged Diffusion constants of the respective subunit in a single cell. **(D)** Fraction of receptor subunits classified as immobile in absence and presence of IFNγ or mIFNγ. Each data point represents a single cell. Statistical analysis was done in an unpaired students t-test: ns, non-significant; *, $P \leq 0.05$; **, $P \leq 0.01$; ***, $P \leq 0.001$.

4.1.2.4 Stoichiometry and model of IFNGR complex assembly

We wanted to understand the stoichiometry and arrangement of IFNGR complexes on living cells. To this extend, we combined homo- and hetero-dimerization in a 4-color SMFM experiment (**Figure 17**). By using a quadruple beam splitter in the emission path, we could simultaneously image IFNGR subunits labeled with up to four different dyes. HeLa cells expressing mXFPm-IFNGR1 and mXFPe-IFNGR2 were incubated with 5 nM of each MI-ATTO488, MI-Rho11, EN-ATTO643 and EN-DY752 and subsequently imaged as previously described. We observed homo- and hetero-dimerization between all IFNGR subunits, which was in line with our previous results (**Figure 17** B, D). Additionally, rarely co-tracking of up to three receptor subunits (two IFNGR1 and a single IFNGR2) could be observed (**Figure 17** E). However, co-tracking of two IFNGR2 and a single IFNGR1 could not be observed, which is in line with the low levels of IFNGR2 homo-

dimerization and the high endogenous expression level of IFNGR1. In accordance with previous results, mIFNγ did induce hetero-dimerization but no homo-dimerization (**Figure 17** B). Likewise, co-tracking of three different receptor subunits could not be observed after stimulation with mIFNγ. We could rule out that the observed co-tracking of three IFNGR subunits was caused by co-tracking of different IFNGR complexes by performing dual-color SMFM experiments on un-transfected cells simultaneously incubated with IFNγ-Rho11 and IFNγ-Dy647 (**Figure 17** A). As each chain of the IFNγ homodimer was labeled with a dye, we co-incubated IFNγ-Rho11 and IFNγ-Dy647 for 30 min before adding it to the cells to allow potential mixing of differently labeled IFNγ chains in one homodimer, which would result in false positive receptor complex co-tracking. As expected, in neither experiment IFNγ-Rho11 and IFNγ-Dy647 did show co-tracking, indicating that individual IFNGR complexes do not oligomerize. Hence, the observed correlated diffusion of several IFNGR subunits must represent the stoichiometry of individual receptor complexes.

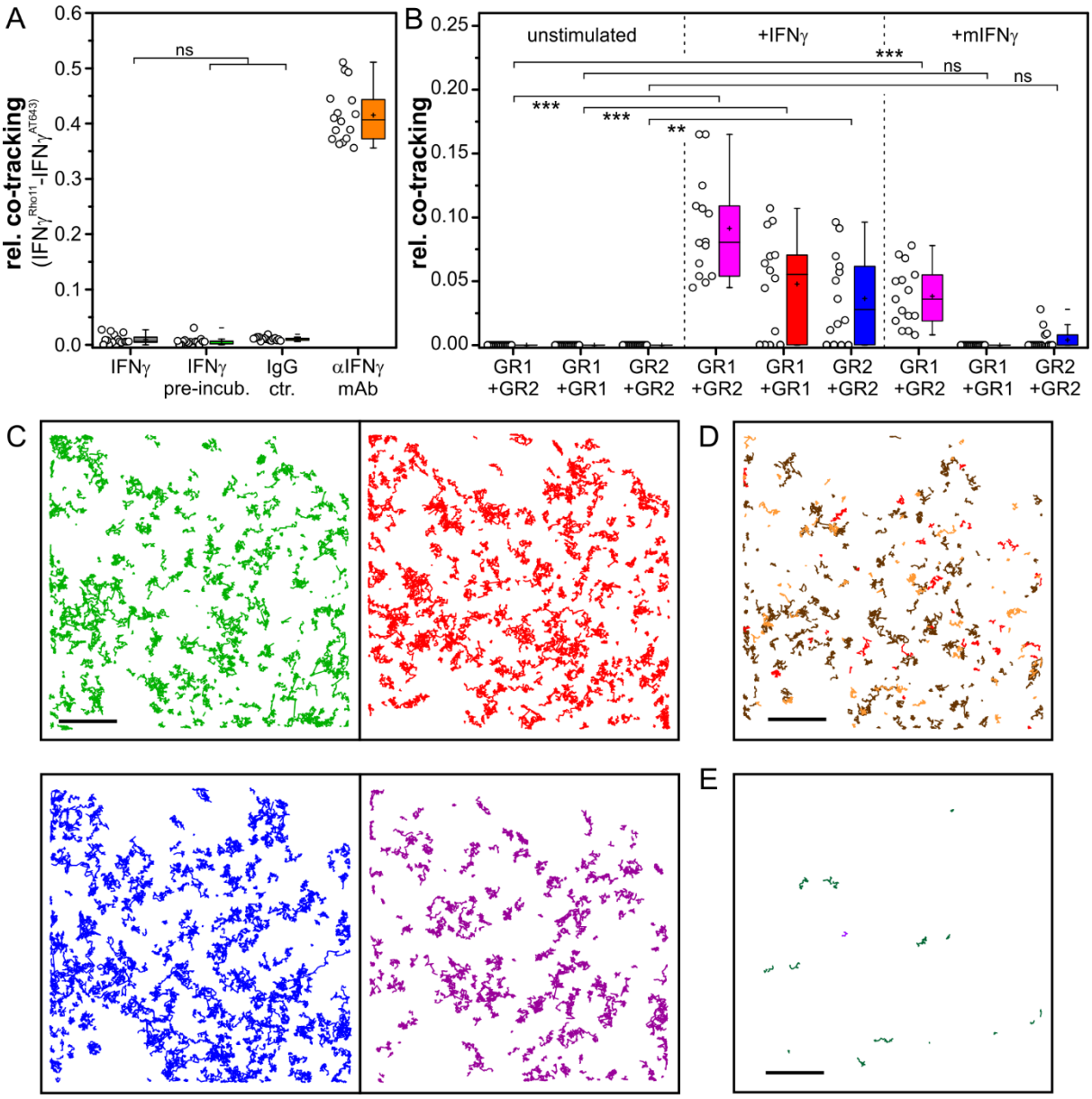

Figure 17: 4-color single molecule localization and tracking analysis of the IFNGR complex. (A) Co-tracking analysis of IFNγ-Rho11 and IFNγ-AT643 in otherwise untreated HeLa cells. Controls: Both IFNγ variants were pre-incubated on ice for 30 minutes (IFNγ pre-incub.), IgG control that does not bind IFNγ (IgG ctr.) and an anti-IFNγ monoclonal antibody (αIFNγ mAb) were added in addition to IFNγ-Rho11 and IFNγ-AT643. **(B)** Co-tracking analysis of IFNGR subunits labeled with 4 colors. Each receptor subunit was labeled with equal concentrations of two differently labeled NB. Hetero-dimerization of IFNGR1-IFNGR2 (GR1-GR2), homo-dimerization of IFNGR1 (GR1-GR1) and homo-dimerization of IFNGR2 (GR2-GR2). Statistical analysis: unpaired students t-test: ns, non-significant; *, $P \leq 0.05$; **, $P \leq 0.01$; ***, $P \leq 0.001$. **(C)** Single channel trajectories of IFNGR1 (green, red) and IFNGR2 (blue, magenta). **(D)** All co-trajectories from two channels combinations. Each color represents another channel combination. **(E)** Three color co-trajectories. Scale bar 5 µm.

Based on these observations we defined our model for IFNGR complex assembly (**Figure 18**): Binding of IFNγ to a single IFNGR1 subunit on the surface of a target cell initiates complex assembly (1). In the next step either another IFNGR1 (2a) is recruited to the IFNGR1:IFNγ complex, which is followed by binding of IFNGR2 (3a), or an IFNGR2 subunits (2b) is recruited to the IFNGR1:IFNg complex followed by a second IFNGR1 subunit (3b). Which of both steps occurs first most likely depends on the expression level of IFNGR2 on the surface of the target cell.

In the last step the second IFNGR2 binds to the intermediate IFNGR complex (4) and thereby completes the hexameric (2:2:2) structure. Specifically, this last step is governed by the expression level of the IFNGR subunits and the binding affinity of IFNGR2 to the ligand, so that eventually only a minor fraction of the complex reaches the hexameric structure.

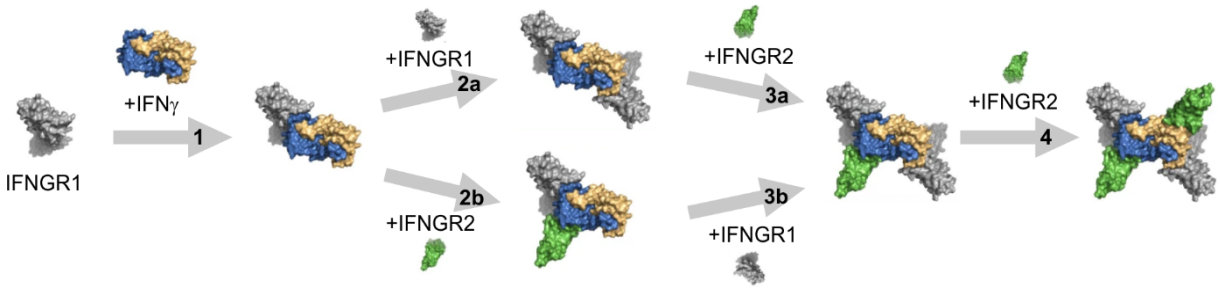

Figure 18: Model of IFNGR complex assembly.

4.1.3 Pleiotropy of IFNGR signaling

The type II interferon IFNγ is a potent immunomodulatory cytokine with many pleiotropic effects on the innate and adaptive immune systems due to the broad expression of its receptors on immune cells. IFNγ exhibits an array of immunostimulatory, immunosuppressive, anti-proliferative and antiviral activities that are vital to normal immune homeostasis and has a key role in tumor surveillance. Among the most important actions of IFNγ are activating macrophages and dendritic cells and inducing upregulation of MHC molecules to enhance presentation of bacterial, viral and tumor antigens. However, despite its central role in many important functions related to disease, IFNγ has not achieved therapeutic utility owing to its pleiotropy and counterbalancing immunostimulatory and immunomodulatory activities.

Intervening in type II interferon signaling to efficiently manipulate signaling responses in a cellular context demands knowledge about how pleiotropic cellular effects are encoded in the IFNGR signaling pathway. To address this question properly, understanding of the precise molecular mechanism underlying IFNGR complex assembly was required. A structure of IFNγ in complex with IFNGR1 revealed the mode of binding of the high-affinity receptor subunit. However, the structure of the complete extracellular hexameric (2:2:2 IFNγ–IFNGR1–IFNGR2) signaling complex has not been solved, principally because of the extremely low affinity of the IFNGR2 subunit within the complex. Determination of the structure of the complete IFNGR complex would not only be essential for understanding of signal activation and complex assembly, but also provide a blueprint for cytokine engineering to access the full therapeutic potential of IFNγ in cancer and immune diseases.

4.1.3.1 Crystal structure of complete IFNγ receptor complex

The data presented in chapter 4.1.2 has clearly shown that under physiological experimental conditions IFNγ receptor complex formation takes place only after binding of its specific ligand IFNγ. Additionally, using a yeast surface display approach of IFNGR1, it could be shown that IFNGR2 only binds to the preformed IFNGR1-IFNγ complex, but not IFNγ alone [78]. These findings implied that a composite binding surface is formed between IFNGR1 and IFNγ, which subsequently recruits IFNGR2. We sought to use this readout of cooperativity to engineer and select for a stabilized interaction with IFNGR2, which should eventually yield an IFNGR complex sufficiently stable to generate protein crystals. To this end, we combined non-biased error-prone PCR with gene shuffling to select for IFNGR1 variants with improved affinity (**Figure 19** A). After a single round of selection, the highest-affinity IFNGR1 variant was IFNGR1-F05 (**Figure 19** B), which contains six mutations (T149I, M161K, Q167K, K174N, Q182R and H205N). The two most common mutations (M161K and Q167K) among the selected clones were located in the D2 FNIII domain of IFNGR1 (**Figure 19** C) in an area commonly observed forming receptor–receptor, or 'stem' contacts in other dimeric cytokine–receptor complexes [189]. We co-expressed mXFPm-IFNGR1-F05 and mXFPe-IFNGR2 in HeLa cells and performed dual-color co-tracking analysis as previously described. In line with enhanced binding kinetics, IFNGR1-F05 did show an increased hetero-dimerization level compared to wild-type IFNGR1 when stimulated with mIFNγ (**Figure 19** D), showing that IFNGR1-F05 does increase IFNGR complex stability. However, this effect could not be observed after stimulation with the dimeric IFNγ.

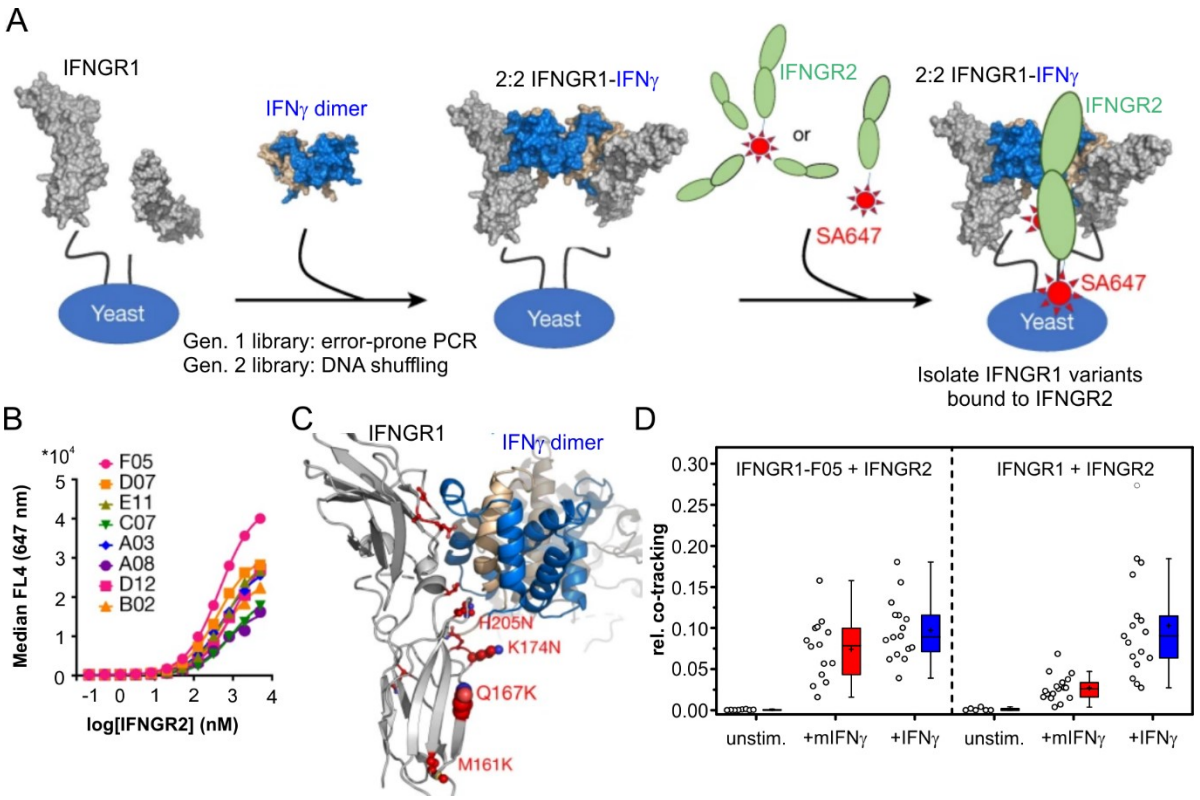

Figure 19: Engineering of a high affinity variant of IFNGR1. (A) Experimental design for engineering higher-affinity IFNGR1 variants. IFNGR1 (grey) is displayed on yeast and, in the presence of unlabeled IFNγ dimer (blue and tan), forms the intermediate 2:2 IFNγ–IFNGR1 complex (middle), enabling detection of variants binding to either tetrameric or monomeric IFNGR2 (green; labeled with streptavidin–Alexa Fluor 647 (SA647)). Using this platform, a first-generation library was generated using non-biased error-prone PCR followed by DNA shuffling. **(B)** After a single round of selection, eight clones were titrated to estimate their relative binding to IFNGR2. **(C)** Sites of mutation on IFNGR1-F05. **(D)** Co-tracking analysis of IFNGR1-F05 and IFNGR2 in presence of wild type or monomeric IFNγ. Each data point represents a single cell.

Using the soluble, affinity-improved IFNGR1-F05 we could obtain crystals of the complete extracellular IFNGR complex and determine the structure (Protein Data Bank (PDB): 6E3K, 6E3L) [78] by molecular replacement using previously determined structures of the 2:2 IFNγ-IFNGR1 intermediate complex (PDB: 1FG9) [221] and IFNGR2 (PDB: 5EH1) [222]. The hexameric (2:2:2) IFNγ receptor complex is star-shaped with a two-fold symmetry imposed by the IFNγ homodimer (**Figure 20** A). The structure reveals six total interaction sites: two site 1 interfaces shared between IFNγ and IFNGR1, two site 2 interfaces shared between IFNγ and IFNGR2, and two site 3 interfaces shared between IFNGR1 and IFNGR2. IFNGR2 binds to the composite interface formed by the high affinity IFNγ-IFNGR1 interaction, which enables IFNGR2 to contact the open face of IFNγ site 2, as well as make extensive stem contacts with IFNGR1 site 3 (**Figure 20** A, top left). Each of the two site 2 interfaces of IFNγ presents a concave surface that buries a total area of 1,243 Å² formed by helices A, D and E, and the N terminus of the cytokine (**Figure 20** A). In contrast to the site 1 interfaces, in which both chains of IFNγ form the IFNGR1 binding interfaces, only one IFNγ chain is needed to form each IFNGR2 binding site in the site 2 interface. IFNGR2 binds to IFNγ principally through a cluster of aromatic residues in loop 3 (F67, Y69 and F75) and through F109

in loop 4 of IFNGR2, which insert into a small pocket formed by helices A and D of IFNγ. The site 3 stem interfaces (1,469 Å² of total buried surface area) consist of primarily flat surfaces between IFNGR1 and IFNGR2 that interact through extensive van der Waals interactions. Both critical mutations, that were commonly found among the high affinity variants of IFNGR1, M161K and Q167K, are located at the site 3 interfaces. IFNGR1(M161K) shares a hydrogen bond with T149 of IFNGR2, and IFNGR1(Q167K) forms a salt bridge with D164 of IFNGR2; both interactions are likely to contribute to the stabilization of the site 3 interfaces. Although the IFNγ signaling complex is 'doubled' into a 2:2:2 hexamer (compared to typical 1:1:1 trimeric cytokine-receptor complexes [189]) because of the homo-dimeric nature of the ligand, each 1:1:1 half of the hexamer shares structural similarities with the type III IFN trimeric (1:1:1) IFNλ receptor complex (PDB: 5T5W) (**Figure 20** B), including the relative binding modes of the high (IFNLR1) and low (IL-10R2) affinity receptors binding to one end of the helical bundle of the respective cytokines [189]. Also, the IFNGR structure topologically resembles the hexameric (2:2:2) structure of the IL-10 receptor complex [57], which also contains IL-10R2. By contrast, the IFNγ complex uses a structural paradigm that is distinct from the trimeric (1:1:1) type I IFN complex in both the relative geometries of the ligand–receptor complexes and the mode of binding to each receptor (**Figure 20** C).

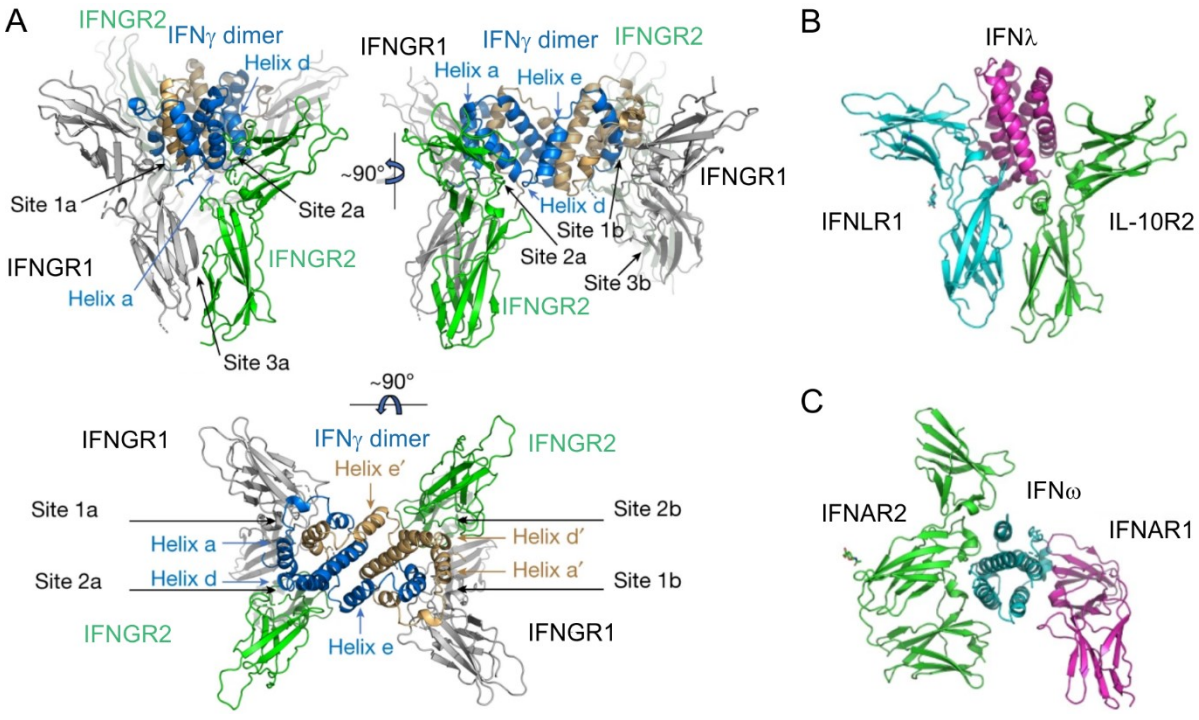

Figure 20: Structure of complete hexameric IFNGR complex. (A) The structure of the IFNγ hexameric complex reveals the mechanism of IFNGR2 (green) recognition of IFNγ (blue and tan) and IFNGR1 (grey). IFNGR2 receptors make extensive contacts with the IFNγ dimer at sites 2a and 2b, and site 3a and 3b makes stem–stem contacts with IFNGR1. **(B)** Structure of the IFNλ–IFNLR1–IL-10R2 signaling complex (PDB: 5T5W) [189] shares a similar geometry with the IFNγ signaling complex. The binding mode of IFNGR2 is nearly identical to that of IL-10R2. **(C)** Structure of a type I IFN receptor complex (PDB: 3SE4) [69] with distinct ligand–receptor geometries compared to either type II or III IFNs.

4.1.3.2 Structure-guided design of partial agonists

We aimed to understand how complex stoichiometry of IFNGR influences signal activation and downstream signaling. Therefore, we used the structural information gained from the site II binding interface to design a mutant that retained binding to IFNGR1 but abrogated binding to IFNGR2. Based on our structure, we rationally designed the IFNγ (K74A, E75Y, N83R) triple mutant and confirmed loss of measurable binding to IFNGR2 by surface plasmon resonance (SPR) analysis (**Figure 21** C). Additionally, binding of site I interface could be disrupted by a known point mutation in IFNγ (H111D) (**Figure 21** A) [205, 223]. Finally, connecting of the C-terminus of the first IFNγ chain with the N-terminus of the second chain enabled us to engineer asymmetric single chain mutants with different combinations of the previously mentioned mutants.

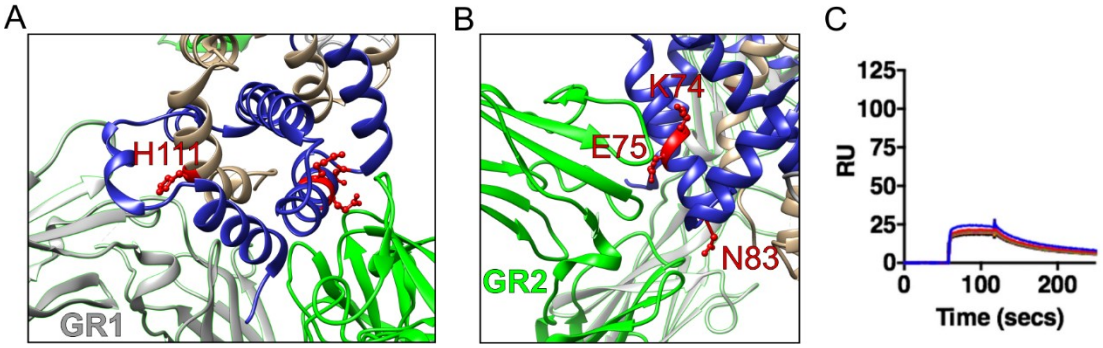

Figure 21: Site-specific mutations of IFNγ disrupt IFNGR binding. IFNGR1 (grey), IFNGR2 (green), IFNγ (blue and tan). **A)** IFNγ (H111D) disrupts IFNGR1 binding at site I [205]. **B)** IFNγ (K74A, E75Y, N83R) disrupts IFNGR2 binding at site II. **C)** When complexed with IFNGR1, the IFNγ (K74A, E75Y, N83R) results in the loss of detectable binding to IFNGR2 (up to 100 μM) as determined by SPR. The titration data are from a single experiment.

We created a set of partial agonists that control both the number and location of the receptors in the complex, mimicking each intermediate step of IFNGR complex assembly (**Figure 22** A). To confirm the receptor stoichiometry induced by the partial agonists we performed SMFM dual color hetero- (**Figure 22** B) and homo-dimerization (**Figure 22** D, E) experiments of the IFNGR in presence of 50 nM agonist (as described in 4.1.2.2). IFNγ variant 1, termed GIFN1, which was supposed to bind two IFNGR1 and a single IFNGR2, could induce IFNGR hetero-dimerization and IFNGR1 homo-dimerization comparable to IFNγ, but no IFNGR2 homo-dimerization as expected. Likewise, IFNγ variant 2, termed GIFN2, which could only bind a single copy of each receptor subunit, failed to induce any receptor homo-dimerization, but retained the ability to induce IFNGR hetero-dimerization, even though at a much lower extend that IFNγ. Lastly, IFNγ variant 3, termed GIFN3, which should only bind two IFNGR1 and no copies of IFNGR2, did induce IFNGR1 homo-dimerization comparable to IFNγ, but did not induce any IFNGR hetero-dimerization or IFNGR2 homo-dimerization. With these partial agonists in hand, we could measure the phosphorylated STAT1 (pSTAT1) in stimulated cells as a direct indicator for IFNGR signaling activity (**Figure 22** C). We observed that there was a relationship between the number and location of receptors bound

and the maximal pSTAT1 signal, Emax. The 2:2 IFNγ–IFNGR1 complex (using GIFN3) exhibits a 25% pSTAT1 Emax, whereas addition of only 1 copy of IFNGR2, to create a 2:2:1 IFNγ–IFNGR1–IFNGR2 intermediate complex (using GIFN1), results in 100% pSTAT1 Emax compared to the complete hexameric complex. The second copy of IFNGR2 therefore appears to be functionally redundant; this also demonstrates the extreme sensitivity of IFNγ responsive cells to expression levels of IFNGR2 and is in line with the overall low IFNGR2 homo-dimerization levels observed in these experiments. Of note, the 2:1:1 complex (using GIFN2) of IFNγ–IFNGR1–IFNGR2 exhibits a 50% Emax for pSTAT1 and appears to be 'capped' until a third receptor subunit binds (using IFNγ variant GIFN1).

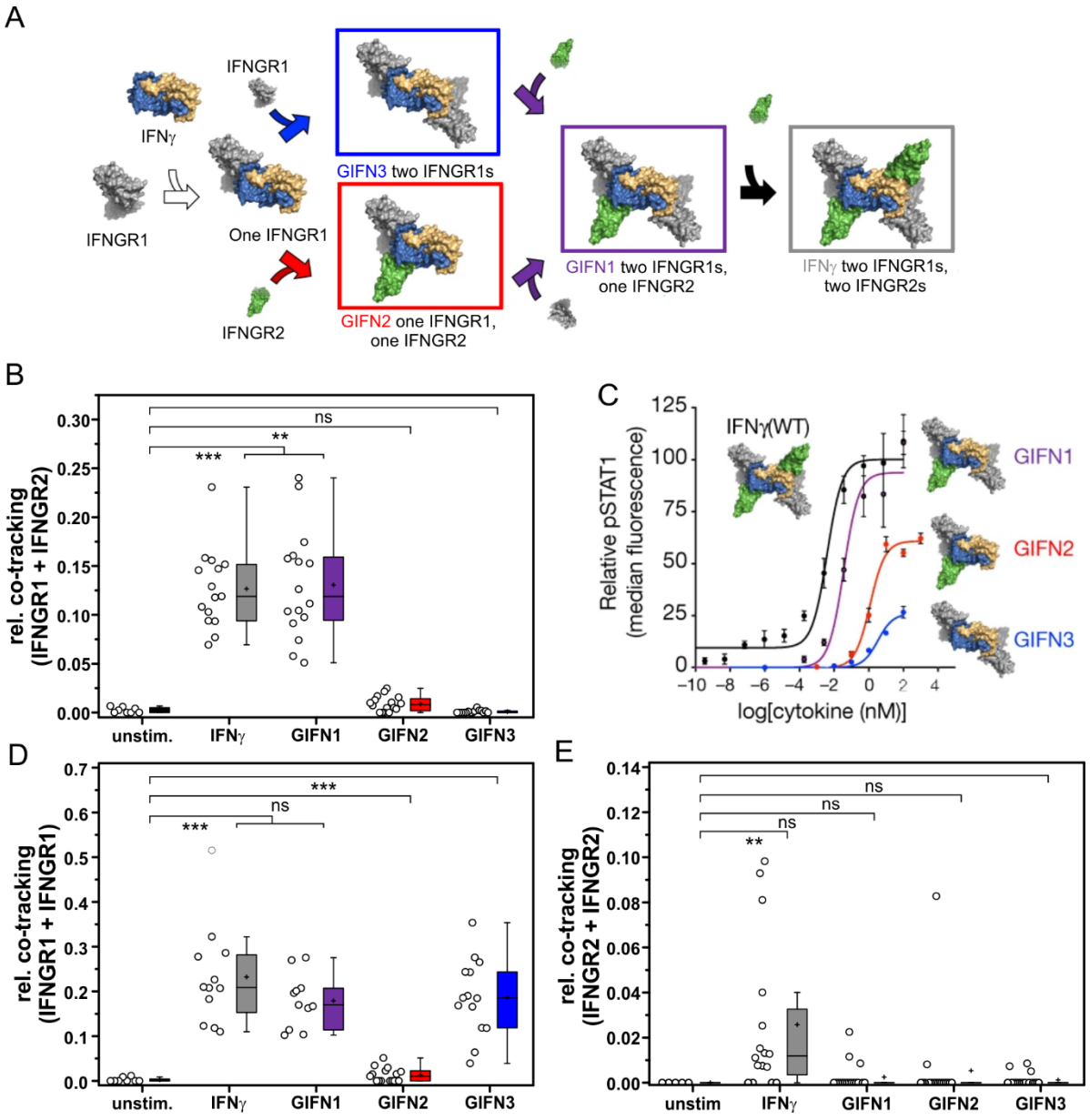

Figure 22: Partial IFNGR agonists were designed to induce receptor complexes with varying receptor number and locations. A) Model of IFNGR complex assembly. Each partial agonist can induce one of the intermediate IFNGR complexes. **B)** Hetero-dimerization of IFNGR1 and IFNGR2 on the surface of HeLa cells before (unstim.) and after incubation with 50 nM of IFNγ or a partial agonist. Dimerization was quantified by co-tracking of fluorescently labeled

IFNGR in a dual color SMFM experiment. Each data point represents an individual cell. **C)** Relative STAT1 phosphorylation was quantified in Hap1 cells stimulated with IFNγ or a partial agonist by flow cytometry. Curves were fitted to a first-order logistic model. Data are mean ± s.e.m.; n = 3 biologically independent experiments. **D)** Homo-dimerization of IFNGR1 after stimulation with IFNγ or a partial agonist quantified as in B). **E)** Homo-dimerization of IFNGR2 after stimulation with IFNγ or a partial agonist quantified as in B).

4.1.3.3 Decoupling of IFNγ induced gene expression

Next, we wanted to know how biased IFNγ signaling by intermediate complexes contributed to cellular responses. Therefore, we performed a next-generation sequencing based gene expression analysis for more than 20,000 genes in A549 cells treated with either wild-type IFNγ or GIFN variants. The previously presented GIFN variants were complemented with GIFN4, a variant that binds both subunits IFNGR1 and IFNGR2 with reduced affinity [78]. As expected, we observed a general trend of the partial agonists inducing lower levels of gene expression in accordance with their pSTAT1 Emax potencies (**Figure 23** A). However, we found that a subset of genes exhibited discordant, biased expression patterns (**Figure 23** B). For example, we identified CD274 among the subset of tunable genes, which is commonly known as programmed death ligand 1 (PD-L1). Its expression was greatly reduced in response to the partial agonists (**Figure 23** B, left), whereas MHC class I (HLA-A) remained highly expressed (**Figure 23** B, right). Additionally, we measured induction of surface expression of MHC class I and PD-L1 in response to IFNγ or GIFN variants by reverse transcription with quantitative PCR (**Figure 23** C) and flow cytometry with fluorescently labeled antibodies (**Figure 23** D). The partial agonists retained nearly wild-type levels of activity in inducing upregulation of MHC class I in A549 cells but induction of PD-L1 expression by the partial agonists was greatly reduced.

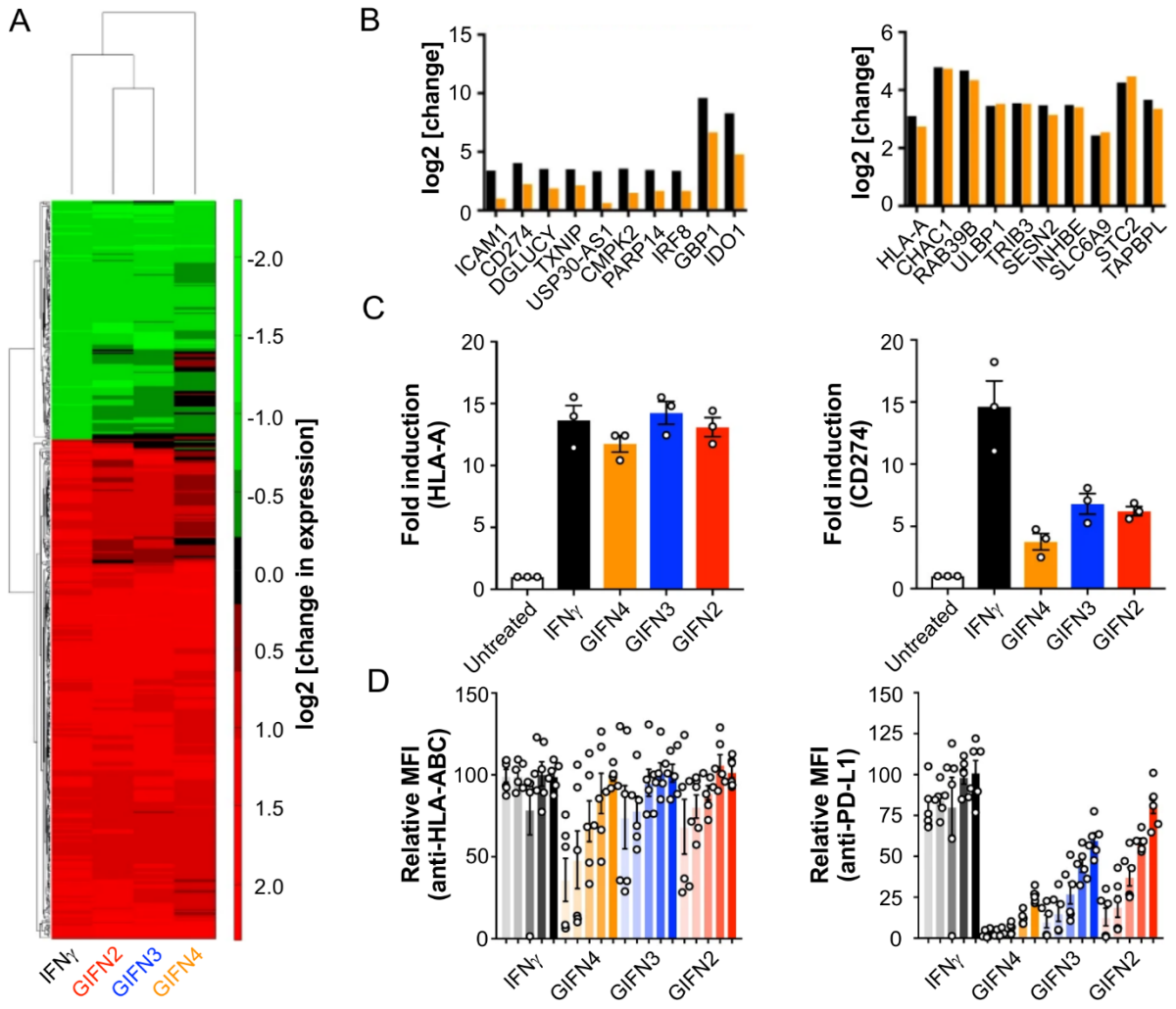

Figure 23: IFNγ variants induced biased gene expression patterns in A549 cells. A) Heat map depicting the relative expression (log_2[change in expression]) of 1,000 genes from the human transcriptome. **B)** Left: Tunable genes showing significantly lowered expression after treatment with GIFN4 (orange) compared to wild-type IFNγ (black). Right: Genes that show comparable expression after either IFNγ (black) or GIFN4 (orange) treatment. **C)** Cells were treated with IFNγ or partial agonists for 48 hours. Upregulation of MHC class I antigen and PD-L1 expression were quantified by reverse transcription with quantitative PCR (RT–qPCR). Ligand concentration, 62.5 nM; mean ± s.e.m., n = 3 biologically independent experiments. **D)** Cells were treated as in C). Upregulation of MHC class I antigen and PD-L1 expression were quantified by flow cytometry using fluorescently labelled HLA-ABC antibody or PD-L1 antibody. MFI, median fluorescence intensity; ligand concentrations 0.1, 0.5, 2.5, 12.5 and 62.5 nM (left to right, respectively, for each agonist); mean ± s.e.m., n = 6 independent experiments.

To ensure, that decoupling of MHC I to PD-L1 expression by partial IFNGR agonists is a general effect and not specific to A549 cells, we screened an additional six cancer cell lines, including Hap1, MeWo, HT-29, Hep G2, HeLa and Panc-1 cell lines. We quantified the ratio of MHC I to PD-L1 expression for cells stimulated with partial agonists relative to wild-type IFNγ and found that partial agonists consistently decouple MHC I to PD-L1 expression to different degrees depending on the cell line (**Figure 24**). This uncoupling of MHC I and PD-L1 expression shows that engineered agonists biased in affinity and complex stoichiometry can uncouple an important pleiotropic activity of IFNγ. In general, different cellular responses to IFNγ may require different thresholds of activation. That could be potentially exploited in the context of immunotherapy, as these IFNγ variants could enhance presentation of tumor antigens by MHC I upregulation without

the concomitant immuno-suppression through checkpoint expression, such as PD-L1, that occurs in response to wild-type IFNγ.

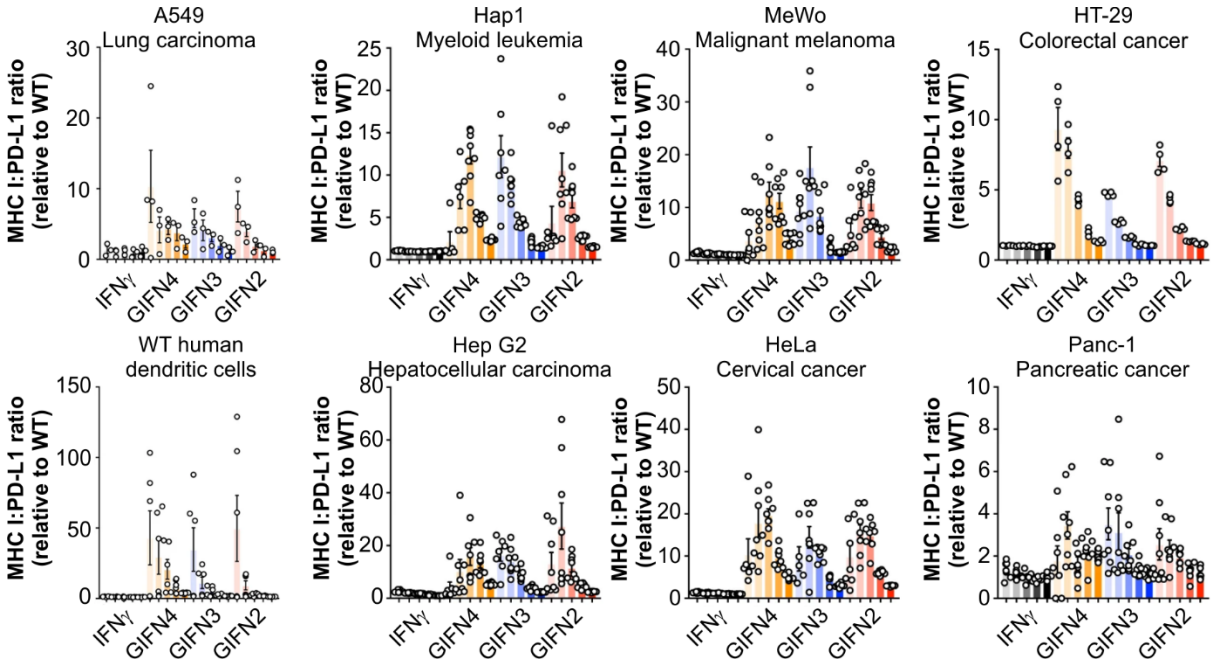

Figure 24: Uncoupling of MHC I:PD-L1 expression in different cancer cell lines by partial IFNGR agonists. Ligand concentrations 0.1, 0.5, 2.5, 12.5 and 62.5 nM from left to right for IFNγ and each partial agonist, respectively. MHC I:PD-L1 ratios were quantified by flow cytometry using fluorescently labeled HLA-ABC and PD-L1 antibodies. Dendritic cells were enriched from human blood.

4.1.4 Pathophysiology of IFNGR signaling

Type II Interferon signaling plays a fundamental role in the mammalian immune system, as it marks the transition point from innate immunity to adaptive immunity. Mendelian Susceptibility to Mycobacterial Diseases (MSMD) is a rare congenital syndrome typically found associated with IFNγ signaling disorders. Patients suffering from MSMD exhibit a predisposition for severe and recurrent infections with weakly pathogenic environmental mycobacteria occasionally accompanied by *Salmonella* non-typhi infections. Most disease-causing genetical defects linked to MSMD do either directly affect IFNγ signaling (*IFNGR1*, *IFNGR2* and *STAT1*) or indirectly, by targeting IL-12 signaling (*IL12RB1* and *IL12B*), which in turn mediates IFNγ secretion in T cells [224].

Among an impressive number of mutations in IFNGR subunits, which in most cases lead to premature stop codons or frame shifts [85], IFNGR2(T168N) probably stands out the most, as it is reported to create a new N-glycosylation site [225]. Lately, this mutation has been hypothesized to partition in lipid and actin nanodomains of the plasma membrane, thereby preventing conformational changes of the IFNGR complex required for activation of Jak1 and hence downstream signaling of IFNGR [197]. In addition to conventional inborn genetic factors autoantibodies against IFNγ have emerged as cause of MSMD in adults recently [226].

Understanding the molecular mechanisms underlying these defects could be an important milestone in the development of IFNGR signaling-related treatments for MSMD.

4.1.4.1 Pathogenic mechanism of the gain of N-glycosylation mutation IFNGR2-T168N

To understand the mechanism evoking type II interferon signaling deficiency in IFNGR2-T168N homozygous patients, it was necessary to investigate the conformation of IFNGR2 within the IFNGR complex. In chapter 4.1.3.1 we presented the structure of IFNGR2 within the type II interferon receptor complex for the first time ever, giving us exclusive insights into the localization and orientation of the T168 residue of IFNGR2. This structure revealed that in the IFNGR complex T168 of IFNGR2 is positioned directly at the stem-stem contact site (binding site 3) of IFNGR1 and IFNGR2 (**Figure 25**). Thus, we hypothesized that the bulky N-linked glycan gained at T168N of IFNGR2 promotes steric clashes at the site 3 interface and consequently prevents recruitment of IFNGR2 into the IFNGR complex.

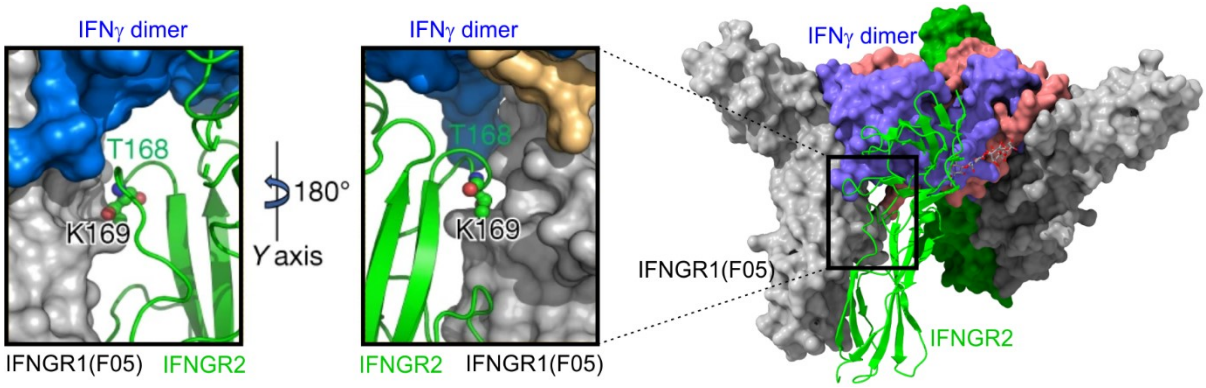

Figure 25: Position of gain of N-glycosylation mutation IFNGR2-T168N within the type II interferon signaling complex. The neogylcosylation site of IFNGR2-T168N is localized at the site3a interface.

To test this hypothesis, we combined two different approaches. Using a recombinantly produced form of the neo-glycan mutant IFNGR2-T168N extracellular domain we could test binding of IFNGR2 to the IFNγ-IFNGR1 intermediate complex *in vitro*. First, we verified that IFNGR2 was glycosylated at the T168N position with almost quantitative occupancy (**Figure 26** A). Using SPR, we measured the affinity of either wild-type IFNGR2 (**Figure 26** B, left) or the neo-glycan mutant IFNGR2-T168N (**Figure 26** B, right) for IFNγ-IFNGR1. We detected a loss of binding between IFNGR2-T168N for IFNγ-IFNGR1. In a second approach, we investigated the ability of IFNGR-T168N to engage IFNGR complexes *in vivo* on the surface of living cells, by performing SMFM as presented previously (chapter 4.1.2.2). In line with our previous results IFNγ induced a significant level of IFNGR1-IFNGR2 heterodimers in cells expressing the wild-type IFNGR2. In contrast, no IFNGR1-IFNGR2 heterodimers could be observed regardless of ligand stimulation in cells expressing the T168N mutant of IFNGR2 (**Figure 26** C). Recent studies have tried to remove the N-glycosylation of IFNGR2-T168N by treatment with purified Peptide:N-Glycosidade (PNGase) F [197]. However, controlled *in vitro* enzymatic reactions on living cells are quite challenging,

especially because we cannot exclusively remove the N-linked glycan at position N168 and more importantly, we cannot predict what would happen to an extra cellular membrane protein lacking essential N-linked glycans. Also, we lacked a clear way to check whether the N-glycosylation at position 168 was eventually removed. Instead, we chose a direct and clean way to eliminate the N-glycosylation at T168N: We disrupted the known N-glycosylation consensus sequence -N-X-T/S- [227] by introducing an alanine at T170 (IFNGR2-T168N-T170A, **Figure 26** D). Strikingly, the T168N-T170A double mutant did restore wild-type levels of IFNGR hetero-dimerization.

All together, these findings support our hypothesis, that the bulky N-linked glycan introduced at the binding interface of IFNGR2 by the T168N mutation simply prevents recruitment of IFNGR2 into the receptor complex and thus downstream signaling of the type II interferon.

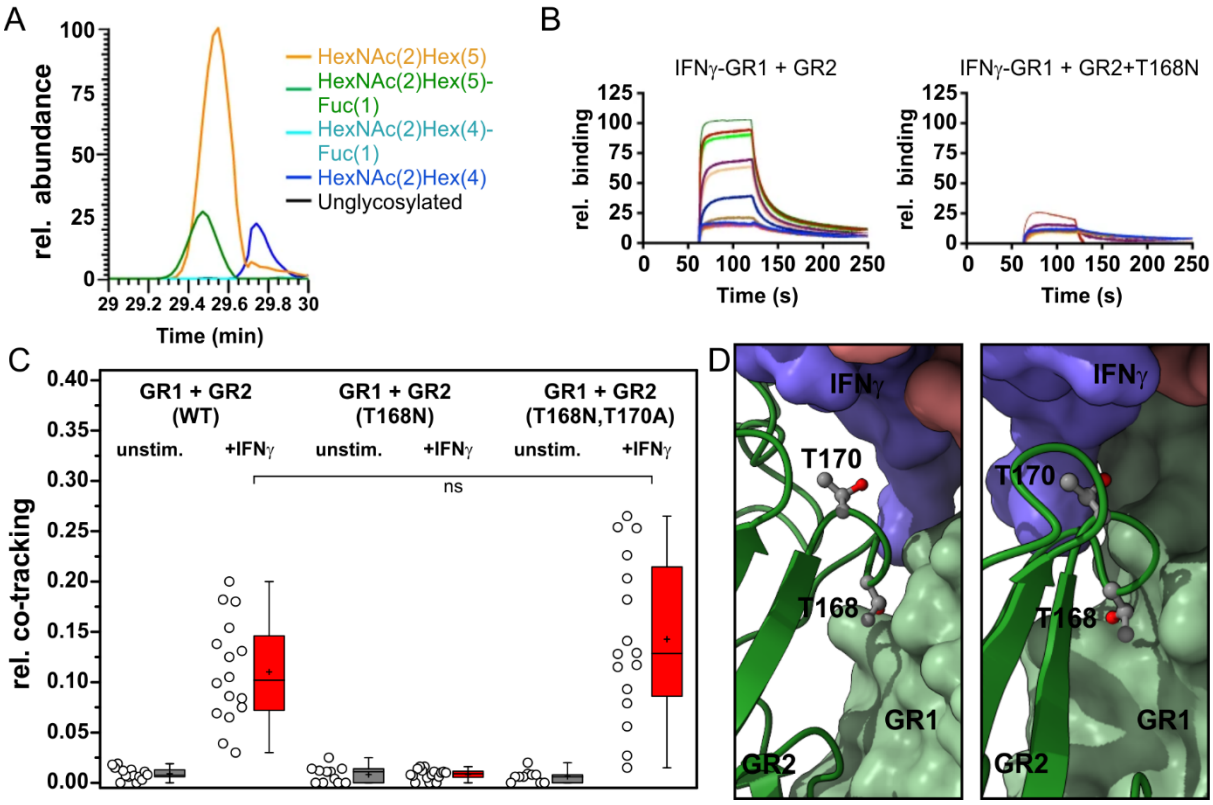

Figure 26: N-glycosylation at T168N of IFNGR2 does disturb IFNGR interaction. (A) IFNGR2-T168N was expressed in HEK293S GnTI-cells and analysed by nano-liquid chromatography followed by tandem mass spectrometry (LC-MS/MS). The peptide containing N168 was identified and relative amounts of various glycoforms were determined by extracted ion chromatograms. The data shown are from a single experiment. **(B)** SPR analysis was used to determin the affinity of IFNGR2 to the 2:2 IFNγ-IFNGR1 intermediate complex (K_D ~5 µM, left), whereas IFNGR2-T168N results in a loss of binding (right). The titration data are from a single experiment. **(C)** Single molecule co-tracking analysis of IFNGR1 and IFNGR2. Wild type IFNGR2 was compared to T168N and T168N/T170A double mutant after ligand stimulation. Each data point represents a single cell. Statistical analysis: unpaired students t-test: ns, non-significant. **(D)** 3D structure of IFNGR1:IFNGR2 interface showing position T170. Blue and Red; IFNγ; Gray, IFNGR1; Green, IFNGR2.

4.1.4.2 Pathogenic mechanism of anti-IFNγ autoantibodies

Since 2004 more than 500 adult patients have been diagnosed with an autoimmune disease linked to anti-IFNγ autoantibodies (AIGA), almost all of which originated in Southeast Asia [226]. This high prevalence of AIGAs in patients from Southeast Asia, particularly Thailand and Taiwan, is

strictly associated with specific human leukocyte antigen class II haplotypes and is regarded as a genetic predisposition [228]. The late onset of immunodeficiency evoked by AIGAs expands the spectrum of MSMD promoted by inborn errors of immunity in the IFNγ/IL-12 axis [85]. Like patients with MSMD, AIGAs-related diseases also develop infections with *Mycobacterium tuberculosis* and non-typhoidal salmonella [226, 229]. Despite their apparent connection to type II interferon signaling, the molecular mechanism of AIGAs is not well-characterized. In fact, recent studies on AIGA plasma levels in patients have revealed a lack of correlation between antibody titer and severity of disease [230], challenging immune complexes to be the mode of action as anticipated previously.

To understand the molecular mechanism of AIGAs we isolated and characterized 19 monoclonal Antibodies (mAb) targeting IFNγ from AIGA-secreting peripheral memory B cells of patients showing disseminated mycobacterial infections. We performed Bio-layer interferometry (BLI) to assess the binding affinity and epitopes of the isolated mAbs. All tested mAbs had a high binding affinity to IFNγ with a K_D in nanomolar range (**Figure 27** A). In addition, we subjected the isolated mAbs to an epitope binning experiment based on in-tandem BLI cross-competition (**Figure 27** B). For this purpose, biotinylated IFNγ was captured on a streptavidin biosensor and different mAbs were added successively. Thereby we found three non-overlapping binding epitopes, that were recognized by the isolated mAbs, and classified the mAbs accordingly (**Figure 27** C). Lastly, we investigated the neutralizing capabilities of the isolated mAbs in HeLa cells transfected with a gamma-interferon activation site (GAS) luciferase reporter plasmid. Surprisingly, there were neutralizing and non-neutralizing mAbs in both groups, site II, and site III, whereas the single site I mAb E1 did neutralize IFNγ signaling (**Figure 27** D). These finding indicated that the neutralizing effect of AIGAs is not a generic mAb feature and it cannot be solely attributed to the epitope which they recognize. We proceeded to explore the mechanism of neutralization that individual AIGAs exert on IFNγ signaling.

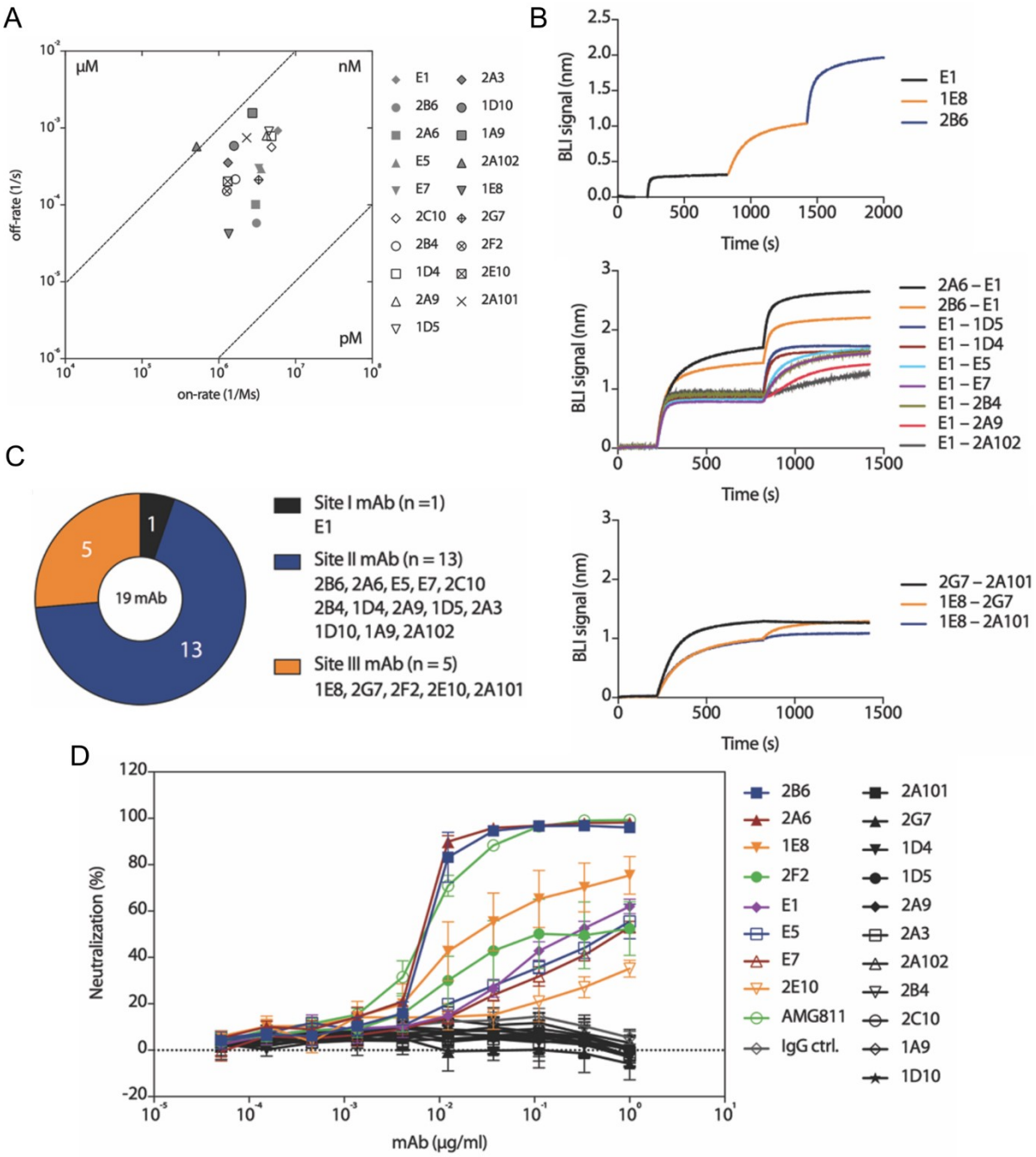

Figure 27: Binding characteristics of anti-IFNγ autoantibodies (AIGA) extracted from patients. (A) Scatter chart of equilibrium dissociation constant (K_D) values, corresponding to the binding affinity. KD values were determined from the association (K_a) and dissociation (K_d) rates of the mAbs ($K_D = K_a/K_d$). **(B)** Kinetic values of monoclonal AIGAs were determined by Bio-Layer inferometry (BLI). Representative graphs showing the in-tandem cross-competition assay for the mAbs and categorizing their binding groups. **(C)** Pie chart showing the three groups of AIGAs (Site I, n = 1; II, n = 13 and III, n = 5). **(D)** In vitro neutralization by monoclonal AIGAs (n = 19) in HeLa GAS reporter cells treated with IFNγ in addition to a serial three-fold dilutions of mAb, beginning at 1 μg/ml. Percentage of neutralization was estimated based on Luciferase activity. Means ± SD of replicate assays are shown (n = 3 – 6 per mAb).

A simple yet effective way to inhibit IFNγ signaling might be accomplished by AIGAs through sterically preventing IFNγ-IFNGR1 binding by epitope recognition. This would result in a competition of mAbs and IFNGR1 for IFNγ. We tested this hypothesis by performing an enzyme-linked immunosorbent assay (ELISA), in which the high-affinity subunit IFNGR1 was immobilized

on plates, and the reactivity of biotin-IFNγ was measured in the presence of AIGAs (**Figure 28** A). Biotin-IFNγ and AIGAs were pre-incubated before performing ELISA to assist potential competition effects. Biotin-IFNγ binding was detected on the plates with increasing amounts of control IgG (**Figure 28** A). Among all AIGAs tested, E1 (the only site I mAb) was the only one that decreased biotin-IFN-γ reactivity in a dose-dependent manner (**Figure 28** A). By contrast, AIGAs targeting sites II and III did not interfere in any clear way with biotin-IFNγ reactivity (**Figure 28** A). The neutralizing mAbs of these groups disrupted cytokine-receptor interaction incompletely, as they only partially inhibited reactivity at a concentration of 100 nM (molar ratio of 1:10). Next, we checked if AIGAs could positively crosslink IFNγ to immune complexes through homotypic bivalent binding. We investigated the contributions of affinity and epitope recognition to immune complex constitution, by performing size-exclusion high-performance liquid chromatography (SEC-HPLC) on equimolar mixtures of mAbs and IFNγ. mAbs from the site I or III groups bound to IFNγ at comparably low levels, resulting in very few immune complexes (**Figure 28** B). Only 2G7 was able to generate larger amounts of immune complex with IFNγ, probably due to a difference in configuration on site III of IFNγ (**Figure 27** B and **Figure 28** B). By contrast, monoclonal AIGAs from site II tended to generate larger amounts of immune complex, even at lower binding affinities, such as 2A102 (KD > 10-10 M) (**Figure 28** B). In particular, 2A6 and 2B6 mAbs generated higher molecular weight immune complexes (over 1000 kDa) with IFNγ (**Figure 28** B). Our data suggest that epitope recognition at site II of IFNγ leads to generation of immune complexes that precedes AIGA–IFNγ binding affinity. However, several non-neutralizing AIGAs (2G7, 2A102 and 1D4) generated immune complexes, suggesting that immune complex formation is not the main driver of neutralization (**Figure 28** B). In addition, binding of neutralizing as well as non-neutralizing mAbs to IFNγ did not prevent initialization of IFNGR complex assembly by binding to the high affinity receptor subunit IFNGR1. This implies that the neutralization mechanism of AIGAs might involve impairing of IFNGR complex assembly.

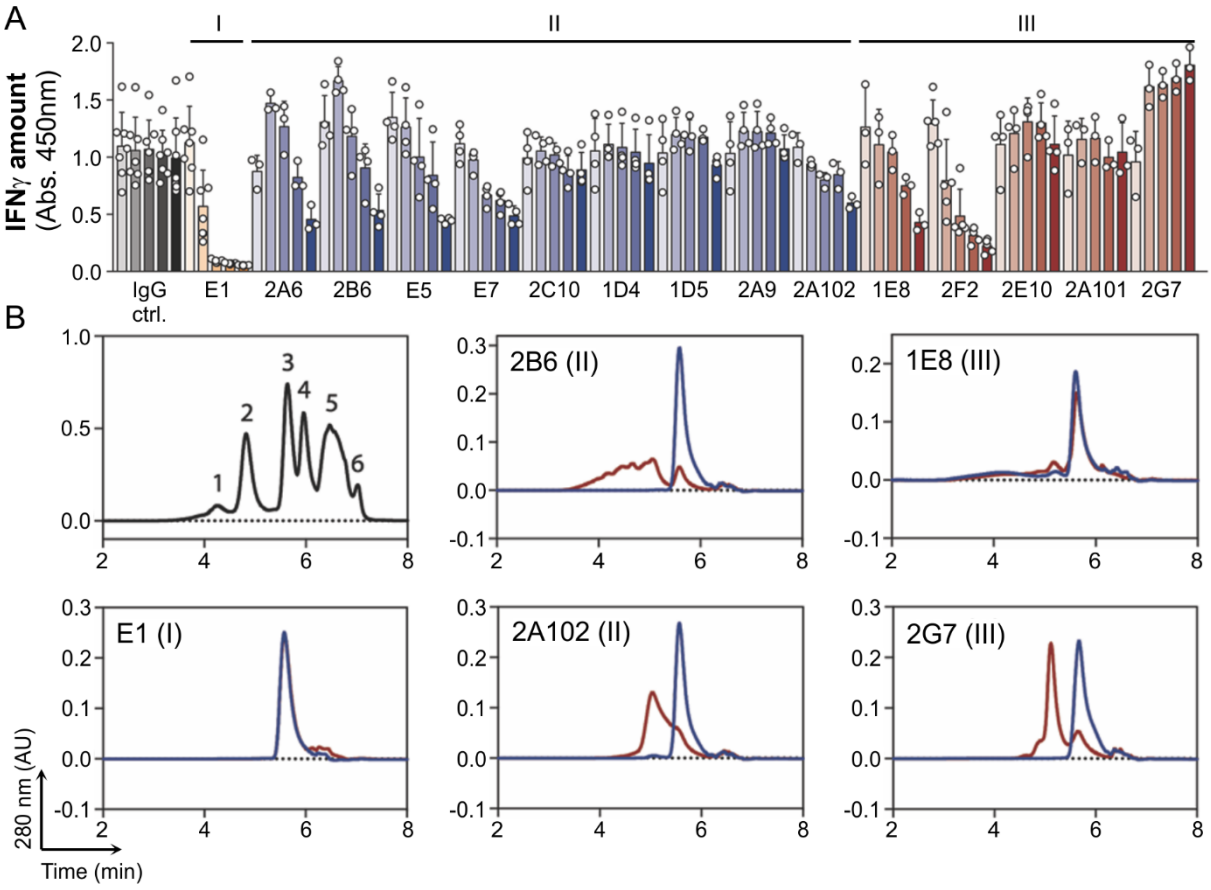

Figure 28: Competition of AIGAs with IFNγ:IFNGR1 interaction. (A) ELISA of 10 nM biotin-IFNg and immobilized IFNGR1 in the presence of mAbs (0, 5, 10, 20 and 100 nM, left to right). Yellow: site I mAb, blue: site II mAbs, red: site III mAbs. Means ±SD of replicate assays are shown (n = 3 – 7 per mAb). Bar graph shows the signal for biotin-IFNγ binding to IFNGR1 after addition of pre-incubated biotin-IFNγ-mAb mixture. **(B)** Size-exclusion chromatography profiles of samples containing a single antibody with (red) or without (blue) IFNγ. Control top-left: 1) Thyroglobulin Dimer 1,320 kDa, 2) Thyroglobulin 660 kDa, 3) IgG 150 kDa, 4) BSA 66.4 kDa, 5) Myoglobin 16.7 kDa, 6) Uracil 0.112 kDa. Only mAbs are shown that were chosen for the following experiments: the single site I mAbs and one neutralizing and one non-neutralizing from site II and site III group.

In the previous chapters we could show that SMFM allows us to display the behavior of single IFNGR subunits on the surface of living cells in real time, an essential prerequisite to dissect the effect of AIGAs on the intermediate steps of IFNGR complex assembly. Therefore, we utilized SMFM to identify the IFNγ-neutralizing mechanism of AIGAs. We decided to combine two approaches to get an overview of spatiotemporal dynamic of IFNGR assembly in presence of AIGAs in its entirety. First, we employed IFNγ labeled with either Rho11 or DY649 to assess binding of IFNγ to its cognate high affinity receptor subunit IFNGR1 (**Figure 29** B) on the cell surface in presence of AIGAs, as well as to investigate if IFNγ-AIGA complexes are still able to bind IFNGR1 (**Figure 29** A). We performed this experiment on non-transfected HeLa cells since we have shown that HeLa cells do express IFNGR1 endogenously and hence show binding of labeled ligand at suitable single molecule levels (chapter 4.1.1). We expected AIGAs recognizing an overlapping epitope to have a similar impact on the IFNγ-IFNGR interaction. Thus, we chose a neutralizing and a non-neutralizing mAbs from each epitope group, except for site I from which we

only had one mAb. We co-incubated mAbs and IFNγ on ice for 30 min at a 2:1 molar ratio before performing TIRF microscopy to allow saturation of AIGA-IFNγ binding. This potentially helped us to minimize binding competition effects as each fluorescently labeled IFNγ binding to a cell surface receptor most likely has already bound at least one mAb. All mAb tested induced significantly more ligand dimers than the IgG control, which should not bind IFNγ (**Figure 29** A). Simultaneously, the density of IFNγ bound to the cell surface was reduced in the presence of all mAbs but 2G7 (**Figure 29** B). In a second approach we tested hetero-dimerization of IFNGR1-IFNGR2 (**Figure 29** C) and homo-dimerization of IFNGR2-IFNGR2 (**Figure 29** D) as described in chapter 4.1.2.2 after addition of the pre-incubated IFNγ-AIGA mix. Consistently with previous results we observed the lowest IFNγ dimerization in presence of E1. Simultaneously, the surface density of labeled IFNγ was drastically reduced compared to the IgG control, but neither IFNGR hetero-dimerization nor IFNGR2 homo-dimerization was significantly reduced in presence of E1. This indicated that E1 inhibits IFNγ signaling by preventing binding to IFNGR1 but cannot fully block IFNγ at the concentrations applied in this experiment. Strikingly, for the neutralizing mAbs of site II (2B6) and site III (1E8) we observed an almost complete prevention of both IFNGR hetero-dimerization and IFNGR2 homo-dimerization. In comparison, the non-neutralizing site II mAb (2A102) did show a comparable density of surface-bound IFNγ but seem not to have any impact on the IFNGR hetero-dimerization.

Taken together these results suggested that neutralizing AIGAs of the site II and site III group did inhibit IFNγ signaling primarily by preventing recruitment of IFNGR2 into the IFNGR complex, comparable to the gain of N-glycosylation IFNGR2-T168N mutation. Whereas the inhibitory mechanism underlying the site I mAb E1 relies on impairing IFNGR assembly by blocking of ligand binding to the high affinity receptor subunit IFNGR1.

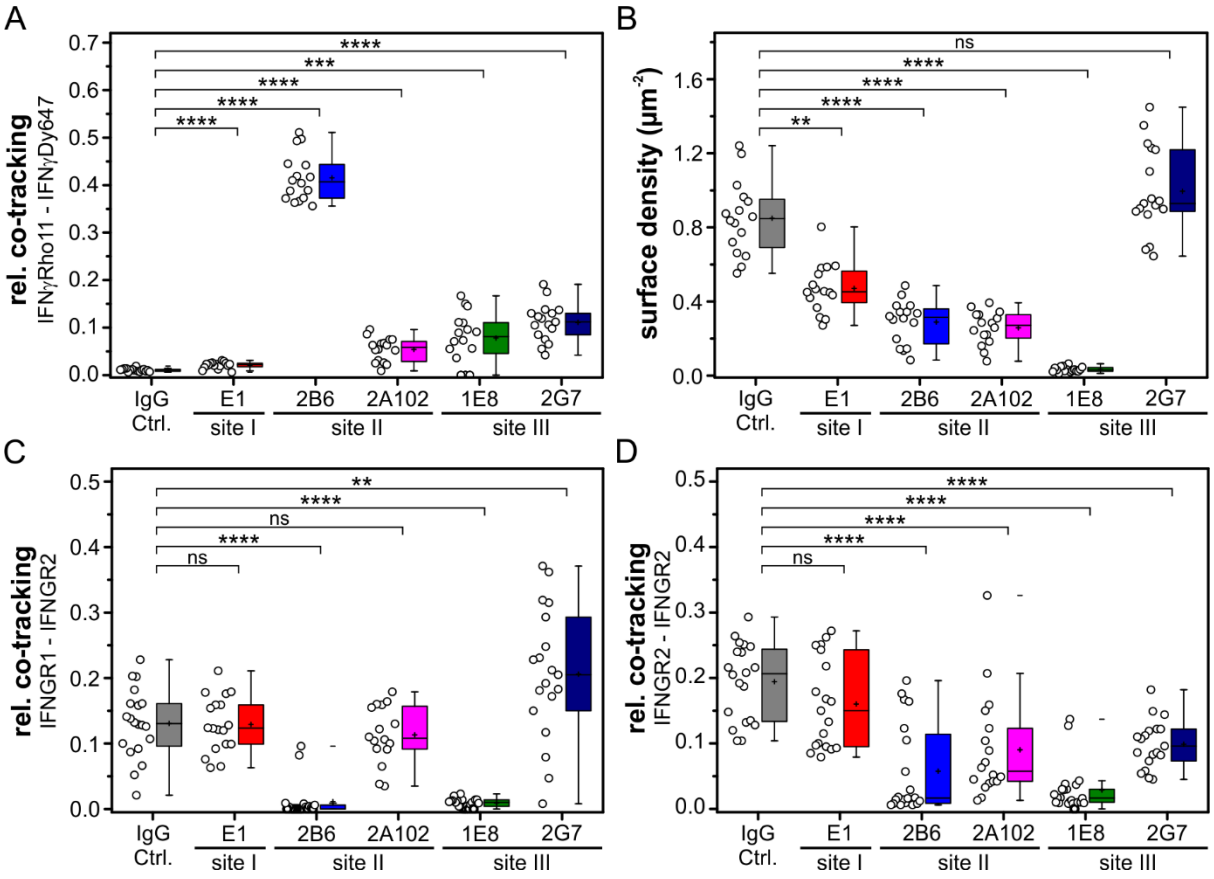

Figure 29: Receptor and IFNγ co-tracking analysis in presence of different AIGAs. (A) Co-tracking of differntly labeled IFNγ bound to the surface of HeLa cells after pre-incubation with mAb. (B) Total density of surface bound IFNγ. (C) Hetero-dimerization of IFNGR1 and IFNGR2 induced by pre-incubated IFNγ and mAbs determined by single molecule co-tracking analysis. (D) Homo-dimerization of IFNGR2 induced by pre-incubated IFNg and mAbs determined by co-tracking analysis. Each data point represents the mean value of a single cell. Statistical analysis: unpaired students t-test: ns, non-significant; *, $P \leq 0.05$; **, $P \leq 0.01$; ***, $P \leq 0.001$; ****, $P \leq 0.0001$.

4.1.5 Contributions and publications

H. Kenneweg and G. Hikade assisted me with protein and plasmid production, respectively. T. Meyer helped with the flow cytometry analysis in chapter 4.1.2.2.

O. Birkholz and F. Eull contributed to chapter 4.1.2.1 by designing and purifying the GFP variants mXFPm/mECFP and mXFPe/mEGFPe. They also conducted the single molecule competitive binding and FRET experiments.

J. L. Mendoza engineered IFNGR1-F05, designed and prepared all recombinant IFNGR partial agonists used in chapter 4.1.2.4, 4.1.3 and 4.1.4.1. He crystallized and subsequently solved the structure of the complete IFNGR complex. K. M. Jude helped in refining the protein structure. Furthermore, J. L. Mendoza performed the SPR and cytokine secretion assays. J. L. Mendoza and L. Su performed cytokine secretion assays and screened cancer cell lines for MHC I:PD-L1 bias. N. K. Escalante performed PD-L1 and MHC class I upregulation assays. S. J. Berardinelli performed mass spectrometry analysis of IFNGR2-T168N neo N-glycosylation site. J. L. Mendoza measured gene expression by qPCR and prepared samples for next-generation sequencing of a

human gene expression AmpliSeq panel. Finally, J. L. Mendoza performed flow cytometry experiments of pSTAT1 on IFNGR complex intermediates.

In chapter 3.1.4.2 H.-T. Ting, T.-Y. Wu and Y.-N. Lin carried out the preparation and purification of monoclonal antibodies. H.-P. Shih carried out the cellular cytotoxicity assays with the help of Y.-F. Lo and analyzed them with Y.-H. Tsai.

Publications

Mendoza, J.L., N.K. Escalante, K.M. Jude, J. Sotolongo Bellón, L. Su, T.M. Horton, N. Tsutsumi, S.J. Berardinelli, R.S. Haltiwanger, J. Piehler, E.G. Engleman, and K.C. Garcia, *Structure of the IFNgamma receptor complex guides design of biased agonists.* Nature, 2019. **567**(7746): p. 56-60.

Sotolongo Bellon, J., O. Birkholz, C.P. Richter, F. Eull, H. Kenneweg, S. Wilmes, U. Rothbauer, C. You, M.R. Walter, R. Kurre and J. Piehler, *Four-color single-molecule imaging with engineered tags resolves the molecular architecture of signaling complexes in the plasma membrane.* Cell Reports Methods, 2022. https://doi.org/10.1016/j.crmeth.2022.100165.

Han-Po Shih, Jing-Ya Ding, Junel Sotolongo Bellón, Yu-Fan Lo, Pei-Han Chung, He-Ting Ting, Jhan-Jie Peng, Tsai-Yi Wu, Chia-Hao Lin, Chia-Chi Lo, You-Ning Lin, Chun-Fu Yeh, Jiun-Bo Chen, Ting-Shu Wu, Yuag-Meng Liu, Chen-Yen Kuo, Shang-Yu Wang, Kun-Hua Tu, Chau Yee Ng, Wei-Te Lei, Yu-Huan Tsai, Jou-Han Chen, Ya-Ting Chuang, Jing-Yi Huang, Félix A Rey, Hung-Kai Chen, Tse-Wen Chang, Jacob Piehler, Chih-Yu Chi, Cheng-Lung Ku, *Pathogenic autoantibodies to IFN-γ act through the impedance of receptor assembly and Fc-mediated response.* J Exp Med, 2021. (submitted)

4.2 Part II: The interleukin-10 receptor complex

4.2.1 Spatiotemporal dynamics of interleukin-10 receptor assembly

4.2.1.1 Homo- and hetero-dimerization of IL-10R subunits

We utilized SMFM to understand the mechanism of IL-10 receptor (IL-10R) assembly. First, we decided to probe homo-dimerization of the high affinity binding subunit IL-10R1 by dual-color single molecule co-tracking analysis (**Figure 30** A, ii). Therefore, we transiently transfected HeLa cells with mXFPm-IL-10R1 at single molecule relevant surface expression levels. During the experiment, IL-10R1 was specifically labeled by simultaneous incubation with 5nM of MI-Rho11 and MI-AT643 each. In absence of IL-10 no homo-dimerization of IL-10R1 could be observed. On the contrast, after stimulation with 40 nM of IL-10 a substantial increase (26 ±11.5%) in IL-10R1 co-tracking could be observed (**Figure 30** C, left). A similar observation was made for homo-dimerization of the low affinity accessory subunit IL-10R2 (**Figure 30**, right), when we expressed mXFPe-IL-10R2 on the surface of HeLa cells and labeled it by simultaneous incubation with 5nM of EN-Rho11 and EN-AT643. Here, it was necessary to provide sufficient IL-10R1 at the cell surface, as IL-10R2 cannot bind IL-10 alone and requires the ligand receptor complex IL-10R1:IL-10 for binding [231]. We expected IL-10R1 not being expressed in HeLa cells naturally and therefore co-transfected the cells for the experiment with mXFPm-IL-10R1. Over expression of IL-10R1 was proven on a single cell level by labeling with MI-AT488 (**Figure 30** A, iii). Just as for IL-10R1, we could not observe IL-10R2 homo-dimerization in absence of IL-10, whereas after incubation with 40 nM IL-10 a significant increase in IL-10R2 homo-dimerization (7.1 ±3.58%) was detectable (**Figure 30** C, right). The homo-dimerization observed for IL-10R2 was significantly lower than the homo-dimerization of IL-10R1, which is in line with the published binding affinities of the IL-10 receptor subunits for its ligand (IL-10R1 for IL-10 $K_D < 1\ nM$; IL-10R2 for IL-10R1:IL-10 $K_D \sim 350\ \mu M$) [231]. As expected, no ligand-induced homo-dimerization of IL-10R2 could be observed without IL-10R1 co-transfection. Next, we tested hetero-dimerization of IL-10R1 and IL-10R2 (**Figure 30** A, i). HeLa cells were transiently transfected with mXFPm-IL-10R1 and mXFPe-IL-10R2, which were orthogonally labeled with MI-Rho11 and EN-AT643 respectively, as previously described in chapter 4.1.2.1. In absence of ligand stimulation hetero-dimerization of IL-10R1 and IL-10R2 was not detectable, whereas after incubation with 40nM of IL-10 IL-10R hetero-dimerization increased substantially to 7.9 ±2.91% (**Figure 30** B). After incubation with a functional monomeric IL-10 (mIL-10) receptor hetero-dimerization was reduced to 3.5 ±1.82% (**Figure 30** B), which was comparable to the reduction in IFNGR hetero-dimerization that we observed for mIFNγ. Our receptor dimerization results of IL-10R suggest a similar dimerization pattern and thus a similar receptor complex assembly and activation mechanism as the IFNGR. This is further supported by overall striking similarities in receptor

complex stoichiometry and orientation, as well as binding affinities of individual receptor subunits [204, 231].

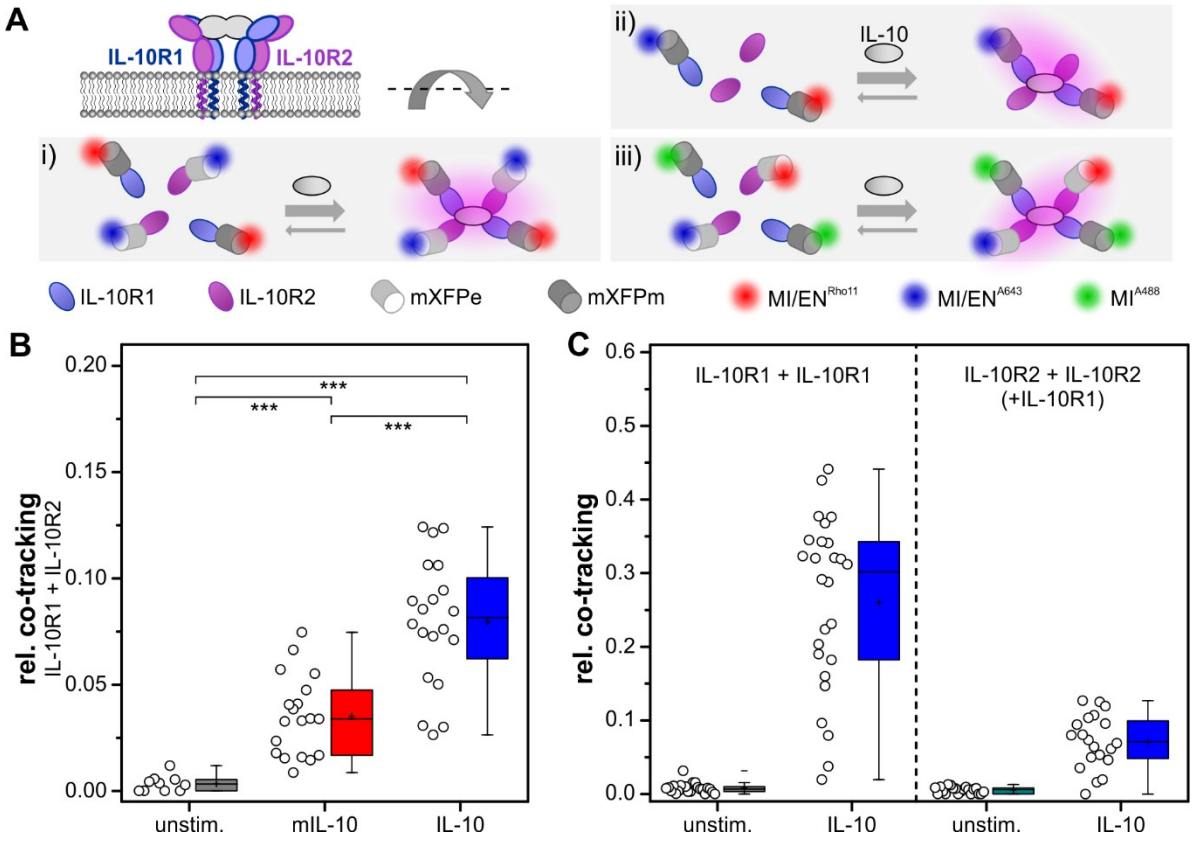

Figure 30: Spatiotemporal dynamic of IL-10R assembly at the cell surface. A) Depiction of labelling strategy utilized to label IL-10R1 and IL-10R2 in **(ii, iii)** homo-and **(i)** hetero-dimerization experiments orthogonally. Magenta area represents receptor complexes that were detected as dimers in receptor co-tracking analysis. **B)** Quantification of IL-10R1 and IL-10R2 hetero-dimerization as identified by receptor co-tracking analysis. Each data point represents a single cell. Statistical analysis: unpaired students t-test; ***, $P \leq 0.001$. **C)** Quantification of (left) IL-10R1 and (right) IL-10R2 homo-dimerization as identified by receptor co-tracking analysis. Each data point represents a single cell.

4.2.1.2 Mobility and diffusion properties of IL-10R

We sought to further compare IFNGR and IL-10R complex assembly by investigating mobility and diffusion properties of the IL-10R subunits. Therefore, trajectories of IL-10R subunits were subjected to MSD and mobility analysis (**Figure 31**). In absence of ligand IL-10R1 did show a mean diffusion constant of D_{R1} = 0.156 ±0.0267 µm²/s, which was comparable to diffusion constants previously observed for IFNGR subunits. Surprisingly, the diffusion constant of IL-10R2 was drastically reduced (D_{R2} = 0.070 ±0.0162 µm²/s) compared to IL-10R1 (**Figure 31** A). Likewise, the fraction of immobile IL-10R1 molecules (8 ±3.6%) was comparable to that of IFNGR subunits, whereas the immobile fraction of IL-10R2 was approximately 3-fold increased (25 ±4.8%, **Figure 31** B), even higher than what we typically observe for cytokine receptor complexes. Strikingly, after ligand stimulation IL-10R1 did adapt the diffusion constant and immobile fraction of IL-10R2 (**Figure 31** A, B). We went a step further and compared the step-size distribution of IL-

10R subunits in absence of IL-10 (**Figure 31** C). In the case of frame-to-frame step-sizes (lag time: τ = 32 ms) both subunits, IL-10R1 and IL-10R2, showed a population of slow diffusive molecules with a mean step-size of 33.5 ±2.48 nm and 24.2 ±0.56 nm respectively (**Figure 31** C), which are close to the theoretical mean step-size for immobile molecules (28 nm) calculated from a mean photon-based localization precision of 20 nm. It should be noted that the population of slow diffusive molecules detected by step-size distribution nicely match the previously estimated immobile fraction of both receptor subunits (**Figure 31** B). Interestingly, when compared to step-size distribution (**Figure 31** C) for longer lag times ($\tau \approx$ 1s) the population of immobile IL-10R2 was drastically reduced (10.4 ±0.58%), whereas the population of immobile IL-10R1 remained in a similar range (6.2 ±0.28%). These observations pointed in the direction that IL-10R2 molecules seem to change their mobility over time, whereas other class II cytokine receptor subunits, such as IL-10R1 or IFNGR1, show a limited fraction of immobile molecules, but on the contrast, these molecules remain immobile for longer dwell times. This stimulation-induced temporary arrest of lateral diffusion (STALL)-like [232] behavior of IL-10R2 could be nicely visualized by plotting the x and y position over the time (**Figure 31** D, E) of representative single IL-10R2 trajectories. This lengthy and pronounced STALL-like diffusion of IL-10R2 is unique among the class II cytokine receptors. Considering that IL-10R2 is a shared receptor subunit of the IL-10R family [233] these observations might have implications for the assembly and activation mechanism of several class II cytokine receptors.

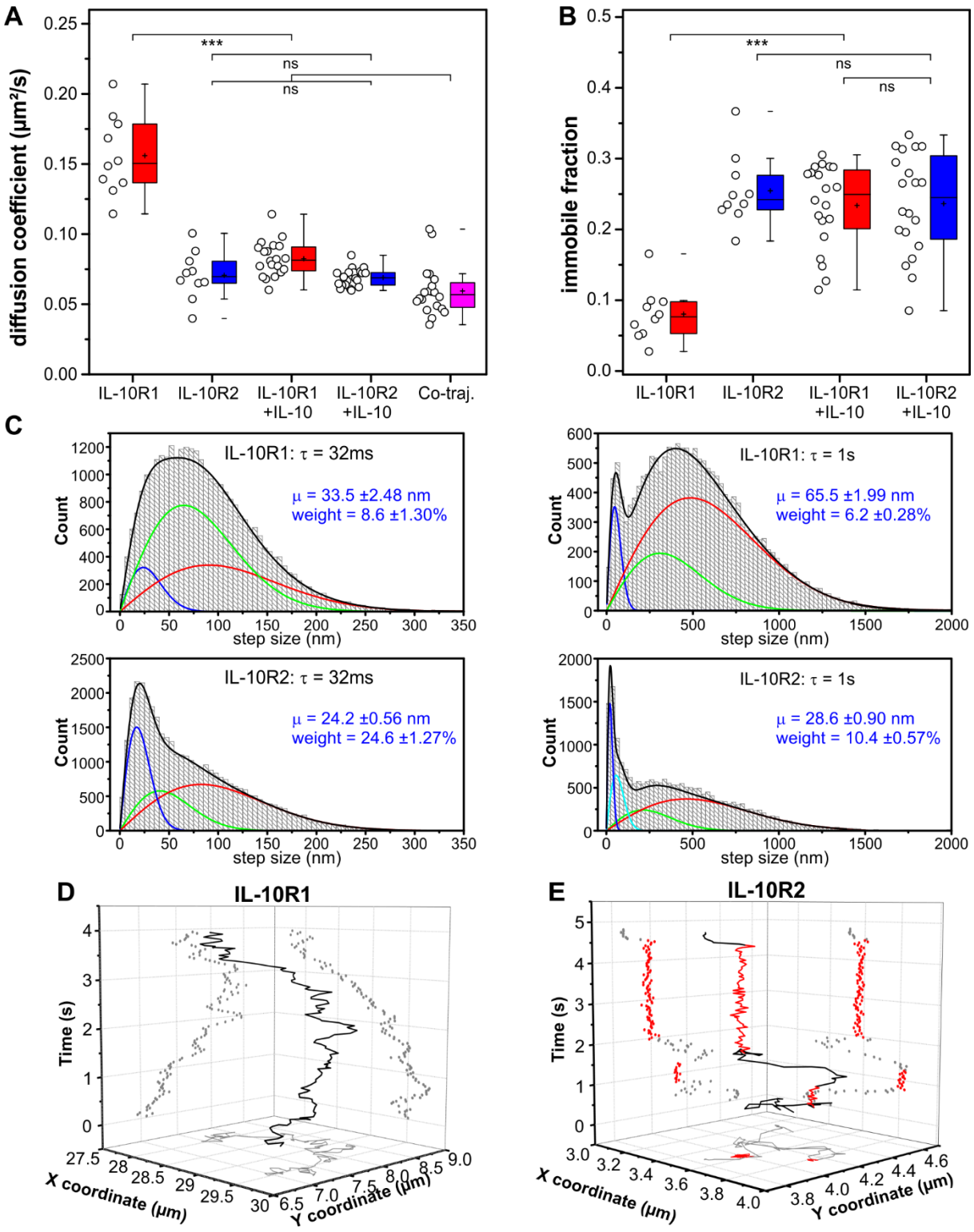

Figure 31: Mobility and diffusion properties of IL-10R1 and IL-10R2 subunits. (A) Diffusion coefficient of IL-10R1 (red), IL-10R2 (blue) and co-tracked dimers (magenta) calculated from MSD analysis. Each data point represents the mean value of a single cell. **(B)** Fraction of IL-10R1 (red) or IL-10R2 (blue) molecules classified as immobile particles in absence and presence of IL-10. **(C)** Step size distribution of IL-10R1 (top) and IL-10R2 (bottom) for a lag time of τ = 32 ms (left) or τ = 1s (right). Three to four populations of differently diffusing particles were fitted as peak functions for the total probability density function (PDF) to fit the empiric distribution. Population size (weight) and mean step size of the slowest diffusing population are shown in blue. **(D, E)** 3D projection of a representative trajectory of a single IL-10R1 (left) and IL-10R2 (right). Immobile state of the trajectory is highlighted in red.

4.2.2 Abnormal diffusion properties of IL-10R2

We decided to further investigate the molecular mechanism underlying the STALL-like diffusion of IL-10R2. Initially, we hypothesized that the observed temporary arrest of lateral diffusion may originate from transient protein-protein interactions. This potential interaction partner had to be very immobile itself in the time scale imaged, such as the membrane skeleton or the endocytic machinery [234]. First, we designed serial truncations of IL-10R2 to determine which part of the transmembrane receptor is responsible for STALL-like diffusion (**Figure 32**): IL-10R2-delECD (Δ19-209) lacked the extra cellular domain (**Figure 32** C). IL-10R2-delICD (Δ304-325) lacked most of the intra cellular domain while still containing the predicted TYK2 binding region (**Figure 32** D) [161]. IL-10R2-delTYK2 (Δ251-325) lacked the entire intra cellular domain including the TYK2 binding region (**Figure 32** E). IL-10R2-TMD (210-250) contained only the predicted transmembrane domain of IL-10R2 (**Figure 32** F). We expressed these IL-10R2 variants each N-terminally tagged with mXFPe in HeLa cells and labeled them by incubation with 5 nM of EN-AT643. All truncations including wild type IL-10R1 and IL-10R2 were subjected to single molecule tracking analysis. Subsequently single representative trajectories were used to portray the diffusion property of the construct by plotting the frame-to-frame square displacement (SD) over time. Typical Brownian-like diffusion of cytokine receptors was shown by IL-10R1 (**Figure 32** A). Whereas all IL-10R2 truncations, including wild type IL-10R2, did show STALL-like diffusion (**Figure 32** B – F), indicating that the transmembrane is triggering this abnormal diffusion behavior.

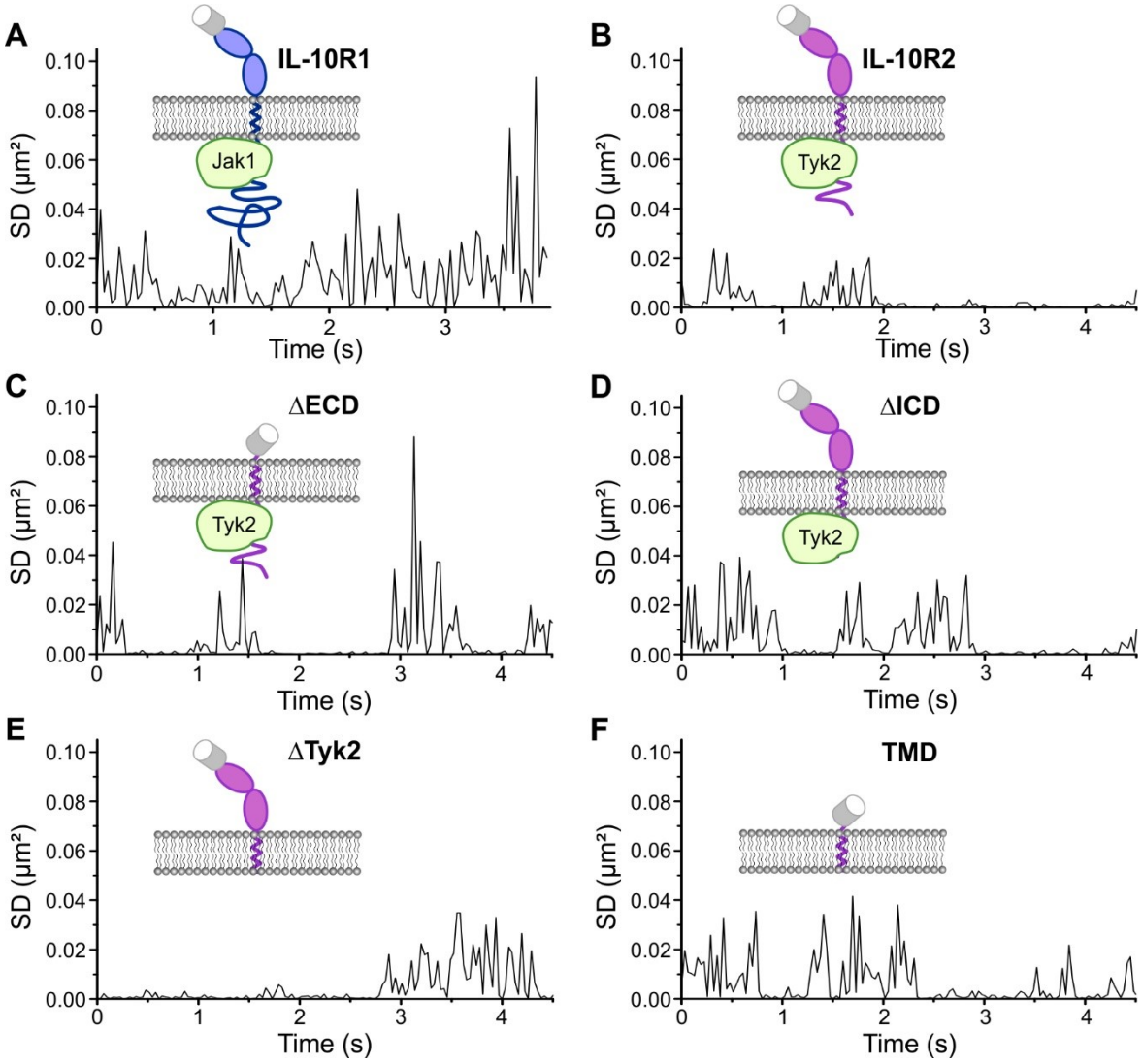

Figure 32: STALL-like diffusion behavior is aroused by the TMD of IL-10R2. Frame-to-frame square displacement (SD) (|Δx*Δy|) of representative trajectories of IL-10R2 truncations plotted against the time. During transient lateral arrest receptor subunits are severely confined, hence the frame-to-frame SD lingers around 0 µm² for a defined time window.

Next, we inspected the transmembrane domain of IL-10R2 in more detail (**Figure 33** A). Thereby we found three cysteine residues near the C-terminus of the TMD of IL-10R2. Membrane proximal cysteines are commonly found in the intra cellular domain of transmembrane adaptor proteins, such as Linker for activation of T cells, and provide palmitoylation sites, which are necessary for protein function [235, 236] and were closely associated with plasma membrane confinement [237]. We exchanged both membrane proximal cysteines, C241 and C247, for alanine, but left C235 untouched, as it was supposed to be buried in the plasma membrane (**Figure 33** A). Single molecule tracking analysis revealed a similar diffusion pattern as the wild-type IL-10R2 (**Figure 33** D). Additionally, we noticed that the TMD of IL-10R2 is remarkable 33 amino acids big, if you consider the entire hydrophobic part between the two charged residues E216 and K250 to be the TMD. This is roughly ten amino acids bigger than the average size of TMD of plasma membrane proteins of vertebrates [238]. We hypothesized that the size of the TMD provides IL-10R2 flexibility in its

orientation in the plasma membrane. This flexibility could potentially lead to membrane confinement and thus translate into STALL-like diffusion. To test this idea, we limited the size of the TMD by introducing a lysine residue at A224 or A243 respectively (**Figure 33** A). For both constructs we could observe a drastic reduction of STALL-like diffusion (**Figure 33** B), while still a minor part of the IL-10R2 did show STALL-like diffusion (**Figure 33** C). These observations indicated that IL-10R2 STALL-like diffusion most probably involves temporal, unfavorable orientation of the TMD inside the plasma membrane or membrane confinement. This could be in line with the overall flat IL-10R complex structure [57] and the rotation between both IL-10 subunits, that might force the receptor subunits to be inclined to a more horizontal orientation rather than vertical.

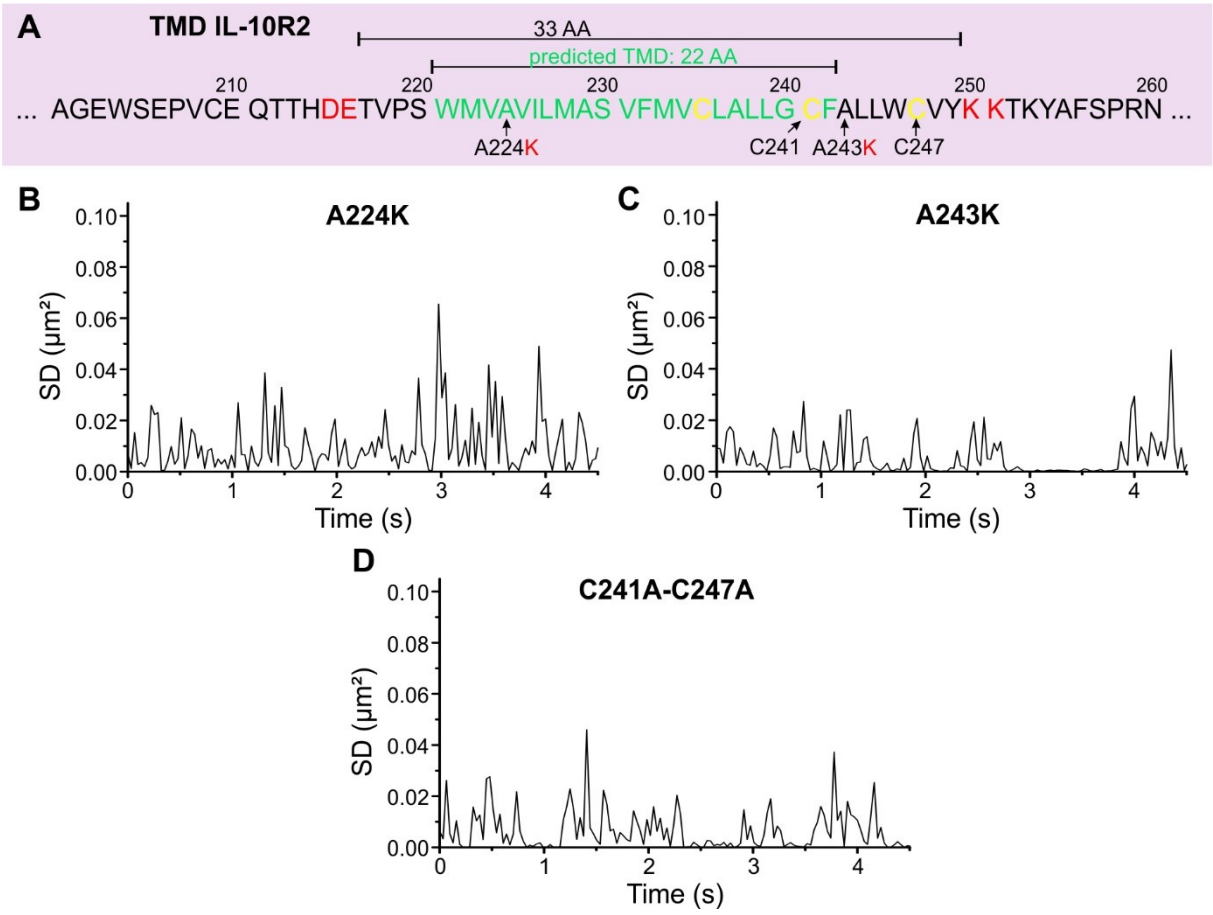

Figure 33: Restricting the length of the TMD of IL-10R2 reduces its propensity to show STALL-like diffusion. (A) Amino acid (AA) sequence of transmembrane domain (TMD) of IL-10R2 showing the position of introduced mutations. Predicted TMD is highlighted in green. Charged residues flanking the predicted TMD are highlighted in red. **(B, C)** Frame-to-frame square displacement plotted against the time for extra cellularly confined TMD (A224K) or intra cellularly confined TMD (A243K). **(D)** Frame-to-frame square displacement plotted against the time for IL-10R2-C241A-C247A. Data represent a single representative trajectory.

4.2.3 Pleiotropy of IL-10R signaling

In its critical role as immune regulator IL-10 contributes to maintaining immune homeostasis by precisely balancing its immune suppressive and immune stimulatory effects in the event of pathogen infection. IL-10 regulates the adaptive arm of the immune response by reducing the

antigen presentation potential of innate cells by decreasing their surface major histocompatibility complex (MHC) levels and costimulatory molecules [123, 124]. In addition, IL-10 potently suppresses the production of proinflammatory cytokines from various cell types including monocytes, macrophages, and T cells [119, 239]. In addition to its anti-inflammatory activities, IL-10 can increase the cytotoxic function of CD8+ T cells, augmenting their ability to target tumors and boosting the anticancer response [240].

The importance of IL-10 signaling for a healthy immune response is highlighted by the finding that IL-10 deficient patients develop severe autoimmune diseases such as Crohn's diseases and colitis [241, 242]. In addition, several viruses have developed different IL-10 homologs that hijack the IL-10 signaling pathway and selectively activate solely its immune suppressive responses. These viral modulations of IL-10 signaling responses imply that there are opportunities to engineer human IL-10 (hIL-10) to fine-tune signaling into the desired direction. Understanding the molecular mechanism of pleiotropic IL-10 cellular responses could potentially offer an advantage in developing medical applications.

4.2.3.1 Viral IL-10 homologous hijack human immune system

From all currently known viral IL-10 homologs the variant from the Epstein-Barr virus (ebvIL-10) and the human Cytomegalovirus (cmvIL-10) are the only two that mainly target human IL-10R [153]. Both viral IL-10 homologs evolved independently from each other, as indicated by large differences in amino acid sequence while simultaneously possessing remarkable homologies in the protein structure [152, 243]. ebvIL-10 shares high sequence similarity with hIL-10 but has a 250-fold reduced binding affinity towards IL-10R1 compared to hIL-10 [244]. On the contrast, cmvIL-10 has a strongly conserved protein structure of the receptor binding interfaces with respect to hIL-10 but has a larger intermolecular angle between both cmvIL-10 subunits [152]. However, cmvIL-10 shows similar binding affinities to IL-10R compared to hIL-10 [152], which suggest, that both viruses have found distinct ways to achieve a similar result, that is escaping the human immune system after viral infection.

To resolve the immune escape mechanism underlying the viral IL-10 homologs, it was necessary to understand how viral IL-10 homologs decouple the pleiotropy of IL-10 signaling. Former studies have provided valuable in-depth *in vitro* characterization of both IL-10 homologs [152, 243, 244], but few have studied the effect of viral IL-10 on IL-10R assembly. Therefore, we utilized SMFM to investigate the spatiotemporal dynamic of IL-10R complex assembly induced by viral IL-10 variants on living cells (**Figure 34**). Because ebvIL-10's reduction in binding affinity toward IL-10R seems primarily to come from IL-10R1 binding [244], we expected a more distinct effect on the fraction of IL-10R1 homodimers and consequently tested IL-10R1 homo-dimerization in presence of viral IL-10 (**Figure 34** A). Like in previous experiments, in absence of ligand

essentially all IL-10R1 remained monomeric, but incubation with 40 nM hIL-10 led to a strong increase (36.8 ±4.76%) in IL-10R1 homo-dimerization. According to its reduced binding affinity, ebvIL-10 induced less IL-10R1 homo-dimerization (10.6 ±3.79%), even at higher concentrations (12.7 ±2.86%, **Figure 34** A). A single Isoleucine residue at position 87 of hIL-10 has been known to be essential for the immunostimulatory response of the IL-10 signaling pathway [245]. Restoring this Isoleucine in ebvIL-10(A87I) has not only restored immunostimulatory signaling responses but also greatly enhanced the binding affinity of ebvIL-10 for IL-10R1. In line with these observations, ebvIL-10(A87I) could drastically enhance the IL-10R1 homo-dimerization (26 ±5.39) but not entirely restore wild-type IL-10R1 homo-dimerization levels (**Figure 34** A). Unexpectedly, cmvIL-10 only induced limited levels of IL-10R1 homo-dimerization (3.2 ±2.95%), contradicting reported IL-10R1 binding affinity comparable to hIL-10 [152]. Overall, the diffusion constants gained from MSD analysis further supported these observations (**Figure 34** B). IL-10R1 homodimers induced by all tested IL-10 variants showed nearly identical diffusion properties, hinting that signaling complexes formed by the IL-10 variants were also quite similar in terms of plasma membrane confinement and stoichiometry. On the contrast, mean diffusion constants of all IL-10R1 after stimulation with different IL-10 variants reflected the observed IL-10R1 homo-dimerization levels (**Figure 34** A, B), indicating that IL-10R1 homo-dimerization is required for noticeable change in diffusion properties of IL-10R complexes.

These first observations seem to positively link an immunostimulatory signaling response to IL-10R complex assembly threshold and as a consequent to signaling strength. The viral IL-10 homologs fail to induce sufficient IL-10R complexes, despite potentially higher ligand concentrations and thereby ensure that only immunosuppressive signaling responses are activated.

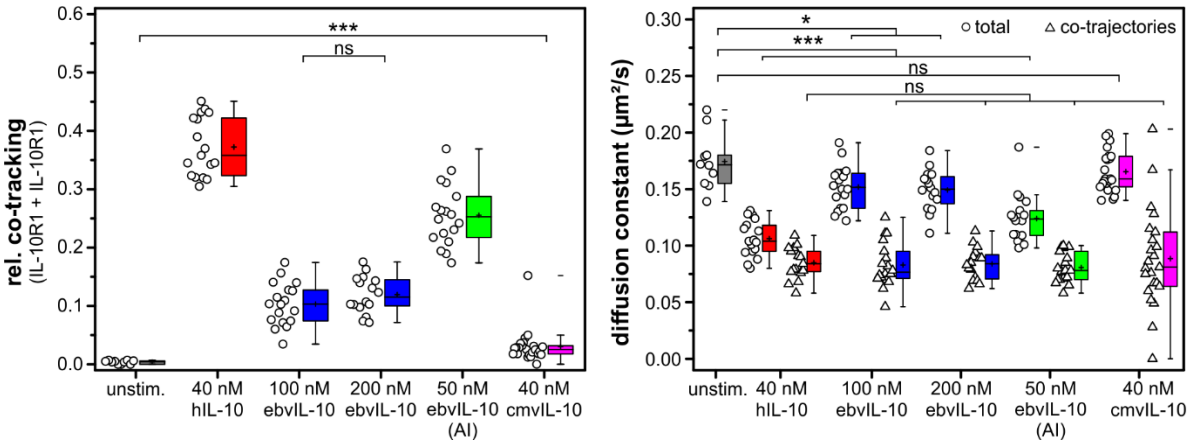

Figure 34: IL-10 receptor assembly induced by viral IL-10 homologs. (A) IL-10R1 homo-dimerization quantified by dual color single molecule TIRF microscopy. **(B)** Mean diffusion constant of all IL-10R1 trajectories (circle) or only co-tracked receptors (triangle). hIL-10 = human IL-10, ebvIL-10 = IL-10 homologue from Epstein-Barr virus, AI = ebvIL-10(A87→I), cmvIL-10 = IL-10 homologue from human Cytomegalovirus. Each data point represents a single cell. Statistical analysis: unpaired t test: ns, non-significant; *, $P \leq 0.05$; **, $P \leq 0.01$; ***, $P \leq 0.001$.

4.2.3.2 Engineering of an affinity maturated IL-10 variant

The viral IL-10 homologs had shown that different IL-10 cellular signaling responses might need different signaling potency thresholds to be activated. Due to its potent anti-inflammatory properties, recombinant IL-10 therapy was regarded as an attractive biological approach to treat autoimmune disorders, such as inflammatory bowel disease. Unfortunately, IL-10 therapies have failed to elicit beneficial results in the clinic, with several clinical trials showing only mild efficacy and biased responses in patients [246, 247]. Especially in the case of Crohn's disease, a leading hypothesis to explain these effects was, that low levels of this cytokine reach the gastrointestinal track and consequently fail to produce an effective response [248]. Having an IL-10 variant with the ability to elicit robust responses at therapeutically relevant doses could potentially help to avoid this limitation.

In chapter 4.2.1 we could show that IL-10 initiates receptor complex formation by fast binding to its high affinity receptor subunit IL-10R1 and subsequently the low affinity receptor subunit IL-10R2 is recruited into the complex in a rate-limited fashion. According to this model we hypothesized that by improving the IL-10R2 binding affinity we could create a ligand that elicits robust cellular responses even at lower ligand concentrations. To test this hypothesis, we engineered IL-10 using yeast surface display to bind IL-10R2 with increased binding affinity (**Figure 35**). A caveat to engineering IL-10 is its dimeric nature, which makes the correct display of this cytokine on the yeast surface challenging. We used a previously described monomeric IL-10 variant [203] as an engineering scaffold to overcome this limitation. The monomeric IL-10 was generated by extending the connecting linker between helices D and E in IL-10 by six peptides, consequently allowing helices E and F to fold into its own hydrophobic core to form an IL-10 monomer (**Figure 35** B). Monomeric IL-10 recruits one molecule each of IL-10R1 and IL-10R2 to form an active signaling trimeric complex. Although monomeric IL-10 can trigger IL-10–mediated responses, it does so with lower potency than its dimeric counterpart [203, 231]. First, we transfected yeast with the monomeric IL-10 construct to test whether binding to IL-10R1 and IL-10R2 receptor subunits was preserved in the context of the yeast surface. We used biotinylated ectodomains of IL-10R1 and IL-10R2 receptors in combination with Alexa Fluor 647 fluorescently labeled streptavidin to measure receptor binding by flow cytometry (**Figure 35** A). Without a crystal structure of IL-10 bound to IL-10R2 to guide us in the design of a site-directed mutant library, we undertook an unbiased error-prone approach to generate IL-10 mutants with enhanced affinity for IL-10R2. The gene encoding the monomeric IL-10 variant was subject to error-prone polymerase chain reaction (PCR) and the amplified PCR product subsequently electroporated into the Saccharomyces cerevisiae strain EBY100 following previously described protocols [189, 249]. Eight rounds of selection were performed, in which the concentration of IL-10R1 was gradually decreased to isolate variants of IL-10 that bound to IL-10R2 with enhanced affinity (**Figure 35** C). Initial rounds of

selection were performed with high concentrations (1 µM) of biotinylated IL-10R2 in the presence of 100 nM nonbiotinylated IL-10R1 to stabilize the surface complex and recover low-affinity binding variants. After round 6 of selection, the library was composed of variants that bound to IL-10R2 even in the absence of IL-10R1, and by round 8, the library contained variants that bound to concentrations of IL-10R2 in the low nanomolar range. At this point, we picked individual yeast colonies and isolated several clones (A11, B11, and R5A11) that bound to IL-10R2 with enhanced affinity when compared to WT IL-10 (**Figure 35** E). In the IL-10 structure, these mutations localized to the region along helices A and D that was previously predicted to bind IL-10R2 [189], thereby validating our selection process (**Figure 35** D).

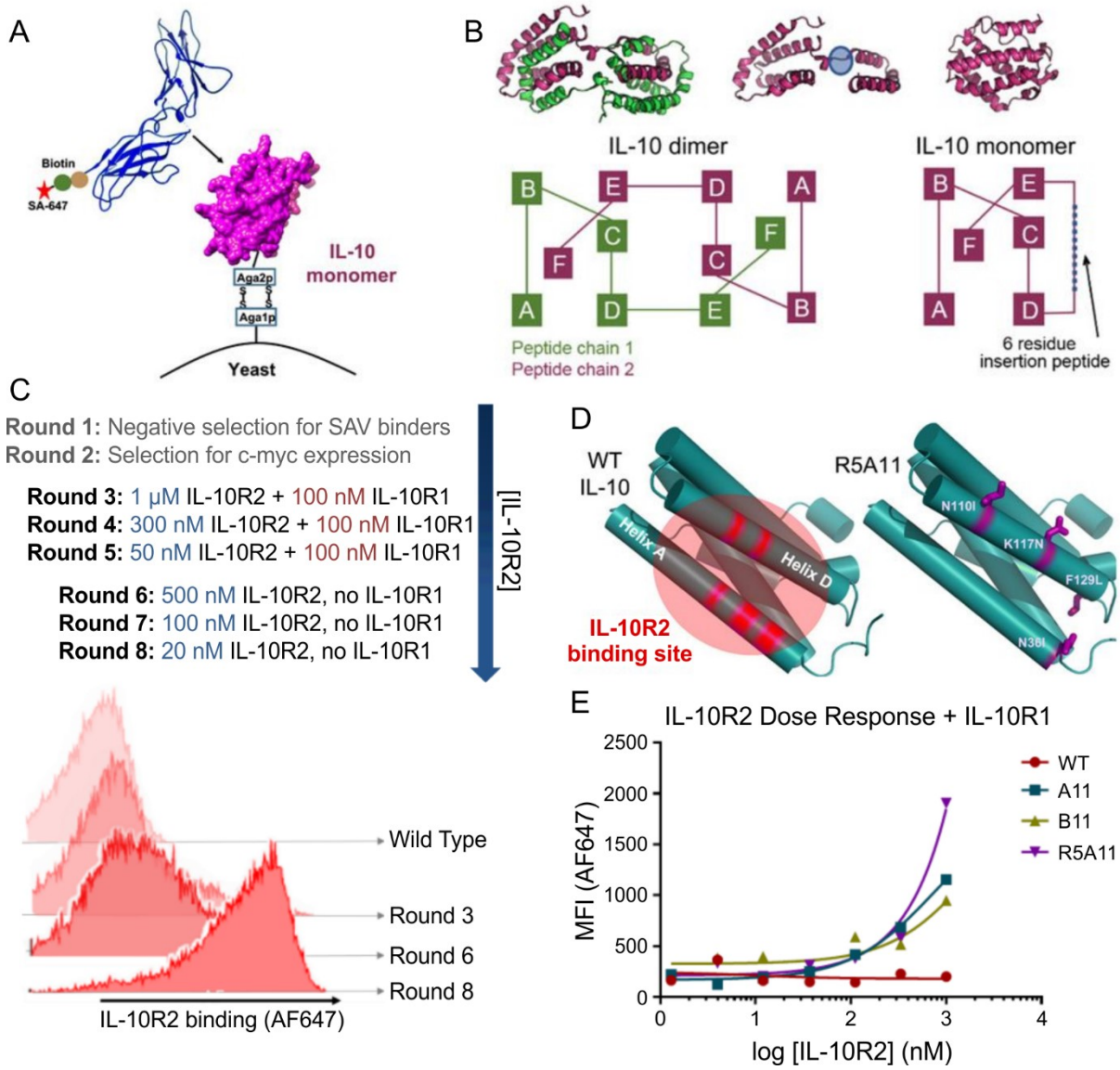

Figure 35: Improving of IL-10 binding to IL-10R2 by yeast surface display. (A) Representation of IL-10 displayed on yeast cell surface used in screen with fluorescently labeled IL-10R2. **(B)** Depiction of IL-10 dimer and monomer protein structure and helix organization. Insertion of a 6-residue linker allows folding of a single chain to a monomeric IL-10 protein. **(C)** Top: Ligand conditions used in each yeast display selection round. Bottom: Representative histograms

of IL-10R2 binding (AF647) on yeast displaying wild type IL-10 from depicted rounds of selection. **(D)** Left: WT IL-10 structure with helices A and D emphasized in red as the area predicted to be the IL-10R2 binding site [189]. Right: Cartoon representation of the IL-10 monomer with the positions of the mutations found in the high-affinity variant R5A11 highlighted in purple. **(E)** Dose response for IL-10R2 binding for single clones from yeast display library. The highest IL-10R2 concentration is 1 µM with a 1:3 serial fold dilution over 7 concentrations. Non-biotinylated IL-10R1 was added at 100 nM to improve cooperative binding.

4.2.3.3 Affinity maturated IL-10 variant enhances IL-10R complex assembly at the plasma membrane

Thus far, the protein engineering methodologies applied have demanded the use of the monomeric form of the cytokine. To study the native IL-10/IL-10R complex stoichiometry, we recombinantly expressed our high-affinity IL-10 mutant, R5A11, in dimeric form (R5A11D) in addition to the monomeric form (R5A11M). We selected this mutant based on its higher expression yields compared to other isolated variants. Comparisons between these variants, IL-10, and mIL-10 allowed us to examine how increased binding affinity and stoichiometry contributed to IL-10's molecular and cellular activities. To test how increasing the binding affinity to IL-10R2 supported receptor assembly at the plasma membrane of living cells, we probed diffusion and interaction of both receptor chains by dual-color TIRF microscopy. We expressed mXFPm-IL-10R1 and mXFPe-IL-10R2 in HeLa cells and labeled them by incubation with MI-Rho11 and EN-AT643 as previously described. Hetero-dimerization of IL-10R1 and IL-10R2 in presence of R5A11 was quantified by co-tracking analysis. R5A11D induced a substantially higher level of receptor heterodimers (**Figure 36** A). This finding was also confirmed for the monomeric versions of both wild type and high-affinity IL-10 variants although at lower levels than seen for the dimeric versions (**Figure 36** B). This observation is in line with the 50% reduced probability to observe heterodimers expected for the monomeric compared to dimeric ligand. We also probed homodimerization of IL-10R1 and IL-10R2, respectively. Stimulation with the dimeric IL-10 induced strong homodimerization of IL-10R1 with no difference between both cytokine variants because the IL-10R1 binding interface was unaltered in R5A11 (**Figure 36** A). Instead, homodimerization of IL-10R2 was significantly increased for the engineered variant R5A11D compared to IL-10. For mIL-10 variants, all homodimerization experiments failed to induce receptor homodimers, in agreement with the monomeric nature of the ligands (**Figure 36** B) [203]. Together, these results confirmed that, compared to wild type IL-10, the engineered R5A11 variants increased recruitment of IL-10R2 into the signaling complex at the plasma membrane.

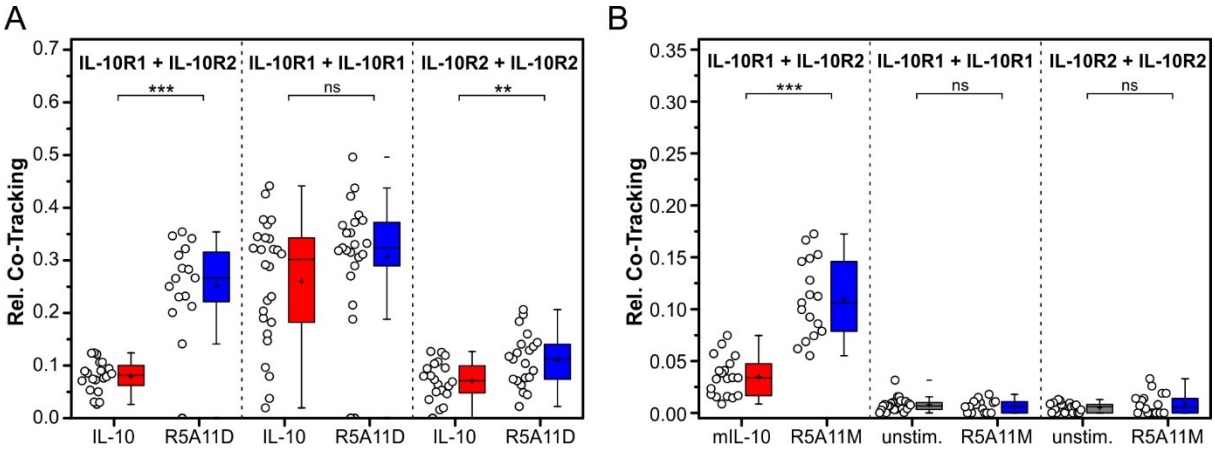

Figure 36: Dimerization of IL-10R induced by affinity maturated R5A11 ligands. (A) Hetero and homo-dimerization induced by R5A11D compared to wild type IL-10 estimated by single molecule co-tracking analysis. **(B)** Hetero-dimerization of IL-10R induced by R5A11M compared to monomeric IL-10 and homo-dimerization of either IL-10R1 or IL-10R2 induced by R5A11M compared to homo-dimerization of unstimulated receptor subunits. Statistical analysis: unpaired t-test; ns, non-significant; **, $P \leq 0.01$; ***, $P \leq 0.001$.

4.2.3.4 Effect of engineered ligands on immunosuppressive IL-10 signaling response

In the last chapter we could show that the affinity maturated IL-10 variant R5A11 does recruit IL-10R2 more efficiently into the IL-10R complex and subsequently leads to an increased number of IL-10R complexes at the cell surface of living cells. Next, we wanted to investigate which effect does this affinity improvement and altered surface receptor complex level exert on IL-10 specific cellular responses.

IL-10 inhibits inflammatory processes by modulating the activities of different innate cells including monocytes. We next performed signaling and activity assays in human monocytes to investigate the anti-inflammatory potential of our engineered variants. Monocytes (CD14+ cells) were isolated from human buffy coats and stimulated with IL-10 and R5A11 for 15 min for measurement of STAT1 and STAT3 phosphorylation or rested for 2 days before a 24-hour stimulation for measurement of human leukocyte antigen–DR isotype (HLA-DR) levels (**Figure 37**). Levels of STAT1 and STAT3 phosphorylation upon ligand stimulation were measured by flow cytometry because these two transcription factors represent the major signaling pathway engaged by IL-10 [172, 250]. At saturating concentrations, R5A11D and IL-10 activated STAT1 and STAT3 to a comparable extent (**Figure 37** A). However, R5A11D induced enhanced phosphorylation of both STAT1 and STAT3 at subsaturating concentrations, which translated into a decrease in median effective concentration (EC_{50}) values compared to IL-10 (**Figure 37** A, B). mIL-10 showed poor activation of STAT1 and STAT3 with amplitudes of activation, reaching less than 50% of those elicited by IL-10 (**Figure 37** A). Although IL-10, R5A11D, and R5A11M showed similar pSTAT1:pSTAT3 ratios, the bias of mIL-10 in inducing more pSTAT3 than pSTAT1 (**Figure 37** C) agrees with previous observations describing biased signaling by short-lived cytokine-receptor complexes [251]. R5A11M induced the activation of both STAT1 and STAT3 to levels comparable

to those induced by the dimeric cytokines at saturating doses, suggesting that the defective signaling elicited by mIL-10 results from its weak IL-10R2 binding affinity (**Figure 37** A, B). Time course analyses showed that the signaling profiles of the variants were not caused by differences in signaling kinetics. The four IL-10 ligands triggered comparable signaling kinetics in human monocytes (**Figure 37** D), confirming that their different signaling profiles result from their different binding affinities for IL-10R2.

IL-10 exerts its anti-inflammatory properties by inhibiting antigen presentation in innate cells such as monocytes and dendritic cells [252]. Thus, we next studied whether IL-10 binding affinity to IL-10R2 influenced its ability to decrease HLA-DR expression in human primary monocytes. IL-10 and R5A11D reduced the levels of HLA-DR surface expression to a similar extent (50%) at saturating doses, in agreement with their comparable signaling profiles (**Figure 37** E). At subsaturating doses, however, R5A11D induced greater inhibition of HLA-DR expression (**Figure 37** E). mIL-10 induced a mild reduction of HLA-DR surface levels (20%), which paralleled its poor signaling potency (**Figure 37** E). R5A11M induced only a 30% reduction of the surface HLA-DR levels, despite activating STAT1/STAT3 to a similar extent as the dimeric ligands (**Figure 37** E), suggesting an additional dimer-dependent mechanism by which IL-10 reduces HLA-DR expression. We next investigated how IL-10R2 binding affinity correlated with IL-10's ability to inhibit proinflammatory cytokine production by monocytes. We measured IL-6 secretion from monocytes upon lipopolysaccharide (LPS) stimulation in the presence of various doses of IL-10 and R5A11D (**Figure 37** F). At saturating concentrations, IL-10 and R5A11D effectively inhibited IL-6 secretion to a similar extent (**Figure 37** F). However, at subsaturating doses, R5A11D retained the ability to inhibit IL-6 secretion, unlike IL-10 (**Figure 37** F). Together, our data highlight that IL-10 variants exhibiting enhanced binding toward IL-10R2 gain a functional advantage at subsaturating doses, such as those that would be attained during therapeutic interventions.

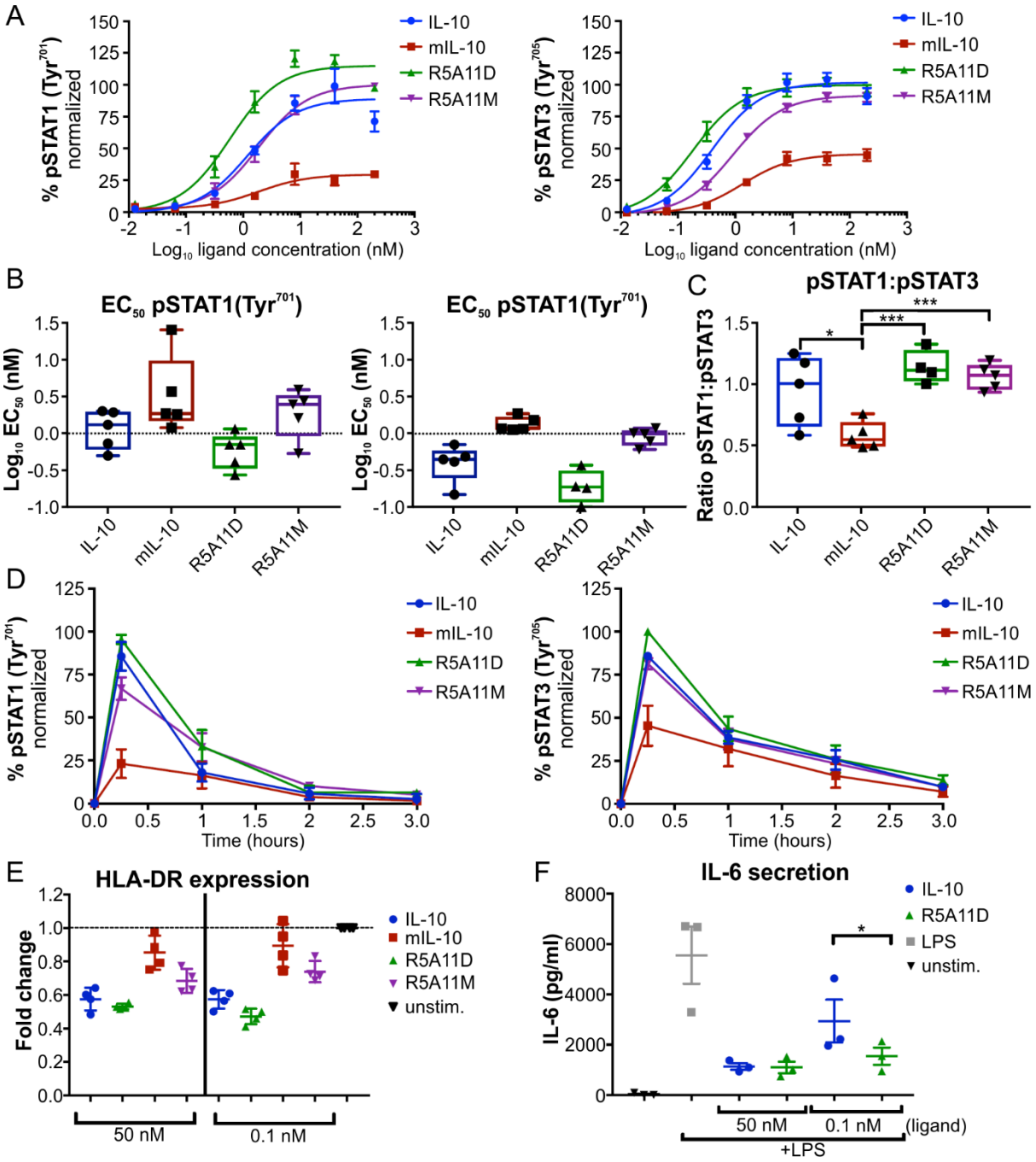

Figure 37: Activation of IL-10R signaling in human primary monocytes. (A) Dose response curve of STAT1 (left) and STAT3 (right) phosphorylation in human primary monocytes treated with IL-10. Cells were stimulated with monomeric or dimeric wild type IL-10 (mIL-10 and IL-10) and engineered variant (R5A11M and R5A11D) for 15 min. Phosphorylation of STAT1/STAT3 was quantified by phosphor-flow cytometry. Sigmoidal curves were fitted with GraphPad Prism software. Data shown are the mean of five biological replicates with error bars depicting the SEM. Each biological replicate was normalized by assigning the highest MFI value to the top concentration as 100% and the lowest MFI value of an untreated control as 0%. The rest of the samples and conditions were normalized accordingly. **(B)** Log_{10} EC_{50} values for pSTAT1/pSTAT3 from dose response curves in (A). **(C)** Ratios of pSTAT1 to pSTAT3 in IL-10-stimulated monocytes were calculated by dividing pSTAT1 by pSTAT3 values. Statistical analysis: two-tailed paired t-test; *, $P \leq 0.05$; ***, $P \leq 0.001$. **(D)** Kinetics of pSTAT3 and pSTAT1 induced by IL-10. Monocytes were stimulated with IL-10 for the indicated time periods before fixation. **(E)** Measurement of HLA-DR cell surface expression in monocytes after 24 hours of IL-10 treatment. **(F)** Measurement of IL-6 secretion by monocytes stimulated with LPS for 8 hours in presence of IL-10. Statistical analysis: two-tailed paired t-test; *, $P \leq 0.05$.

Our initial studies in monocytes were focused on two classical markers attenuated by IL-10, HLA-DR levels, and IL-6 expression. To gain a broader understanding of how our variants affect human

monocyte activities, we performed a detailed transcriptional analysis of human monocytes stimulated with the different IL-10 ligands for 24 hours. Wild type IL-10 treatment elicited strong transcriptional changes in human monocytes. We observed increased expression of 741 genes and decreased expression of 1084 genes (**Figure 38** A). Kyoto Encyclopedia of Genes and Genomes (KEGG) pathway analysis showed that IL-10 treatment affected the expression of several metabolic genes, including pyruvate metabolism, glycolysis, and lipid biosynthesis [253]. In addition to metabolism-related genes, IL-10 treatment induced changes in the expression of genes encoding cytokines, chemokines, and their receptors [253], revealing a broad regulation of monocyte biology that included fine-tuning energy homeostasis, migration, and trafficking. Interestingly, 27% of the genes regulated by IL-10 at saturating doses (50 nM) were found to be expressed differentially at subsaturating IL-10 doses (0.1 nM) (**Figure 38** C), whereas changes in the expression of the other 73% of the genes were induced to a similar extend under both conditions. 95% of those differentially expressed genes corresponded to genes attenuated by IL-10 treatment and include those encoding critical pro-inflammatory chemokines and cytokines (**Figure 38** B, C). Our data show that at low doses, IL-10 loses the ability to reduce the expression of genes encoding key cytokines and chemokines that critically contribute to enhance the inflammatory response. Next, we studied how the engineered IL-10 variants affected gene expression programs in monocytes. 40% of the genes whose expression was altered by IL-10 showed reduced regulation in response to R5A11M (**Figure 38** D). This effect contrasted with its ability to activate STAT1 and STAT3 to levels comparable to those induced by the dimeric ligands, suggesting that STAT activation does not directly correlate with transcriptional activity in response to IL-10. In agreement with our signaling studies, R5A11D induced a more robust gene expression profile at subsaturating doses when compared to IL-10. At these doses, R5A11D treatment enhanced the expression of 19% of genes compared to IL-10 treatment, with only 6% of genes showing increased expression upon IL-10 treatment compared to R5A11D treatment (**Figure 38** D). Of the top 10 genes with increased or decreased expression by IL-10, most displayed more pronounced changes in response to R5A11D treatment (**Figure 38** E). Genes encoding key proinflammatory cytokines were inhibited to a greater extent by R5A11D compared to IL-10 at the same subsaturating dose (**Figure 38** E). Overall, our transcriptional data show that IL-10 controls monocyte biology at different levels and that by exhibiting enhanced affinity toward IL-10R2, R5A11D elicits more robust responses at low ligand concentrations, thus suggesting that it may make IL-10–based therapies

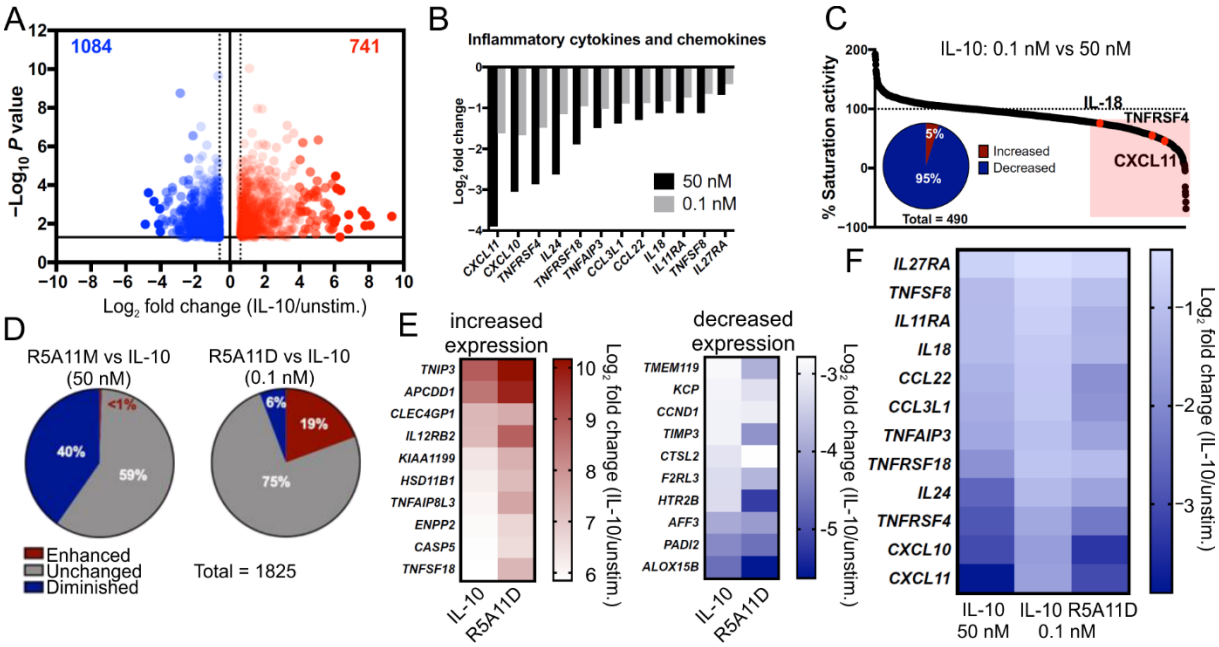

Figure 38: Changes in monocyte gene expression after IL-10 treatment. (A) Volcano plot of changes in gene expression in monocyte stimulated with 50 nM of IL-10. Only genes whose expression was significantly increased by IL-10 (≥ 0.6 log_2 fold change, red) or significantly decreased (≤ -0.6 log_2 fold change, blue) compared to non-stimulated cells were plotted. Fold change was calculated by dividing values of gene expression under stimulated condition by values of unstimulated for each donor. The average fold change was calculated and the log_2 of this value was plotted. P values were calculated by paired two-tailed t-test. **(B)** Log_2 fold change for a sample of inflammatory cytokine and chemokine genes after 50 and 0.1 nM IL-10 treatment, respectively. **(C)** Percentage activity of low dose (0.1 nM) compared to high dose (50 nM) IL-10. Genes which show ≤75% of high-dose activity (490 genes) are highlighted in red. Insert shows the percentage of these genes whose expression was increased or decreased by IL-10. **(D)** Comparison of the expression of monocyte genes in response to R5A11M (50 nM, left) or R5A11D (0.1 nM, right) and IL-10. Log_2 fold change of R5A11/unstimulated was divided by the log_2 fold change of IL-10/unstimulated. The proportion of genes that show enhanced expression (>1.5-fold change) are shown in red; the proportion of genes that show diminished expression (<0.67-fold change) are shown in blue; and genes that show similar responses under both ligands are shown in grey. **(E)** Heatmap of the log2 fold change of the top 10 genes whose expression was increased (left) or decreased (right) by 0.1 nM IL-10 compared to 0.1 nM R5A11D. **(F)** Heatmap of inflammatory cytokine and chemokine genes whose expression was inhibited by IL-10 at 50 and 0.1 nM and R5A11D at 0.1 nM. Monocytes from three donors were analyzed in (A) to (F).

4.2.3.5 Effect of engineered ligands on immunostimulatory IL-10 signaling response

In addition to its potent anti-inflammatory effects, IL-10 also stimulates cytotoxic CD8+ T cells under specific circumstances, thereby enhancing the production of effector molecules and increasing their cytotoxic activity [254]. We next investigated whether the enhanced activities exhibited by our affinity-matured variants in monocytes would translate into CD8+ T cells. Human primary CD8+ T cells were grown and activated, and the phosphorylation of STAT1 and STAT3 in response to the indicated concentrations of IL-10 variants was measured by flow cytometry (**Figure 39** A). IL-10 and R5A11D induced similar STAT phosphorylation levels at saturating doses, but R5A11D showed a decreased EC_{50} value and stronger signaling at subsaturating doses (**Figure 39** B), agreeing with our results in monocytes. R5A11D induced a more potent activation of STAT1 over STAT3, which we did not observe in monocytes, suggesting that long-lived IL-10R complexes are more effective at activating STAT1 in CD8+ T cells. mIL-10 produced weak activation of STAT1 and STAT3, inducing less than 25% of the activation amplitudes elicited by

the dimeric molecules, and exhibited a bias toward STAT3 activation (**Figure 39** A-C). In contrast to our observations in monocytes, R5A11M also elicited a STAT3-biased response, activating STAT3 to 80% of the levels induced by the dimeric molecules and STAT1 to 60% of the levels induced by the dimeric molecules (**Figure 39** A-C), suggesting that signaling downstream of the IL-10R complex differs between monocytes and CD8+ T cells. As with monocytes, the observed differences in signaling output by the different IL-10 ligands were not a result of altered signaling activation kinetics in CD8+ T cells (**Figure 39** D). Granzyme B is a potent cytotoxic effector molecule that is increased in CD8+ T cells upon IL-10 stimulation [255]. At saturating concentrations, IL-10 and R5A11D enhanced granzyme B production to a similar extent, 2.5-fold higher than granzyme B levels induced by TCR stimulation alone (**Figure 39** E). mIL-10 poorly induced granzyme B production, consistent with its weak STAT activation. At a subsaturating concentration, we again observed a stronger increase in granzyme B levels induced by R5A11D. R5A11M stimulation resulted in two major populations, with half of the cells expressing granzyme B at levels similar to those in mIL-10-treated cells and the other half showing increased granzyme B to levels comparable to those induced by the dimeric molecules. Overall, our results show that enhanced affinity for IL-10R2 bestows IL-10 with robust activities over a wide range of ligand doses and immune cell subsets.

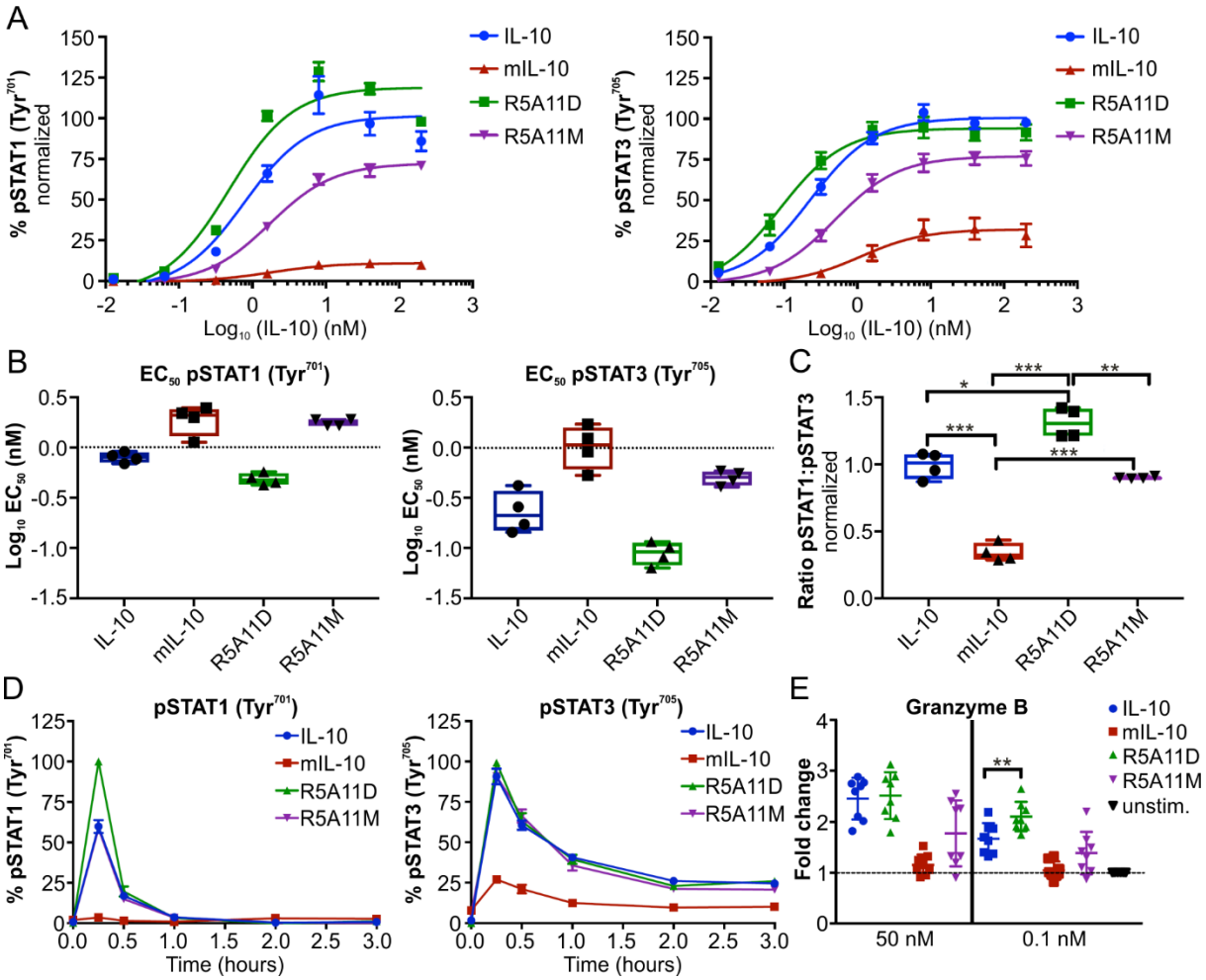

Figure 39: Activation of IL-10R signaling in CD8+ T cells. (A) Dose response curves for pSTAT1 (left) and pSTAT3 (right) in CD8+ cells that were stimulated with IL-10 variants for 15 min. Data shown are the mean of four biological replicates with error bars depicting SEM. Each biological replicate was normalized by assigning the highest MFI value of the top concentration as 100% and the lowest MFI value of an untreated control as 0%. **(B)** Log_{10} EC_{50} values for phosphorylated STAT1 and STAT3 from dose response curves in (A). **(C)** Ratio of pSTAT1 to pSTAT3 in CD8+ T cells stimulated by 40 nM of IL-10 variants. Ratios were calculated by dividing the percentage pSTAT1 value by the percentage pSTAT3 value of each biological replicate. Each data point represents a biological replicate with a line indicating the mean and error bars showing the minimum and maximum values. Statistical analysis: paired *t* tests; *, $P \leq 0.05$; **, $P \leq 0.01$; ***, $P \leq 0.001$. **(D)** Kinetic of pSTAT1 and pSTAT3 induced by IL-10 variants. CD8+ T cells were fixated after activation with IL-10 variants for the indicated time periods. Data was normalized as in (A). **(E)** Measurement of granzyme B protein abundance in activated CD8+ T cells (grown and stimulated as in (A)) in the presence of IL-10 variants. Granzyme B protein was quantified by flow cytometry of fixed and permeabilized cells. Fold change was calculated by normalizing to a non–treated control for each donor. Each data point represents a biological replicate (n = 8), and error bars indicate the standard deviation. Statistical analysis: paired *t* test; **, $P \leq 0.01$.

To obtain a greater understanding of how IL-10 influences CD8+ T cell responses, we next performed transcriptional studies on CD8+ T cells treated with the different IL-10 ligands. Human CD8+ T cells were purified by positive selection and activated in the presence of IL-10 and our variants over 6 days. Fewer transcriptional changes were induced by IL-10 in CD8+ T cells than in monocytes. 1050 genes were significantly changed, with 78% of those genes' expression being decreased by IL-10 treatment (**Figure 40** A). We observed that IL-10 induced a decrease in expression of genes classically associated with CD8+ T cell exhaustion (**Figure 40** C) and thereby may enhance CD8+ T cell activities by preventing their exhaustion. We also observed a significant

decrease of IL-2Rα by IL-10 treatment both at the mRNA and protein level [253], which was associated with a reduction of expression of IL-2 dependent genes, such as IL-13, LIF, SLC1A4, and NFIL3 [253, 256]. Our results suggest that IL-10 increases the cytotoxic activity of CD8+ T cells by limiting their sensitivity to IL-2. As with monocytes, subsaturating doses of IL-10 differentially affected a subset of genes whose expression was changed by IL-10, with the expression of most of those genes being decreased by IL-10 treatment (**Figure 40** B). At subsaturating doses, IL-10 failed to decrease the expression of classical IL-2 dependent genes like IL-13 and LIF to the same extent as the saturating dose, suggesting that inhibition of IL-2 activities by IL-10 requires high IL-10 doses (**Figure 40** C).

As seen for monocytes, R5A11M enhanced the transcriptional response when compared to mIL-10 but induced expression at levels below those induced by the dimeric ligands despite similar STAT signaling profiles (**Figure 40** D). 58% of the genes that showed altered expression in response to IL-10 were changed to a lesser extent by the high-affinity monomer R5A11M (**Figure 40** D). Similar to the results obtained with monocytes, R5A11D at 0.1 nM produced enhanced transcriptional responses compared to IL-10 at 0.1 nM, supporting its ability to act effectively at low concentrations (**Figure 40** D). 39% of the genes showed enhanced expression in response to R5A11D compared to IL-10 (**Figure 40** D), as reflected in the comparison of the top 10 genes with the greatest increase or decrease in expression in response to IL-10 and R5A11D at 0.1 nM (**Figure 40** E). Classical IL-2–dependent genes showed greater inhibition by R5A11D compared to IL-10 at this low concentration (**Figure 40** F). Together, our data confirms that IL-10 variants with enhanced affinity for IL-10R2 exhibit more robust activity at a wider range of ligand concentrations, which opens new avenues to boost IL-10–based anticancer immune therapies.

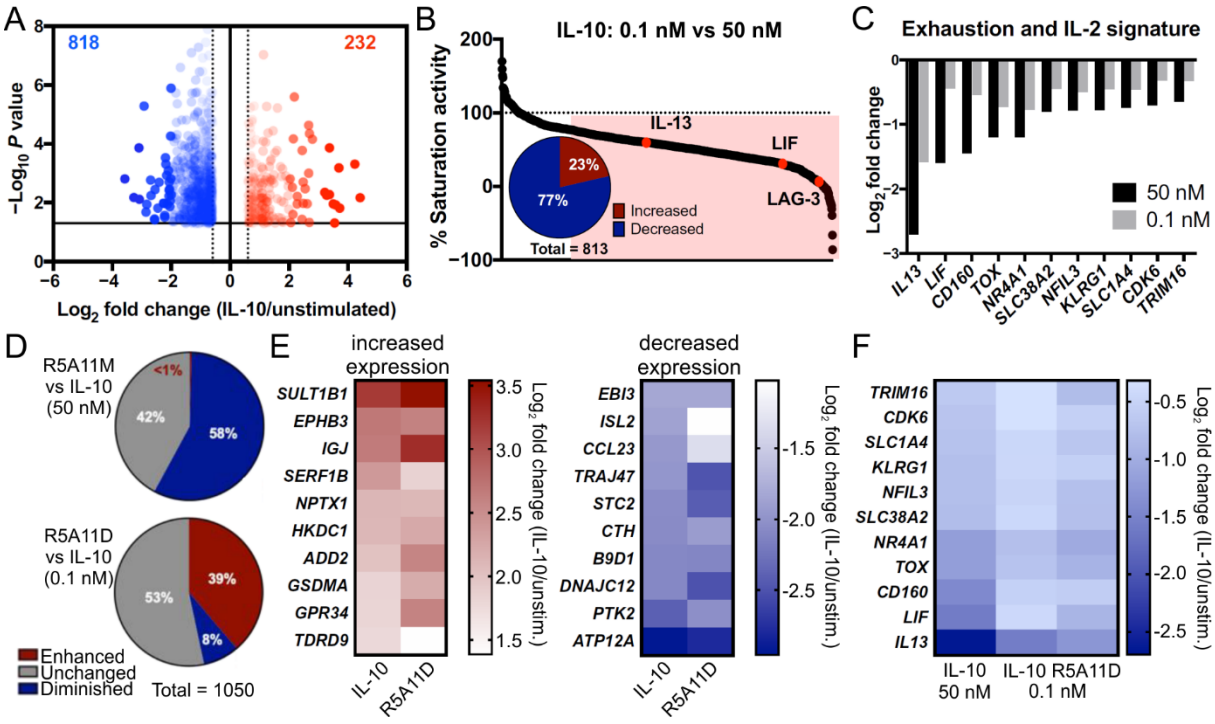

Figure 40: Changes in CD8+ T cells gene expression after IL-10 treatment. (A) Volcano plot of changes in gene expression in CD8+ T cells stimulated with 50 nM of IL-10. Only genes whose expression was significantly increased by IL-10 (≥ 0.6 log_2 fold change, red) or significantly decreased (≤ -0.6 log_2 fold change, blue) compared to non-stimulated cells were plotted. Fold change was calculated by dividing values of gene expression under stimulated condition by values of unstimulated for each donor. The average fold change was calculated and the log_2 of this value was plotted. P values were calculated by paired two-tailed t-test. **(B)** Percentage activity of low dose (0.1 nM) compared to high dose (50 nM) IL-10. Genes which show ≤75% of high-dose activity (813 genes) are highlighted in red. Insert shows the percentage of these genes whose expression was increased or decreased by IL-10. **(C)** Log_2 fold change for genes associated with CD8+ T cell exhaustion and IL2 stimulation after treatment with 50 and 0.1 nM IL-10, respectively. **(D)** Comparison of the expression of CD8+ T cell genes in response to R5A11M (50 nM, top) or R5A11D (0.1 nM, bottom) and IL-10. Log_2 fold change of R5A11/unstimulated was divided by the log_2 fold change of IL-10/unstimulated. The proportion of genes that show enhanced expression (>1.5-fold change) are shown in red; the proportion of genes that show diminished expression (<0.67-fold change) are shown in blue; and genes that show similar responses under both ligands are shown in gray. **(E)** Heatmap of the log2 fold change of the top 10 genes whose expression was increased (left) or decreased (right) in CD8+ T cells treated with 0.1 nM IL-10 compared to 0.1 nM R5A11D. **(F)** Heatmap of exhaustion or IL-2 associated genes whose expression was reduced after treatment with 50 and 0.1 nM of IL-10 and 0.1 nM of R5A11D. CD8+ T cells from three donors were analyzed in (A) to (F).

4.2.4 Contributions and publications

C. Gorby performed the IL-10 engineering studies in chapter 4.2.1 and 4.2.3. C. Gorby and P. K. Fyfe performed recombinant protein production and SPR binding measurements. C. Gorby, S. Wilmes and E. Pohler performed signaling and cellular experiments. C. Gorby performed RNA sequencing studies.

Publications

Gorby, C., J. Sotolongo Bellón, S. Wilmes, W. Warda, E. Pohler, P.K. Fyfe, A. Cozzani, C. Ferrand, M.R. Walter, S. Mitra, J. Piehler, and I. Moraga, *Engineered IL-10 variants elicit potent immunomodulatory effects at low ligand doses.* Sci Signal, 2020. **13**(649).

5 Conclusion

5.1 Mechanism of class II cytokine receptor assembly and activation

After decades of studies, both hexameric class II cytokine receptors, IFNGR and IL-10R, are known for their crucial role as immunoregulators. Despite fundamental understanding of key players of their signaling pathways and cellular responses, the mechanism of receptor assembly and activation are controversially debated. While originally for several cytokine receptor systems a ligand-induced two-step assembly was proposed, this view is challenged by models of pre-assembled receptor complexes which are activated by a conformational change upon ligand binding. These two opposing models probably stems from the fact that many prior studies relied either on *in vitro* experiments or on live-cell experiments conducted at non-physiological conditions, such as receptor over-expression or reporter probes that stabilize interactions. Accordingly, such experiments presumably give limited insights into the complex spatiotemporal dynamics of cytokine receptors in living cells. This thesis addressed this question by investigating class II cytokine receptor complex assembly *in cellulo* at physiologically relevant receptor expression levels with the least possible artificial intervention. Therefore, the submicroscopic localization and diffusion behavior of IFNGR and IL-10R were probed by multicolor single-molecule fluorescence microscopy combined with co-localization and co-tracking analysis.

Visualization of receptor complexes in wild type cells with fluorescently labeled cytokines confirmed a limited cell surface expression of type I and type II interferon receptors. Moreover, it underlined the requirement for single molecule microscopy to investigate cytokine receptor assembly under physiological conditions. In this respect, we developed an orthogonal protein labeling strategy based on GFP-tags and anti-GFP nanobodies, which achieved fast and efficient labeling in up to four spectral channels. Utilizing our labeling strategy in combination with single molecules TIRF microscopy we investigated diffusion and interaction of single cytokine receptor subunits in the plasma membrane of living cells in real time. This analysis revealed that IFNGR and IL-10R subunits remain monomeric on the cell surface in absence of ligand and only after ligand binding persistent receptor complexes are assembled, verifying the ligand-induced receptor complex assembly model for both cytokine receptors. As this ligand-induced receptor assembly mechanism has been shown to apply to several hetero-dimeric [59, 69, 208] and homo-dimeric [188, 257] cytokine receptors, we are convinced, that this is the common mechanism throughout the entire family of class I/II cytokine receptors.

We observed above all substantial homo-dimerization of the binding subunit, but also receptor hetero-dimerization, whereas the homo-dimerization level of the accessory subunit was distinctly lower. Four-color single molecule co-localization and co-tracking of IFNGR showed a similar dimerization pattern as well as simultaneous interaction of two IFNGR1 and one IFNGR2.

Unfortunately, we could not detect simultaneous interaction of two IFNGR1 and two IFNGR2. One possible explanation could be that the number of hexameric complexes on the cell surface is quite low, as indicated by the low IFNGR2 homo-dimerization, and therefore hexameric receptor complexes carrying on each dye are unlikely to encounter. Furthermore, our experiments were conducted in wild type HeLa cells, which express endogenous IFNGR2 on their cell surface and thus further decreases the probability to observe receptor hexamers. Based on these observations, we developed a model for IFNGR and IL-10R assembly on the cell surface, in which homo- and heterodimerization of the monomeric receptor subunits is initiated by ligand binding to the high affinity binding receptor subunit, followed by lateral recruitment of further binding and accessory receptor subunits. In the last step, a second accessory receptor subunit is recruited to complete the hexameric receptor complex containing a dimeric ligand and two of each binding and accessory receptor subunit. Crystal structure of whole extracellular receptor complexes [57, 78] and single molecule FRET analysis supported our model. The crystal structure of the IFNGR complex revealed that IFNGR2 binds to a composite interface formed by the high affinity IFNγ-IFNGR1 interaction; hence, both IFNγ and IFNGR1 are required for IFNGR2 to be recruited into the receptor complex. Recently, the crystal structure of the IL-10R complex was resolved, revealing an identical binding mode for IL-10R2, but a twisting of cytokine subunits, which translates into ~90° rotation and large intermolecular angle between both IL-10R1 resulting in a larger distance between both IL-10R1-IL-10R2 heterodimers and an over-all flatter conformation [57]. The complex structures of IFNGR and IL-10R have pointed out a strong resemblance between their ternary complexes, that is one of each receptor subunit dimerized by the ligand, and the ternary complex of type III IFN receptor (IFNLR) [189], which in contrast to the hexameric class II cytokine receptors does not bind dimeric cytokines and hence assembles into ternary complexes only.

Patients with IFNγ signaling disorders often suffer from Mendelian Susceptibility to Mycobacterial disease (MSMD) syndrome. Homozygous T168N mutation in IFNGR2 is a prominent cause of MSMD, that has been shown to induce an additional glycosylation at the new Asparagine residue [225]. In the past Lamaze and colleagues have postulated that this new glycosylation affects partitioning of IFNGR in lipid and actin nanodomains hence impeding activation of JAK/STAT downstream signaling [197]. Using single molecules localization and tracking microscopy we did show that this additional glycosylation at 168N prevents IFNGR2 from binding to the IFNGR complex, which consequently prevents downstream signaling. Similarly, newly discovered anti-IFNγ autoantibodies (AIGAs) have been associated with MSMD [226]. While examining the effects of isolated AIGAs on IFNGR complex assembly on the surface of living cells we found that AIGAs with neutralizing effects on IFNγ signaling presumably block IFNGR2 recruitment into the IFNGR complex in a similar fashion to the T168N mutant but by antibody binding to the IFNGR2 binding site.

5.2 Role of hexameric receptor complexes in IFNGR and IL-10R signaling

In the past recombinant monomeric IFNγ and IL-10 have been proven to activate IFNGR and IL-10R signaling and induce STAT1 and STAT3 phosphorylation respectively, questioning the relevance of hexameric receptor complexes for signaling activation and regulation. By testing receptor hetero- and homo-dimerization, we verified that those monomeric cytokines induced ternary complexes only as intended. Knowing the IFNγ-IFNGR interfaces we designed partial agonists to test the effect of intermediate receptor complexes on signal transduction and cellular response. Our analysis pointed out a redundancy of the second IFNGR2 subunit in signal activation, as our agonist lacking one IFNGR2 binding site achieved a similar STAT1 phosphorylation kinetic and amplitude as the wild-type ligand. However, agonists recruiting two IFNGR1 subunits exceeded the monomeric IFNγ in STAT1 phosphorylation amplitude despite supposedly similar IFNGR1 saturation by the agonists. A similar observation was made for IL-10R when we stimulated with monomeric IL-10, but in this case the difference in STAT phosphorylation was even larger. We hypothesized that the very limited number of receptor complexes containing two accessory receptor subunits did not considerably contribute to the over-all cellular response, but the second binding receptor subunit does strongly enhance the STAT phosphorylation capability of the receptor complex. Our data suggest that all four associated JAKs potentially interact and activate each other in the receptor complex, rather than just the JAKs belonging to a ternary complex as in the conventional models. A possible interpretation of our findings could be that JAK1 presumably contributes stronger to STAT phosphorylation than JAK2 or TYK2. An alternative interpretation could be that STAT phosphorylation is limited by recruitment of STATs to the receptor complexes rather than kinase activity. Recruiting a second binding receptor subunit provides an additional STAT binding site to the receptor complex. In either case the STAT phosphorylation rate is limited by how many binding subunits have access to an accessory receptor subunit associated JAK2. Nevertheless, any further interpretations would require deeper understanding of JAK phosphorylation and STAT recruitment kinetics.

5.3 Implications of receptor mobility and diffusion for signaling

Mobility and diffusion analysis revealed a comparable diffusion coefficient for all receptor subunits but IL-10R2 in the plasma membrane. In absence of ligand single cytokine receptor subunits diffused freely throughout the cell surface. After ligand stimulation the diffusion constant was drastically reduced, and the fraction of immobile receptor subunits grew. This phenomenon has been repeatedly observed for other cytokine receptors [59, 188] and attributed to the plasma membrane organization and receptor endocytosis. At the current state plasma membrane organization is subdivided into two distinct components: lipid-dependent arrangement into nanodomains, which are often termed as “lipid rafts”, and confinement by the actin meshwork of

the membrane skeleton [258]. Despite the controversial discussion about the existence of lipid nanodomains, in the past they have been suggested to be necessary for internalization and activation of IFNGR [197, 207]. By contrast, the effect of the actin meshwork on the plasma membrane and embedded proteins has been described in much more detail by the "fence and picket" model [259]. The submembraneous actin filaments resemble fences that form "corrals" with diameters of tens to hundreds of nanometers, whereas many membrane proteins connected to the actin filaments represent the pickets that hold the structure. Within the corrals membrane proteins may diffuse unhindered, while "hopping" between corrals is much more unlikely, thereby constraining membrane protein diffusion in plasma membranes compared to artificial membranes. Receptor assembly is accompanied by an increase in size of the protein structure and hence hopping becomes less likely leading to a decrease of diffusion constant. Accordingly, the diffusion constant of IFNGR and IL-10R ternary complexes induced by monomeric ligands was reduced compared to the monomeric receptor subunits but was still significantly higher than the diffusion constant of hexameric receptor complexes. A similar picture was drawn by the diffusion of endogenous receptors labeled by IFNα2 and IFNγ, which was governed by different actin corral sizes in different cell lines resulting in a comparable diffusion profile for both receptors, whereas the potentially larger IFNGR complex diffused in general slower than IFNAR.

Ligand stimulation was accompanied by an increase in prolonged receptor immobilization at the plasma membrane, which could be ascribed to receptor endocytosis. In contrast, stimulation with monomeric ligands failed to induce receptor immobilization, proposing a potential role of receptor hexamerization in enabling efficient receptor endocytosis. Lately, the role of receptor endocytosis in regulation of cytokine receptor signaling has arisen great interest, as an increasing number of studies are suggesting further functions for endocytosis beyond the original idea of a master switch to turn off cellular responsiveness and receptor signaling. Prior studies from Lamaze and colleagues have shown that in contrast to IFNAR the IFNGR dependent phosphorylation of STAT1 is not affected by inhibition of receptor endocytosis [207] hence proposing that endocytosis does not control IFNGR signaling activation. Nonetheless, receptor endocytosis could fulfill other regulatory functions during IFNGR signaling, such as tuning strength and duration of cellular response, which will require more investigation before we might be able to understand it.

Cell surface IL-10R2 did show a strong intensity of intermittent immobilization that is unique among the receptor subunits studied in this work and resembled the stimulation-induced temporary arrest of lateral (STALL) diffusion of GPI-anchored receptor clusters [232]. By creating receptor truncations, we traced the origin of the STALL-like diffusion and identified primarily the transmembrane domain (TMD) of IL-10R2 to be responsible for this behavior. Furthermore, we noticed that the TMD of IL-10R2 is above-average large with 33 amino acids. Confining the size of the TMD by introducing charged residues at either side of the TMD had major impact on the

STALL-like diffusion of IL-10R2, even restoring normal diffusion for one mutation. We hypothesized that the conspicuous size of the TMD allows IL-10R2 to switch between different orientations within the plasma membrane and some of which are unfavorable and disallow lateral diffusion. This degree of freedom may to be required for the functionality of IL-10R complex, as the crystal structure indicates a very flat complex structure and especially a low-angle membrane entry of IL-10R2. Remarkably, this unique diffusion behavior might be decisive for IL-10R signaling, as IL-10R complexes adapt this trait after assembly whereas IFNLR complexes do not. However, the data presented in this thesis for STALL-like diffusion of IL-10R2 is primarily qualitative and a robust quantitative analysis of STALL length and frequency is still required to really compare and assess the significance of this abnormal diffusion behavior in IL-10R signaling.

5.4 Mechanism of controlling class II cytokine receptor signaling pleiotropy

Understanding the mechanism of signaling pleiotropy of class II cytokine receptors has kept cytokine science busy for decades, also because it could release enormous potential for clinical applications. If we can differentially activate desired cellular responses of a cytokine receptor's signaling repertoire, we will be able to design drugs for specific therapies. Viruses have shown us how it is done by evolving IL-10 homologs that exploit the signaling pleiotropy by activating just a selection of immunosuppressive genes and allowing the virus to bypass immune surveillance. Using our single molecule co-localization and co-tracking approach, we verified a correlation between reduced binding affinity of the viral IL-10 homologs and an observed reduction in receptor dimerization levels at the cell surface despite significantly higher ligand concentrations. Based on this principle, in the past binding affinities of receptor-cytokine interactions have been modified on several occasions, including members of the class II cytokine receptors, which have led to altered cellular signaling [59, 189]. We engineered IFNγ and IL-10 variants with altered receptor binding affinities to investigate the mechanism of signaling pleiotropy in class II cytokine receptors. Thereby we found that altering the binding kinetics of the receptor-ligand interaction would expectedly translate into differential receptor dimerization levels on the cell surface. Strikingly, this differential dimerization levels could be used to decouple pleiotropic cellular responses of IFNGR and IL-10R. Recently, Garcia and colleagues made similar observations on IL-10R and the closely related IL-22R by creating engineered cytokine variants [57, 190]. This increasing number of studies suggest that signaling plasticity and pleiotropy of cytokine receptors being controlled by the degree of receptor activation or rather receptor complex assembly at the cell surface might be a common mechanism of class I/II cytokine receptors. However, more interesting might be the question how this mechanism is used by the organism as both IFNGR and IL-10R do only have a single ligand to induce pleiotropic signaling. One simple explanation could be that the surface expression of at least one receptor subunit is tightly regulated to limit the level of receptor dimers despite ligand abundance, which was already observed for IFNGR2 [95]. In this context, receptor

trafficking and recycling could play a central role in achieving this regulation. This could be particularly relevant for signaling studies, as they are often performed under artificial receptor expression.

5.5 Limitations and future perspectives

The results presented in this thesis were obtained primarily by single molecule co-localization and tracking microscopy. Although single molecule localization microscopy offers in practice a lateral resolution of up to 20 nm and below for a single channel, robust co-localization of two channels required a co-localization search radius of 100 – 150nm. Conversely, single molecule co-localization microscopy alone cannot be used to resolve single receptor subunit interactions below this range. Single molecule Förster resonance energy transfer (smFRET) methods, such as donor recovery after acceptor bleaching and alternate excitation FRET, are frequently used to overcome this limitation. However, these methods contain own limitations, which must be carefully considered. For instance, receptor complexes might exceed the typical Förster radius ~6-8nm in size, requiring cumbersome site-specific labeling strategies to enable FRET in the first place. Instead, we used the additional temporal correlation from single particle tracking to discriminate particle density-based random co-localization from actual receptor dimers at the cell surface. Essentially, co-localization events persisting for more than 300ms represented real receptor dimers, which we assessed experimentally. Conversely, it must be noted that transient interactions below that time limits would potentially slip through our analysis. Thus, we cannot exclude very transient interactions in absence of ligand with certainty. But also, as both receptor subunits directly interact in the receptor complex via stem-stem contact, we expect them to undergo such very transient interactions, which are not sufficiently stable to activate downstream signaling.

Furthermore, the receptor subunits investigated in this thesis, IFNGR1, IFNGR2 and IL-10R2, are endogenously expressed in HeLa cell line. Therefore, we expected an unknown fraction of unlabeled receptor molecules in the background of our experiments, that still would interact with the labeled receptor subunits and be recruited inside the receptor complex, thereby reducing the apparent dimerization rate and the dynamic range of the analysis. To further improve our single molecule localization and tracking microscopy method, we would need to eliminate unlabeled receptor subunits. An elegant way to do so would be tagging of endogenous receptors using genome editing methods such as CRISPR/cas9 [260]. One benefit of this idea would be that thereby we avoid any kind of additional expression and concomitant effects. However, the endogenous receptor expression could exceed the particle density acceptable for single molecule tracking, hence simply knocking out and transfecting the desired receptor subunits could be less risky.

We have presented a model of class II cytokine receptor assembly clearly showing complex assembly to be induced by ligand stimulation. A prominent change in mobility and diffusion after

ligand stimulation proposed possible involvement of membrane organization and receptor endocytosis in regulation and activation of class II cytokine receptors. In this sense, future experiments should focus much stronger on receptor trafficking to better understand how cytokine signaling is regulated in cells. As the size of membrane vesicles and some early endosomal structures fall below a few hundred nanometers, receptors inside these structures will be diffraction limited and single molecule tracking will be insufficient to explore them. At the same time, as trafficking receptors depart from the plasma membrane, a versatile microscopy method with good 3D resolution and fast acquisition speed, such as lattice light sheet microscopy, will be needed to explore these processes in living cells.

The here presented partial agonist could be used to further investigate the impact of different receptor sizes on diffusion and subsequently on receptor endocytosis. If we further combine it with receptor truncations, we would be able to explore the effect of kinase and effector binding on the diffusion behavior of cytokine receptors, possibly helping us to understand its significance for class II cytokine receptor signaling.

6 Materials and Methods

6.1 Molecular biology

Preparation of mammalian expression vectors. Class II cytokine receptors were expressed in human cell lines using a modified plasmid cassette based on pSems-26m (Covalys Biosciences) vector. Therefore, cloning cassettes already existing in our group [59] were adjusted to the class II cytokine receptors used in this work. Human cytomegalovirus (CMV) enhancer and promoter were used to express the desired gene in human cell lines. All cytokine receptor constructs contained N-terminally an Ig-κ signal peptide, to target the protein to the plasma membrane, and an HA-tag. This signal sequence was followed by a non-fluorescent mEGFP derivative (mXFPm, mXFPe). C-terminally to this tag the desired receptor sequence lacking its specific signal peptide was added. Mammalian expression vectors (Table 1) were cloned via conventional restriction digest and ligation in *E.coli*. Desired restriction sites were added to the gene of interest by PCR with specifically designed oligo nucleotides.

Table 1: List of plasmids used to express tagged receptors in HeLa cells.

Denomination	Construct (residues)	Description
mXFPm-IFNGR1	pSems leader-seq.-mXFPm-IFNGR1 (18-489)	mXFPm-tagged IFNGR1 used in single molecule microscopy
mXFPm-IFNGR1-F05	pSems leader-seq.-mXFPm-IFNGR1-F05 (18-489)	Affinity increased IFNGR1 (T149I, M161K, Q167K, K174N, Q182R, H205N)
mXFPe-IFNGR2	pSems leader-seq.-mXFPe1-IFNGR2 (30-337)	mXFPe-tagged IFNGR2 used in single molecule microscopy
mXFPe-IFNGR2(T168N)	pSems leader-seq.-mXFPe1-IFNGR2-T168N (30-337)	Gain of N-glycosylation mutant of IFNGR2
mXFPe-IFNGR2(T168N, T170A)	pSems leader-seq.-mXFPe1-IFNGR2-T168N-T170A (29-337)	IFNGR2-T168N mutant with disrupted glycosylation motif
mXFPm-IL-10R1	pSems leader-seq.-mXFPm-IL-10R1 (21-578)	mXFPm-tagged IL-10R1 used in single molecule microscopy
mXFPe-IL-10R2	pSems leader-seq.-mXFPe1-IL-10R2 (19-325)	mXFPe-tagged IL-10R2 used in single molecule microscopy
mXFPe-IL-10R2-delECD	pSems leader-seq.-mXFPe1-IL-10R2 (210-325)	IL-10R2 truncation lacking the extracellular domain
mXFPe-IL-10R2-delICD	pSems leader-seq.-mXFPe1-IL-10R2 (19-250)	IL-10R2 truncation lacking the intracellular domain but not TYK2
mXFPe-IL-10R2-delTYK2	pSems leader-seq.-mXFPe1-IL-10R2 (19-244)	IL-10R2-delICD additionally lacking the TYK2 binding motif
mXFPe-IL-10R2-TMD	pSems leader-seq.-mXFPe1-IL-10R2 (210-250)	IL-10R2 truncation lacking both ECD and ICD
mXFPe-IL-10R2-CC	pSems leader-seq.-mXFPe1-IL-10R2-C241A-C247A (19-325)	C → A replaced in full-length IL-10R2
mXFPe-IL-10R2(A224K)	pSems leader-seq.-mXFPe1-IL-10R2-A224K (19-325)	Extracellularly constrained TMD of full-length IL-10R2

mXFPe-IL-10R2(A243K)	pSems leader-seq.-mXFPe1-IL-10R2-A243K (19-325)	Intracellularly constrained TMD of full-length IL-10R2

Polymerase chain reaction (PCR) was primarily used to add missing restriction sites to the sequence of a specific gene. Alternatively, it was used to create specific point mutation by performing whole-plasmid PCR with a complementary primer pair. Primers were designed based on the DNA sequence to bind specific to the region of interest with 15-20 base pair homology. Whole-plasmid primers were designed with 30-40 base pair homology. PCR was performed as indicated by manufacturers protocol. Master mix was prepared for each sample individually as indicated in Table 2. 5X Q5 High GC Enhancer was used if the PCR product had a GC content higher than 60%. This master mix was split into three 50 µl samples and subjected to standard PCR using Phusion High-Fidelity DNA Polymerase (NEB): Initial denaturation (60s at 98°C); 30 cycles of denaturation (10s at 98°C), primer alignment (30s at 50°C, 55°C and 60°C), elongation (30s per kb at 72°C); final elongation (10min at 72°C). Afterwards, agarose gel electrophoresis was performed to separate and purify DNA fragments.

Table 2: PCR master mix

Compound	**Volume**	**Company**
5X Q5 Reaction Buffer	30 µl	NEB
2mM dNTPs	15 µl	NEB
5X Q5 High GC Enhancer	30 µl	NEB
DMSO	4.5 µl	NEB
Forward Primer (100 nM)	0.75 µl	Merck
Backward Primer (100 nM)	0.75 µl	Merck
DNA template	<1000 ng	n/a
Q5 High-Fidelity DNA Polymerase	1.5 µl	NEB
H_2O	Fill up to 150 µl	n/a

Agarose gel electrophoresis and gel extraction. DNA containing samples from PCR or enzymatic digest were separated in length by agarose gel electrophoresis. Agarose gels were prepared by diluting 1% agarose (Sigma Aldrich) in TAE buffer (40 mM Tris, 40 mM acetic acid, 1 mM EDTA, pH 8.0) and heating it up, until the buffer was clear. For DNA fragments shorter than 500 base pairs 1.5% agarose gels were used. For DNA fragments larger than 4000 base pairs 0.5% agarose gels were used. The hot agarose solution was cooled in a chamber until it solidified. For DNA visualization 5µl of 0.5% ethidium bromide (Roth) were added to 50 ml gel. DNA samples were diluted 6:1 with Gel Loading Dye Purple (6x) (NEB) and subjected to gel electrophoresis. DNA

bands were visualized on a UV table and gel slices containing the bands of interest were cut off with a scalpel and purified using Monarch DNA Gel Extraction Kit (NEB). NanoDrop 2000 (ThermoScientific) was used to identify the concentration of the purified DNA.

Restriction digest. DNA was digested using suitable restriction enzyme pairs (NEB). If available, the high-fidelity version of the enzyme was used. 5µg plasmid DNA or the entire PCR product were mixed with 1 µl of each restriction enzyme, 1 µl of 10x CutSmart buffer (NEB) and filled up with H_2O to a total volume of 10 µl. This sample was incubated at 37°C for 90 min, after 75 min 1µl of quick CIP (NEB) was added to the vector only, to dephosphorylate DNA ends and prevent rebinding of vectors. Subsequently, digested DNA samples were subjected to agarose gel electrophoresis as described previously.

Ligation. After gel extraction, purified DNA fragments were ligated to obtain intact plasmids. Therefore, 1µl of vector DNA, 5µl of insert DNA, 1µl of T4 DNA Ligase (NEB), 1µl of T4 DNA Ligase buffer (NEB) and 2 µl H_2O were mixed and incubated at room temperature for a minimum of 2 hours or overnight. The ligation sample was transformed into *E.coli* DH5a strain as described in the next section.

***E.coli* Transformation and plasmid amplification.** Plasmid amplification was performed in chemically competent *E.coli* DH5α strain (Invitrogen/ ThermoFisher) provided by G.Hikade from the Biophysics Lab, University of Osnabrück. Chemically competent cells were taken from -80°C storage just before transformation and kept on ice during the process. 1 µL of a plasmid containing sample (DNA concentration < 1µg/µL) or ligation sample was added to 60µL of competent DH5a and incubated on ice for 20 minutes. Afterwards 90 second heat-shock at 42°C was performed. Subsequently, DNA-containing cells were incubated on ice for 5 minutes, to entirely cool down the sample and complete the heat-shock. If transformation was performed after ligation, or if the plasmid's selection marker was kanamycin, a phenotypical expression was done afterwards. Therefore, 1 mL of LB medium was added to the sample and cell were incubated for at least 30 minutes at 37°C without any selection marker. This ensures that successfully transformed DH5a express the resistance gene before being plated on an agar petri dish containing the corresponding antibiotics. These agar plates were incubated over night at 37°C to allow colonies to grow. At the following day at least two colonies were picked from the plates, and each inoculated into 10 mL of LB medium containing the respective selection marker as well as on a new selective agar plate as back-up and incubated at 37°C overnight (medium on a shaker). At the following day 10 ml culture were harvested by centrifuge (5000 g, 15 min) and plasmids were extracted using QIAprep Spin Miniprep Kit (QIAGEN). Exact DNA sequence was verified by sequencing (Microsynth sanger sequencing). Correct clones were amplified in a 100 ml culture according to the 10 ml cultures and purified using NucleoBond Xtra Midi (Macherey-Nagel GmbH).

6.2 Protein purification and labeling

Purification and fluorescence labeling of His6-tagged nanobodies. Competent *E.coli* Rosetta (DE3) pLysS cells (Novagen) were transformed with plasmids encoding for NBs. Cells were grown at 37°C in LB medium supplemented with 100 µg·mL^{-1} ampicillin until an OD_{600nm} of 0.6 - 0.8 was reached, when protein expression was induced by the addition of 0.8 mM IPTG followed by overnight culturing at 18°C. Cells were pelleted by centrifugation, resuspended in HEPES-buffered saline (HBS – 20 mM HEPES pH 7.5, 150 mM NaCl) supplemented with DNAse, lysozyme and protease inhibitors and lysed by sonification. After ultracentrifugation (55.000 x g, 25 min, 4°C, Type 70 Ti, Beckman Coulter), the supernatant was applied to an IMAC (5 mL HiTrap Chelating HP, GE Healthcare) by an FPLC system (ÄKTAprime, GE Healthcare). Proteins were eluted by a linear gradient with HBS buffer containing 500 mM imidazole. Collected NB-containing fractions were then fractionated by size exclusion chromatography (SEC) using a Superdex 75 Increase 10/300 GL column (GE Healthcare) in HBS buffer.

Site-specific fluorescence labeling of the NBs was conducted with a two-fold excess of maleimide-fluorophore conjugates (diluted from 10 mM DMSO stocks) for 30 min at room temperature. The reaction was stopped by addition of a three-fold excess of cysteine over the fluorophore and further incubation for 15 min, followed by SEC under the same conditions as described above. The degree of labeling (DOL) of all fluorophore-conjugated nanobodies was determined by UV/Vis spectroscopy using published (fluorescent dyes) or calculated (proteins) extinction coefficients and correction factors. Labeled and unlabeled nanobodies were flash-frozen in liquid nitrogen and stored at -80°C until use.

Expression, refolding, and purification of IFNγ and mIFNγ. Dimeric and monomeric IFNγ were expressed in *E. coli,* refolded, and purified, as previously described [261]. Briefly, cells were grown in LB medium to an absorbance of 0.6 at 600 nm and then induced with 1 mM IPTG for 3 h. Inclusion bodies were isolated and solubilized in 8 M guanidine hydrochloride. Refolding was performed by rapid dilution into 10 mM ammonium acetate buffer (pH 7.0) containing 2.5 mM EDTA and 5 mM benzamidine. The proteins were purified by ion exchange chromatography (HS20 resin, ThermoFisher), followed by size exclusion chromatography (Superose 6, GE Healthcare).

Production and labeling of IFNγ cysteine mutant. IFNγ S66C was produced and purified as the wt. 45 µM of IFNγ S66C were mixed with 105 µM of maleimide functionalized DY-647P1 (Dyomics GmbH) to a final volume of 500 µL and incubated for 45 min in the absence of light at room temperature. Subsequently, the reaction was terminated by addition of L-cysteine (Sigma) at a final concentration of 300 µM and incubation for 15 min under the same condition. Unreacted dye was removed by size exclusion chromatography (Superdex 75 Increase 10/300 GL, GE Healthcare). The DOL of DY-647P1-labeled IFNγ S66C ($^{DY-647}$IFNγ) was estimated using

absorption spectroscopy. The $^{DY\text{-}647}$IFNγ-containing aliquots were shock frozen in LN for long-term storage at -80°C.

6.3 Cell culture

Culturing, passaging, and seeding. HeLa cell line (company) were cultivated in 75T-flasks containing MEM medium supplemented with 10% FCS, HEPES and non-essential amino acids (MEM+). After 3-4 days of growing in 37°C and 5% CO_2 cells reached confluency and were passaged. During this process cells were washed 1-2 times with 5 ml PBS (company) and detached from the T-flasks by incubating with 1 ml Trypsin/EDTA (company) for approximately 5 minutes. Subsequently, the cell suspension was diluted with 5 ml MEM+ to block Trypsin reaction. 1 ml of the cell solution was passed into a new T-flasks containing 5 ml fresh MEM+. If cells should be transfected 300µl – 500µl of the cell solution was passed into a 6cm dish and filled up with 5 ml MEM+.

Transfection. Mammalian cell lines were transfected with mammalian expression vectors either by calcium phosphate precipitation or PEI transfection. For calcium phosphate precipitation cells were prepared as described in 0 a day prior to transfection. Just before transfection cells were washed with 5 ml PBS and supplied with 5 ml fresh MEM+. 5 – 10 µg of DNA were added to 50 µl x mM $CaCl_2$ solution and mixed thoroughly before adding H_2O to a final volume of 500 µl. This solution was added dropwise under constant vortexing into 500 µl HBS (pH 6.95). Subsequently, DNA containing HBS solution was applied dropwise to a 6 cm dish containing cells at 60-80% confluency and incubated 8 – 16 hours at 37°C 5% CO_2. Afterwards cells were washed 4-5 times with 5 ml PBS.

Cells were prepared for PEI transfection as described above. 1.5 µg DNA of each plasmid needed was added to 300 µl 150 mM $NaCl_2$ solution and vortexed for 1 minute. Subsequently, 10 µl PEI solution was added to the DNA and vortexed for 1 minute. This mixture was incubated at room temperature for 15 min before adding it dropwise to a 6 cm dish containing cells at 40-60% confluency. After applying the transfection solution Cells were incubated at 37°C 5% CO_2 for 4-6 hours. Afterwards cells were washed 1-2 times with 5 ml PBS.

6.4 Microscopy

Sample preparation and labeling. For microscopy experiments cells were grown on 25mm high precision glass cover slides (company) coated with Poly-L-Lysine-graft-Poly(ethyleneglycol) functionalized with RGD peptide to enhance cell binding to the surface. Glass cover slides were plasma cleaned (company). Afterwards 8 µl of 1 µg/ml PLL-PEG-RGD were added on a cleaned cover slide and covered with another cleaned cover slide in a sandwich-like way. After 1 hour of

incubation at room temperature residual PLL-PEG-RGD was washed off with H_2O. Ready-to-use cover slides were dried with nitrogen gas and stored at -20°C for later use.

At least 4 hours before performing the microscopy experiments cells were seeded on a PLL-PEG-RGD coated cover slide as described before.

Single-molecule localization microscopy. Single-molecule imaging was carried out by total internal reflection fluorescence microscopy (TIRFM) using an inverted microscope (IX83-P2ZF, Olympus) equipped with a motorized quad-line TIR illumination condenser (cellTIRF-4-Line, Olympus). The dyes ATTO 488, ATTO Rho11, DY-647P1/ATTO 643 and DY-752 were excited using a 100× oil immersion objective (UPLAPO100XOHR, NA 1.5, Olympus) at 488 nm (LuxX 488-200, max. 200 mW, Omicron), 561 nm (2RU-VFL-P-500-560-B1R, MPB Communications), 642 nm (2RU-VFL-P-500-642-B1R, MPB Communications) and 730 nm (LuxX 730-50, max. 50 mW, Omicron), respectively. Fluorescence was filtered by a penta-band polychroic mirror (zt405/488/561/640/730rpc, Semrock) and excitation light was blocked by a penta-band bandpass emission filter (BrightLine HC 440/521/607/694/809, Semrock). Up to four channels could be simultaneously acquired by using the four quadrants of a single back-illuminated EMCCD camera (iXon Ultra 897, Andor Technologies) and a four-color image splitter (QuadView QV2, Photometrics). The latter is equipped with three dichroic beamsplitters at 565 nm, 630 nm, and 735 nm (T565LPXR, 630 DCXR and 735DCXR, Chroma) and four single-band bandpass emission filters (BrightLine HC 520/35, BrightLine HC 809/81, Semrock; ET 600/50, ET 685/50, Chroma). For dual channel imaging, only the orange (ATTO Rho11) and red (Dy647-P1/ATTO 643) channel were acquired. To obtain a pixel size of 100 nm, an additional 1.6x magnification was introduced (IX3-CAS, Olympus). The focus was continuously stabilized during the experiment by a hardware autofocus-system (IX3-ZDC2, Olympus) using an internal laser diode at 830 nm.

Four-color experiments required a fast in-frame alternate excitation scheme, since simultaneous excitation of ATTO488 and cyanine dyes (DY647P1/ATTO643, DY-752) resulted in high photo-bleaching rates of the far-red dyes (Fig. S5b). We therefore established a camera-based alternate triggering mode using two function generators directly linked to the laser sources for ultra-fast on/off switching. Here, the rising edge of the camera exposure signal (TTL signal from camera) serves as the master trigger for the first function generator (HMF2525, Hameg) to pulse the 561 nm, 642 nm, and 730 nm laser lines simultaneously. We typically use a burst of 15 short pulses (1 ms high (laser on)/1 ms low (laser off)) within a single 33 ms long frame. The falling edge of these pulses are triggering a second function generator (AFG-2225, GW Instek) pulsing the 488 nm laser with the same high/low signal. The trigger signals for the 488 nm and the 730 nm laser are directly linked to the electronic shutter of the laser heads shutting down the laser output in less than 2 µs. The 560 nm and the 642 nm laser are switched within < 1µs via an acousto-optical tunable filter

(TF525-250-6-3-GH18A, Gooch & Housego) linked to an eight-channel digital frequency synthesizer (MSD040-150-0.2ADM-A5H-8X1, Gooch & Housego).

In all imaging experiments, an oxygen-scavenging system composed of glucose oxidase (4.5 $U \cdot mL^{-1}$), catalase (540 $U \cdot mL^{-1}$) and glucose (4.5 $mg \cdot mL^{-1}$) was added to increase photostability. Additionally, a photoprotectant redox system composed of ascorbic acid and methyl viologen (both 1 mM) was applied [218]. For each channel, penetration depth of the evanescent field as well as laser excitation intensities (typically 50-500 W/cm²) were optimized to obtain comparable signal to background levels in each channel (Fig S8). Viable cells showing typical surface densities of 0.1-0.8 copies/µm² (Fig. S8) were imaged at 30 frames per second for typically 150 consecutive frames using CellSens 2.2 (Olympus) as acquisition software. For quantifying the DOL by smFRET, frame-by-frame alternating excitation at 642 nm and 560 nm lasers was employed in combination with dual-color image acquisition of donor and acceptor fluorescence by using the image splitter and filters mentioned above.

6.5 Data Evaluation and Statistical Analysis

Single molecule data evaluation. Dual- and quad-color raw images were evaluated using an in-house developed Software for Localization-based Imaging in MATLAB. SLIMfast was used to capture individual protein-protein interaction events by single molecule (co-)localization and (co-)tracking as well as analyze their diffusion behavior.

For channel registration, 200 nm TetraSpeck beads (Thermo Fisher Scientific) as multi-color fiducials visible in all fluorescence channels were used. While the TetraSpeck beads are not labeled with NIR dyes, the high brightness of the far-red channel can be used to obtain a reasonable crosstalk in the NIR-channel upon excitation at 642 nm. After bead localization in all spectral channels, we calculated projective transformation matrices to spatially align up to four channels with sub-pixel accuracy correcting for relative translation-, rotation- and scaling factors with respect to the defined reference channel.

Localization of individual fluorescence emitters against noise was done at a set error probability of 10^{-5} (less than 1 false positive detection per frame) with an apparent point spread function estimated robustly from each respective channel using the multi-target tracking algorithm [262]. Immobile emitters were filtered out by spatiotemporal cluster analysis using a modified density-based spatial clustering of applications with noise algorithm DBSCAN [263, 264]. Briefly, emitters are scored as immobile particle if there exists a significant accumulation of localizations within a spatial (here derived from the localization precision [265]) and temporal window (iteratively decreasing to a set minimum of 5 frames). All emitters belonging to identified clusters of immobile particles are removed before applying the tracking algorithm utrack [266]. Upper boundaries for particle linking were established upon a prior robust evaluation of the frame-to-frame nearest-neighbor distribution.

Gap closing with a maximum of 5 frames were allowed to account for missing localizations due to e.g. fluorescence blinking. Trajectories with an observation time ≥ 10 frames were used for further processing.

To detect complex formation, we performed co-tracking analysis between spectral channels. Frame-by-frame co-localization within a set radius of 150 nm followed by tracking of co-localized emitters with the same parameters as described above [266]. Molecules co-diffusing for ≥ 10 frames (≥ 320 ms) were identified as interaction events. Relative heterodimerization levels were determined based on the fraction of co-localized particles which were previously assigned to mobile trajectories. Moreover, heterodimerization levels were related to the least expressed receptor subunit as this subunit limits the absolute number of co-localization events:

$$rel.\ co-tracking = \frac{AB}{A_0} \quad \text{(Eqn. 1)}$$

Relative homodimerization levels were corrected for dimers stochastically double-labeled with the same fluorophore species:

$$AB^* = \frac{2\times AB}{(A_0+B_0)} \quad \text{(Eqn. 2)}$$

$$rel.\ co-tracking = \frac{AB^*}{2\times\left[\left(\frac{A_0}{A_0+B_0}\right)\times\left(\frac{B_0}{A_0+B_0}\right)\right]} \quad \text{(Eqn. 3)}$$

where A_0, B_0 and AB are the total number of localizations observed for each individual receptor channel and the co-localized receptor subunits, respectively. AB^* represents the observed and uncorrected fraction of co-localized receptor subunits.

Mean squared displacement analysis. Diffusion properties were extracted from pooled single trajectory mean squared displacement (MSD) analysis. Here, MSD plots from different channels correspond to different receptor subunits. MSD plots of receptor complexes were collected from co-trajectories of both channels. The instantaneous diffusion coefficient (first 10 data points; $\tau_{\max} = 330$ ms) was estimated for each cell. Therefore, we calculated MSD-time curves for observed trajectories and performed weighted (by the inverse expected error) fits according to the model for Brownian diffusion [267]:

$$MSD(\tau) = 4D\cdot\tau - \frac{4}{3}Dt_e + 4\cdot\sigma^2. \quad \text{(Eqn. 4)}$$

Here, τ is the lag time, D the diffusion coefficient, t_e the exposure time, and σ the localization precision. Local estimates of the diffusion coefficient showing an excessive standard error on the estimates were discarded. Finally, the cell-wide global average was extracted robustly from the Gaussian distribution of log-transformed diffusion coefficients using the minimum covariance determinant method [268].

For single-molecule FRET analysis, representative trajectories of co-localized receptors were chosen. Donor and acceptor intensities were determined from the fitted 2D Gaussian profile along each trajectory. The FRET efficiency *E* was calculated from the mean donor intensity 500 ms before (I_{DA}) and 500 ms after (I_D) photobleaching of the acceptor

$$E = 1 - \frac{I_{DA}}{I_D}. \quad \text{(Eqn. 5)}$$

The respective donor-acceptor distance was calculated from the FRET efficiency *E* according to the Förster equation:

$$r = \sqrt[6]{(1-E)/E} \cdot R_0 \quad \text{(Eqn. 6)}$$

parameterizing the Förster radius R_0 = 6.9 nm for Rho11/AT643 as provided by the manufacturer (ATTO-TEC GmbH).

Statistical Analysis. Box plots were used for visualization and indicate the data distribution of 2nd and 3rd quartile (box), median (line), mean (square) and 1.5× interquartile range (whiskers). Each data point represents the analysis from one cell with a minimum of 10 cells measured for each condition. Statistical significances were determined performing an unpaired student's t-test. Asterisks represent following P-values: ns - $P > 0.05$; * - $P \leq 0.05$; ** - $P \leq 0.01$; *** - $P \leq 0.001$.

7 References

1. Murphy, K.W., C., *Janeway's Immunobiology*. 9th ed. 2017, New York: Garland Science, Taylor & Francis Group.
2. Morrison, S.J., N. Uchida, and I.L. Weissman, *The biology of hematopoietic stem cells.* Annu Rev Cell Dev Biol, 1995. **11**: p. 35-71.
3. Parkin, J. and B. Cohen, *An overview of the immune system.* Lancet, 2001. **357**(9270): p. 1777-89.
4. Takeuchi, O. and S. Akira, *Innate immunity to virus infection.* Immunol Rev, 2009. **227**(1): p. 75-86.
5. Akira, S., S. Uematsu, and O. Takeuchi, *Pathogen recognition and innate immunity.* Cell, 2006. **124**(4): p. 783-801.
6. Snarr, B.D., S.T. Qureshi, and D.C. Sheppard, *Immune Recognition of Fungal Polysaccharides.* J Fungi (Basel), 2017. **3**(3).
7. Steinman, R.M., *The dendritic cell system and its role in immunogenicity.* Annu Rev Immunol, 1991. **9**: p. 271-96.
8. Alt, F.W., E.M. Oltz, F. Young, J. Gorman, G. Taccioli, and J. Chen, *VDJ recombination.* Immunol Today, 1992. **13**(8): p. 306-14.
9. Pleiman, C.M., D. D'Ambrosio, and J.C. Cambier, *The B-cell antigen receptor complex: structure and signal transduction.* Immunol Today, 1994. **15**(9): p. 393-9.
10. Spellberg, B. and J.E. Edwards, Jr., *Type 1/Type 2 immunity in infectious diseases.* Clin Infect Dis, 2001. **32**(1): p. 76-102.
11. Cohen, S., P.E. Bigazzi, and T. Yoshida, *Commentary. Similarities of T cell function in cell-mediated immunity and antibody production.* Cell Immunol, 1974. **12**(1): p. 150-9.
12. Ozaki, K. and W.J. Leonard, *Cytokine and cytokine receptor pleiotropy and redundancy.* J Biol Chem, 2002. **277**(33): p. 29355-8.

13. Chaudhry, H., J. Zhou, Y. Zhong, M.M. Ali, F. McGuire, P.S. Nagarkatti, and M. Nagarkatti, *Role of cytokines as a double-edged sword in sepsis.* In Vivo, 2013. **27**(6): p. 669-84.
14. Fields, J.K., S. Gunther, and E.J. Sundberg, *Structural Basis of IL-1 Family Cytokine Signaling.* Front Immunol, 2019. **10**: p. 1412.
15. Verstrepen, L., T. Bekaert, T.L. Chau, J. Tavernier, A. Chariot, and R. Beyaert, *TLR-4, IL-1R and TNF-R signaling to NF-kappaB: variations on a common theme.* Cell Mol Life Sci, 2008. **65**(19): p. 2964-78.
16. Stanley, E.R., D.M. Chen, and H.S. Lin, *Induction of macrophage production and proliferation by a purified colony stimulating factor.* Nature, 1978. **274**(5667): p. 168-70.
17. Murga-Zamalloa, C., D.C.M. Rolland, A. Polk, A. Wolfe, H. Dewar, P. Chowdhury, O. Onder, R. Dewar, N.A. Brown, N.G. Bailey, K. Inamdar, M.S. Lim, K.S.J. Elenitoba-Johnson, and R.A. Wilcox, *Colony-Stimulating Factor 1 Receptor (CSF1R) Activates AKT/mTOR Signaling and Promotes T-Cell Lymphoma Viability.* Clin Cancer Res, 2020. **26**(3): p. 690-703.
18. Park, K.S., *Tgf-Beta family signaling in embryonic stem cells.* Int J Stem Cells, 2011. **4**(1): p. 18-23.
19. Clark, D.A. and R. Coker, *Transforming growth factor-beta (TGF-beta).* Int J Biochem Cell Biol, 1998. **30**(3): p. 293-8.
20. Bonecchi, R., E. Galliera, E.M. Borroni, M.M. Corsi, M. Locati, and A. Mantovani, *Chemokines and chemokine receptors: an overview.* Front Biosci (Landmark Ed), 2009. **14**: p. 540-51.
21. Lacalle, R.A., R. Blanco, L. Carmona-Rodriguez, A. Martin-Leal, E. Mira, and S. Manes, *Chemokine Receptor Signaling and the Hallmarks of Cancer.* Int Rev Cell Mol Biol, 2017. **331**: p. 181-244.
22. Bodmer, J.L., P. Schneider, and J. Tschopp, *The molecular architecture of the TNF superfamily.* Trends Biochem Sci, 2002. **27**(1): p. 19-26.
23. Wajant, H., K. Pfizenmaier, and P. Scheurich, *Tumor necrosis factor signaling.* Cell Death Differ, 2003. **10**(1): p. 45-65.
24. Aggarwal, B.B., S.C. Gupta, and J.H. Kim, *Historical perspectives on tumor necrosis factor and its superfamily: 25 years later, a golden journey.* Blood, 2012. **119**(3): p. 651-65.
25. Fu, Y.X. and D.D. Chaplin, *Development and maturation of secondary lymphoid tissues.* Annu Rev Immunol, 1999. **17**: p. 399-433.
26. Locksley, R.M., N. Killeen, and M.J. Lenardo, *The TNF and TNF receptor superfamilies: integrating mammalian biology.* Cell, 2001. **104**(4): p. 487-501.
27. Krammer, P.H., *CD95's deadly mission in the immune system.* Nature, 2000. **407**(6805): p. 789-95.
28. Baker, S.J. and E.P. Reddy, *Modulation of life and death by the TNF receptor superfamily.* Oncogene, 1998. **17**(25): p. 3261-70.
29. Nicola, N.A., *Cytokine pleiotropy and redundancy: a view from the receptor.* Stem Cells, 1994. **12 Suppl 1**: p. 3-12; discussion 12-4.
30. Langer, J.A., E.C. Cutrone, and S. Kotenko, *The Class II cytokine receptor (CRF2) family: overview and patterns of receptor-ligand interactions.* Cytokine Growth Factor Rev, 2004. **15**(1): p. 33-48.
31. Bazan, J.F., *Structural design and molecular evolution of a cytokine receptor superfamily.* Proc Natl Acad Sci U S A, 1990. **87**(18): p. 6934-8.
32. Kaczmarski, R.S. and G.J. Mufti, *The cytokine receptor superfamily.* Blood Rev, 1991. **5**(3): p. 193-203.
33. Leonard, W.J. and J.X. Lin, *Cytokine receptor signaling pathways.* J Allergy Clin Immunol, 2000. **105**(5): p. 877-88.
34. Muller, U., U. Steinhoff, L.F. Reis, S. Hemmi, J. Pavlovic, R.M. Zinkernagel, and M. Aguet, *Functional role of type I and type II interferons in antiviral defense.* Science, 1994. **264**(5167): p. 1918-21.

35. van den Broek, M.F., U. Muller, S. Huang, R.M. Zinkernagel, and M. Aguet, *Immune defence in mice lacking type I and/or type II interferon receptors.* Immunol Rev, 1995. **148**: p. 5-18.
36. Chelbi-Alix, M.K. and J. Wietzerbin, *Interferon, a growing cytokine family: 50 years of interferon research.* Biochimie, 2007. **89**(6-7): p. 713-8.
37. Jonasch, E. and F.G. Haluska, *Interferon in oncological practice: review of interferon biology, clinical applications, and toxicities.* Oncologist, 2001. **6**(1): p. 34-55.
38. Renauld, J.C., *Class II cytokine receptors and their ligands: key antiviral and inflammatory modulators.* Nat Rev Immunol, 2003. **3**(8): p. 667-76.
39. Isaacs, A. and J. Lindenmann, *Virus interference. I. The interferon.* Proc R Soc Lond B Biol Sci, 1957. **147**(927): p. 258-67.
40. Platanias, L.C., *Mechanisms of type-I- and type-II-interferon-mediated signalling.* Nat Rev Immunol, 2005. **5**(5): p. 375-86.
41. Kotenko, S.V. and S. Pestka, *Jak-Stat signal transduction pathway through the eyes of cytokine class II receptor complexes.* Oncogene, 2000. **19**(21): p. 2557-65.
42. Walter, M.R., W.T. Windsor, T.L. Nagabhushan, D.J. Lundell, C.A. Lunn, P.J. Zauodny, and S.K. Narula, *Crystal structure of a complex between interferon-gamma and its soluble high-affinity receptor.* Nature, 1995. **376**(6537): p. 230-5.
43. Field, A.K., G.P. Lampson, A.A. Tytell, M.M. Nemes, and M.R. Hilleman, *Inducers of interferon and host resistance, IV. Double-stranded replicative form RNA (MS2-Ff-RNA) from E. coli infected with MS2 coliphage.* Proc Natl Acad Sci U S A, 1967. **58**(5): p. 2102-8.
44. Ruscanu, S., F. Pascale, M. Bourge, B. Hemati, J. Elhmouzi-Younes, C. Urien, M. Bonneau, H. Takamatsu, J. Hope, P. Mertens, G. Meyer, M. Stewart, P. Roy, E.F. Meurs, S. Dabo, S. Zientara, E. Breard, C. Sailleau, E. Chauveau, D. Vitour, B. Charley, and I. Schwartz-Cornil, *The double-stranded RNA bluetongue virus induces type I interferon in plasmacytoid dendritic cells via a MYD88-dependent TLR7/8-independent signaling pathway.* J Virol, 2012. **86**(10): p. 5817-28.
45. Lee, A.J., B. Chen, M.V. Chew, N.G. Barra, M.M. Shenouda, T. Nham, N. van Rooijen, M. Jordana, K.L. Mossman, R.D. Schreiber, M. Mack, and A.A. Ashkar, *Inflammatory monocytes require type I interferon receptor signaling to activate NK cells via IL-18 during a mucosal viral infection.* J Exp Med, 2017. **214**(4): p. 1153-1167.
46. Kang, S., H.M. Brown, and S. Hwang, *Direct Antiviral Mechanisms of Interferon-Gamma.* Immune Netw, 2018. **18**(5): p. e33.
47. McKenzie, A.N.J., H. Spits, and G. Eberl, *Innate lymphoid cells in inflammation and immunity.* Immunity, 2014. **41**(3): p. 366-374.
48. Billiau, A. and P. Matthys, *Interferon-gamma: a historical perspective.* Cytokine Growth Factor Rev, 2009. **20**(2): p. 97-113.
49. Vivier, E., E. Tomasello, M. Baratin, T. Walzer, and S. Ugolini, *Functions of natural killer cells.* Nat Immunol, 2008. **9**(5): p. 503-10.
50. de Weerd, N.A. and T. Nguyen, *The interferons and their receptors--distribution and regulation.* Immunol Cell Biol, 2012. **90**(5): p. 483-91.
51. Pestka, S., C.D. Krause, D. Sarkar, M.R. Walter, Y. Shi, and P.B. Fisher, *Interleukin-10 and related cytokines and receptors.* Annu Rev Immunol, 2004. **22**: p. 929-79.
52. Ouyang, W., S. Rutz, N.K. Crellin, P.A. Valdez, and S.G. Hymowitz, *Regulation and functions of the IL-10 family of cytokines in inflammation and disease.* Annu Rev Immunol, 2011. **29**: p. 71-109.
53. Sommereyns, C., S. Paul, P. Staeheli, and T. Michiels, *IFN-lambda (IFN-lambda) is expressed in a tissue-dependent fashion and primarily acts on epithelial cells in vivo.* PLoS Pathog, 2008. **4**(3): p. e1000017.
54. Lazear, H.M., J.W. Schoggins, and M.S. Diamond, *Shared and Distinct Functions of Type I and Type III Interferons.* Immunity, 2019. **50**(4): p. 907-923.
55. Walter, M.R. and T.L. Nagabhushan, *Crystal structure of interleukin 10 reveals an interferon gamma-like fold.* Biochemistry, 1995. **34**(38): p. 12118-25.

56. Zdanov, A., C. Schalk-Hihi, A. Gustchina, M. Tsang, J. Weatherbee, and A. Wlodawer, *Crystal structure of interleukin-10 reveals the functional dimer with an unexpected topological similarity to interferon gamma.* Structure, 1995. **3**(6): p. 591-601.
57. Saxton, R.A., N. Tsutsumi, L.L. Su, G.C. Abhiraman, K. Mohan, L.T. Henneberg, N.G. Aduri, C. Gati, and K.C. Garcia, *Structure-based decoupling of the pro- and anti-inflammatory functions of interleukin-10.* Science, 2021. **371**(6535).
58. Couper, K.N., D.G. Blount, and E.M. Riley, *IL-10: the master regulator of immunity to infection.* J Immunol, 2008. **180**(9): p. 5771-7.
59. Wilmes, S., O. Beutel, Z. Li, V. Francois-Newton, C.P. Richter, D. Janning, C. Kroll, P. Hanhart, K. Hotte, C. You, G. Uze, S. Pellegrini, and J. Piehler, *Receptor dimerization dynamics as a regulatory valve for plasticity of type I interferon signaling.* J Cell Biol, 2015. **209**(4): p. 579-93.
60. Piehler, J. and G. Schreiber, *Mutational and structural analysis of the binding interface between type I interferons and their receptor Ifnar2.* J Mol Biol, 1999. **294**(1): p. 223-37.
61. Runkel, L., C. deDios, M. Karpusas, M. Betzenhauser, C. Muldowney, M. Zafari, C.D. Benjamin, S. Miller, P.S. Hochman, and A. Whitty, *Systematic mutational mapping of sites on human interferon-beta-1a that are important for receptor binding and functional activity.* Biochemistry, 2000. **39**(10): p. 2538-51.
62. Roisman, L.C., J. Piehler, J.Y. Trosset, H.A. Scheraga, and G. Schreiber, *Structure of the interferon-receptor complex determined by distance constraints from double-mutant cycles and flexible docking.* Proc Natl Acad Sci U S A, 2001. **98**(23): p. 13231-6.
63. Cajean-Feroldi, C., F. Nosal, P.C. Nardeux, X. Gallet, J. Guymarho, F. Baychelier, P. Sempe, M.G. Tovey, J.L. Escary, and P. Eid, *Identification of residues of the IFNAR1 chain of the type I human interferon receptor critical for ligand binding and biological activity.* Biochemistry, 2004. **43**(39): p. 12498-512.
64. Lamken, P., M. Gavutis, I. Peters, J. Van der Heyden, G. Uze, and J. Piehler, *Functional cartography of the ectodomain of the type I interferon receptor subunit ifnar1.* J Mol Biol, 2005. **350**(3): p. 476-88.
65. Strunk, J.J., I. Gregor, Y. Becker, Z. Li, M. Gavutis, E. Jaks, P. Lamken, T. Walz, J. Enderlein, and J. Piehler, *Ligand binding induces a conformational change in ifnar1 that is propagated to its membrane-proximal domain.* J Mol Biol, 2008. **377**(3): p. 725-39.
66. Chill, J.H., S.R. Quadt, R. Levy, G. Schreiber, and J. Anglister, *The human type I interferon receptor: NMR structure reveals the molecular basis of ligand binding.* Structure, 2003. **11**(7): p. 791-802.
67. Quadt-Akabayov, S.R., J.H. Chill, R. Levy, N. Kessler, and J. Anglister, *Determination of the human type I interferon receptor binding site on human interferon-alpha2 by cross saturation and an NMR-based model of the complex.* Protein Sci, 2006. **15**(11): p. 2656-68.
68. Li, Z., J.J. Strunk, P. Lamken, J. Piehler, and T. Walz, *The EM structure of a type I interferon-receptor complex reveals a novel mechanism for cytokine signaling.* J Mol Biol, 2008. **377**(3): p. 715-24.
69. Thomas, C., I. Moraga, D. Levin, P.O. Krutzik, Y. Podoplelova, A. Trejo, C. Lee, G. Yarden, S.E. Vleck, J.S. Glenn, G.P. Nolan, J. Piehler, G. Schreiber, and K.C. Garcia, *Structural linkage between ligand discrimination and receptor activation by type I interferons.* Cell, 2011. **146**(4): p. 621-32.
70. de Weerd, N.A., J.P. Vivian, T.K. Nguyen, N.E. Mangan, J.A. Gould, S.J. Braniff, L. Zaker-Tabrizi, K.Y. Fung, S.C. Forster, T. Beddoe, H.H. Reid, J. Rossjohn, and P.J. Hertzog, *Structural basis of a unique interferon-beta signaling axis mediated via the receptor IFNAR1.* Nat Immunol, 2013. **14**(9): p. 901-7.
71. Subramaniam, P.S., S.A. Khan, C.H. Pontzer, and H.M. Johnson, *Differential recognition of the type I interferon receptor by interferons tau and alpha is responsible for their disparate cytotoxicities.* Proc Natl Acad Sci U S A, 1995. **92**(26): p. 12270-4.
72. Russell-Harde, D., T.C. Wagner, H.D. Perez, and E. Croze, *Formation of a uniquely stable type I interferon receptor complex by interferon beta is dependent upon particular*

interactions between interferon beta and its receptor and independent of tyrosine phosphorylation. Biochem Biophys Res Commun, 1999. **255**(2): p. 539-44.
73. Lamken, P., S. Lata, M. Gavutis, and J. Piehler, *Ligand-induced assembling of the type I interferon receptor on supported lipid bilayers.* J Mol Biol, 2004. **341**(1): p. 303-18.
74. Jaks, E., M. Gavutis, G. Uze, J. Martal, and J. Piehler, *Differential receptor subunit affinities of type I interferons govern differential signal activation.* J Mol Biol, 2007. **366**(2): p. 525-39.
75. Lavoie, T.B., E. Kalie, S. Crisafulli-Cabatu, R. Abramovich, G. DiGioia, K. Moolchan, S. Pestka, and G. Schreiber, *Binding and activity of all human alpha interferon subtypes.* Cytokine, 2011. **56**(2): p. 282-9.
76. Jaitin, D.A., L.C. Roisman, E. Jaks, M. Gavutis, J. Piehler, J. Van der Heyden, G. Uze, and G. Schreiber, *Inquiring into the differential action of interferons (IFNs): an IFN-alpha2 mutant with enhanced affinity to IFNAR1 is functionally similar to IFN-beta.* Mol Cell Biol, 2006. **26**(5): p. 1888-97.
77. Kalie, E., D.A. Jaitin, R. Abramovich, and G. Schreiber, *An interferon alpha2 mutant optimized by phage display for IFNAR1 binding confers specifically enhanced antitumor activities.* J Biol Chem, 2007. **282**(15): p. 11602-11.
78. Mendoza, J.L., N.K. Escalante, K.M. Jude, J. Sotolongo Bellon, L. Su, T.M. Horton, N. Tsutsumi, S.J. Berardinelli, R.S. Haltiwanger, J. Piehler, E.G. Engleman, and K.C. Garcia, *Structure of the IFNgamma receptor complex guides design of biased agonists.* Nature, 2019. **567**(7746): p. 56-60.
79. Hsieh, C.S., S.E. Macatonia, C.S. Tripp, S.F. Wolf, A. O'Garra, and K.M. Murphy, *Development of TH1 CD4+ T cells through IL-12 produced by Listeria-induced macrophages.* Science, 1993. **260**(5107): p. 547-9.
80. Ma, X., W. Yan, H. Zheng, Q. Du, L. Zhang, Y. Ban, N. Li, and F. Wei, *Regulation of IL-10 and IL-12 production and function in macrophages and dendritic cells.* F1000Res, 2015. **4**.
81. Trinchieri, G., *Interleukin-12 and its role in the generation of TH1 cells.* Immunol Today, 1993. **14**(7): p. 335-8.
82. Mosmann, T.R., H. Cherwinski, M.W. Bond, M.A. Giedlin, and R.L. Coffman, *Two types of murine helper T cell clone. I. Definition according to profiles of lymphokine activities and secreted proteins.* J Immunol, 1986. **136**(7): p. 2348-57.
83. Ma, X., J.M. Chow, G. Gri, G. Carra, F. Gerosa, S.F. Wolf, R. Dzialo, and G. Trinchieri, *The interleukin 12 p40 gene promoter is primed by interferon gamma in monocytic cells.* J Exp Med, 1996. **183**(1): p. 147-57.
84. Grohmann, U., M.L. Belladonna, C. Vacca, R. Bianchi, F. Fallarino, C. Orabona, M.C. Fioretti, and P. Puccetti, *Positive regulatory role of IL-12 in macrophages and modulation by IFN-gamma.* J Immunol, 2001. **167**(1): p. 221-7.
85. Ramirez-Alejo, N. and L. Santos-Argumedo, *Innate defects of the IL-12/IFN-gamma axis in susceptibility to infections by mycobacteria and salmonella.* J Interferon Cytokine Res, 2014. **34**(5): p. 307-17.
86. Manetti, R., P. Parronchi, M.G. Giudizi, M.P. Piccinni, E. Maggi, G. Trinchieri, and S. Romagnani, *Natural killer cell stimulatory factor (interleukin 12 [IL-12]) induces T helper type 1 (Th1)-specific immune responses and inhibits the development of IL-4-producing Th cells.* J Exp Med, 1993. **177**(4): p. 1199-204.
87. D'Andrea, A., M. Aste-Amezaga, N.M. Valiante, X. Ma, M. Kubin, and G. Trinchieri, *Interleukin 10 (IL-10) inhibits human lymphocyte interferon gamma-production by suppressing natural killer cell stimulatory factor/IL-12 synthesis in accessory cells.* J Exp Med, 1993. **178**(3): p. 1041-8.
88. Ohmori, Y. and T.A. Hamilton, *IL-4-induced STAT6 suppresses IFN-gamma-stimulated STAT1-dependent transcription in mouse macrophages.* J Immunol, 1997. **159**(11): p. 5474-82.
89. Ito, S., P. Ansari, M. Sakatsume, H. Dickensheets, N. Vazquez, R.P. Donnelly, A.C. Larner, and D.S. Finbloom, *Interleukin-10 inhibits expression of both interferon alpha- and*

interferon gamma- induced genes by suppressing tyrosine phosphorylation of STAT1. Blood, 1999. **93**(5): p. 1456-63.

90. Gajewski, T.F. and F.W. Fitch, *Anti-proliferative effect of IFN-gamma in immune regulation. I. IFN-gamma inhibits the proliferation of Th2 but not Th1 murine helper T lymphocyte clones.* J Immunol, 1988. **140**(12): p. 4245-52.
91. Gajewski, T.F., E. Goldwasser, and F.W. Fitch, *Anti-proliferative effect of IFN-gamma in immune regulation. II. IFN-gamma inhibits the proliferation of murine bone marrow cells stimulated with IL-3, IL-4, or granulocyte-macrophage colony-stimulating factor.* J Immunol, 1988. **141**(8): p. 2635-42.
92. Demeure, C.E., C.Y. Wu, U. Shu, P.V. Schneider, C. Heusser, H. Yssel, and G. Delespesse, *In vitro maturation of human neonatal CD4 T lymphocytes. II. Cytokines present at priming modulate the development of lymphokine production.* J Immunol, 1994. **152**(10): p. 4775-82.
93. Muraille, E. and O. Leo, *Revisiting the Th1/Th2 paradigm.* Scand J Immunol, 1998. **47**(1): p. 1-9.
94. Boehm, U., T. Klamp, M. Groot, and J.C. Howard, *Cellular responses to interferon-gamma.* Annu Rev Immunol, 1997. **15**: p. 749-95.
95. Schroder, K., P.J. Hertzog, T. Ravasi, and D.A. Hume, *Interferon-gamma: an overview of signals, mechanisms and functions.* J Leukoc Biol, 2004. **75**(2): p. 163-89.
96. Xaus, J., M. Cardo, A.F. Valledor, C. Soler, J. Lloberas, and A. Celada, *Interferon gamma induces the expression of p21waf-1 and arrests macrophage cell cycle, preventing induction of apoptosis.* Immunity, 1999. **11**(1): p. 103-13.
97. Dey, A., L. Kim, and W. Li, *Gamma interferon induces expression of Mad1 gene in macrophage, which inhibits colony-stimulating factor-1-dependent mitogenesis.* J Cell Biochem, 1999. **72**(2): p. 232-41.
98. Behar, S.M., C.J. Martin, M.G. Booty, T. Nishimura, X. Zhao, H.X. Gan, M. Divangahi, and H.G. Remold, *Apoptosis is an innate defense function of macrophages against Mycobacterium tuberculosis.* Mucosal Immunol, 2011. **4**(3): p. 279-87.
99. Bernabei, P., E.M. Coccia, L. Rigamonti, M. Bosticardo, G. Forni, S. Pestka, C.D. Krause, A. Battistini, and F. Novelli, *Interferon-gamma receptor 2 expression as the deciding factor in human T, B, and myeloid cell proliferation or death.* J Leukoc Biol, 2001. **70**(6): p. 950-60.
100. Novelli, F., P. Bernabei, L. Ozmen, L. Rigamonti, A. Allione, S. Pestka, G. Garotta, and G. Forni, *Switching on of the proliferation or apoptosis of activated human T lymphocytes by IFN-gamma is correlated with the differential expression of the alpha- and beta-chains of its receptor.* J Immunol, 1996. **157**(5): p. 1935-43.
101. Bernabei, P., A. Allione, L. Rigamonti, M. Bosticardo, G. Losana, I. Borghi, G. Forni, and F. Novelli, *Regulation of interferon-gamma receptor (INF-gammaR) chains: a peculiar way to rule the life and death of human lymphocytes.* Eur Cytokine Netw, 2001. **12**(1): p. 6-14.
102. Strunk, R.C., F.S. Cole, D.H. Perlmutter, and H.R. Colten, *gamma-Interferon increases expression of class III complement genes C2 and factor B in human monocytes and in murine fibroblasts transfected with human C2 and factor B genes.* J Biol Chem, 1985. **260**(28): p. 15280-5.
103. Erbe, D.V., J.E. Collins, L. Shen, R.F. Graziano, and M.W. Fanger, *The effect of cytokines on the expression and function of Fc receptors for IgG on human myeloid cells.* Mol Immunol, 1990. **27**(1): p. 57-67.
104. Drapier, J.C., J. Wietzerbin, and J.B. Hibbs, Jr., *Interferon-gamma and tumor necrosis factor induce the L-arginine-dependent cytotoxic effector mechanism in murine macrophages.* Eur J Immunol, 1988. **18**(10): p. 1587-92.
105. Cassatella, M.A., F. Bazzoni, R.M. Flynn, S. Dusi, G. Trinchieri, and F. Rossi, *Molecular basis of interferon-gamma and lipopolysaccharide enhancement of phagocyte respiratory burst capability. Studies on the gene expression of several NADPH oxidase components.* J Biol Chem, 1990. **265**(33): p. 20241-6.

106. Gupta, J.W., M. Kubin, L. Hartman, M. Cassatella, and G. Trinchieri, *Induction of expression of genes encoding components of the respiratory burst oxidase during differentiation of human myeloid cell lines induced by tumor necrosis factor and gamma-interferon.* Cancer Res, 1992. **52**(9): p. 2530-7.
107. Cassatella, M.A., L. Hartman, B. Perussia, and G. Trinchieri, *Tumor necrosis factor and immune interferon synergistically induce cytochrome b-245 heavy-chain gene expression and nicotinamide-adenine dinucleotide phosphate hydrogenase oxidase in human leukemic myeloid cells.* J Clin Invest, 1989. **83**(5): p. 1570-9.
108. Pfefferkorn, E.R., *Interferon gamma blocks the growth of Toxoplasma gondii in human fibroblasts by inducing the host cells to degrade tryptophan.* Proc Natl Acad Sci U S A, 1984. **81**(3): p. 908-12.
109. Collins, J.T. and W.A. Dunnick, *Germline transcripts of the murine immunoglobulin gamma 2a gene: structure and induction by IFN-gamma.* Int Immunol, 1993. **5**(8): p. 885-91.
110. Chang, C.H., J. Hammer, J.E. Loh, W.L. Fodor, and R.A. Flavell, *The activation of major histocompatibility complex class I genes by interferon regulatory factor-1 (IRF-1).* Immunogenetics, 1992. **35**(6): p. 378-84.
111. Figueiredo, F., T.J. Koerner, and D.O. Adams, *Molecular mechanisms regulating the expression of class II histocompatibility molecules on macrophages. Effects of inductive and suppressive signals on gene transcription.* J Immunol, 1989. **143**(11): p. 3781-6.
112. Groettrup, M., S. Khan, K. Schwarz, and G. Schmidtke, *Interferon-gamma inducible exchanges of 20S proteasome active site subunits: why?* Biochimie, 2001. **83**(3-4): p. 367-72.
113. Cramer, L.A., S.L. Nelson, and M.J. Klemsz, *Synergistic induction of the Tap-1 gene by IFN-gamma and lipopolysaccharide in macrophages is regulated by STAT1.* J Immunol, 2000. **165**(6): p. 3190-7.
114. Seliger, B., K. Schreiber, K. Delp, M. Meissner, S. Hammers, T. Reichert, K. Pawlischko, R. Tampe, and C. Huber, *Downregulation of the constitutive tapasin expression in human tumor cells of distinct origin and its transcriptional upregulation by cytokines.* Tissue Antigens, 2001. **57**(1): p. 39-45.
115. Guidotti, L.G. and F.V. Chisari, *Noncytolytic control of viral infections by the innate and adaptive immune response.* Annu Rev Immunol, 2001. **19**: p. 65-91.
116. Kropp, K.A., K.A. Robertson, G. Sing, S. Rodriguez-Martin, M. Blanc, P. Lacaze, M.F. Hassim, M.R. Khondoker, A. Busche, P. Dickinson, T. Forster, B. Strobl, M. Mueller, S. Jonjic, A. Angulo, and P. Ghazal, *Reversible inhibition of murine cytomegalovirus replication by gamma interferon (IFN-gamma) in primary macrophages involves a primed type I IFN-signaling subnetwork for full establishment of an immediate-early antiviral state.* J Virol, 2011. **85**(19): p. 10286-99.
117. Moore, K.W., R. de Waal Malefyt, R.L. Coffman, and A. O'Garra, *Interleukin-10 and the interleukin-10 receptor.* Annu Rev Immunol, 2001. **19**: p. 683-765.
118. de Waal Malefyt, R., J. Abrams, B. Bennett, C.G. Figdor, and J.E. de Vries, *Interleukin 10(IL-10) inhibits cytokine synthesis by human monocytes: an autoregulatory role of IL-10 produced by monocytes.* J Exp Med, 1991. **174**(5): p. 1209-20.
119. Fiorentino, D.F., A. Zlotnik, T.R. Mosmann, M. Howard, and A. O'Garra, *IL-10 inhibits cytokine production by activated macrophages.* J Immunol, 1991. **147**(11): p. 3815-22.
120. Berkman, N., M. John, G. Roesems, P.J. Jose, P.J. Barnes, and K.F. Chung, *Inhibition of macrophage inflammatory protein-1 alpha expression by IL-10. Differential sensitivities in human blood monocytes and alveolar macrophages.* J Immunol, 1995. **155**(9): p. 4412-8.
121. Kopydlowski, K.M., C.A. Salkowski, M.J. Cody, N. van Rooijen, J. Major, T.A. Hamilton, and S.N. Vogel, *Regulation of macrophage chemokine expression by lipopolysaccharide in vitro and in vivo.* J Immunol, 1999. **163**(3): p. 1537-44.
122. Koppelman, B., J.J. Neefjes, J.E. de Vries, and R. de Waal Malefyt, *Interleukin-10 down-regulates MHC class II alphabeta peptide complexes at the plasma membrane of monocytes by affecting arrival and recycling.* Immunity, 1997. **7**(6): p. 861-71.

123. de Waal Malefyt, R., J. Haanen, H. Spits, M.G. Roncarolo, A. te Velde, C. Figdor, K. Johnson, R. Kastelein, H. Yssel, and J.E. de Vries, *Interleukin 10 (IL-10) and viral IL-10 strongly reduce antigen-specific human T cell proliferation by diminishing the antigen-presenting capacity of monocytes via downregulation of class II major histocompatibility complex expression.* J Exp Med, 1991. **174**(4): p. 915-24.
124. Willems, F., A. Marchant, J.P. Delville, C. Gerard, A. Delvaux, T. Velu, M. de Boer, and M. Goldman, *Interleukin-10 inhibits B7 and intercellular adhesion molecule-1 expression on human monocytes.* Eur J Immunol, 1994. **24**(4): p. 1007-9.
125. Gruber, M.F., C.C. Williams, and T.L. Gerrard, *Macrophage-colony-stimulating factor expression by anti-CD45 stimulated human monocytes is transcriptionally up-regulated by IL-1 beta and inhibited by IL-4 and IL-10.* J Immunol, 1994. **152**(3): p. 1354-61.
126. Itoh, K. and S. Hirohata, *The role of IL-10 in human B cell activation, proliferation, and differentiation.* J Immunol, 1995. **154**(9): p. 4341-50.
127. Heine, G., G. Drozdenko, J.R. Grun, H.D. Chang, A. Radbruch, and M. Worm, *Autocrine IL-10 promotes human B-cell differentiation into IgM- or IgG-secreting plasmablasts.* Eur J Immunol, 2014. **44**(6): p. 1615-21.
128. Go, N.F., B.E. Castle, R. Barrett, R. Kastelein, W. Dang, T.R. Mosmann, K.W. Moore, and M. Howard, *Interleukin 10, a novel B cell stimulatory factor: unresponsiveness of X chromosome-linked immunodeficiency B cells.* J Exp Med, 1990. **172**(6): p. 1625-31.
129. Ye, Z., H. Huang, S. Hao, S. Xu, H. Yu, S. Van Den Hurk, and J. Xiang, *IL-10 has a distinct immunoregulatory effect on naive and active T cell subsets.* J Interferon Cytokine Res, 2007. **27**(12): p. 1031-8.
130. Groux, H., M. Bigler, J.E. de Vries, and M.G. Roncarolo, *Inhibitory and stimulatory effects of IL-10 on human CD8+ T cells.* J Immunol, 1998. **160**(7): p. 3188-93.
131. Marijanovic, Z., J. Ragimbeau, K.G. Kumar, S.Y. Fuchs, and S. Pellegrini, *TYK2 activity promotes ligand-induced IFNAR1 proteolysis.* Biochem J, 2006. **397**(1): p. 31-8.
132. Qian, J., H. Zheng, W.C. Huangfu, J. Liu, C.J. Carbone, N.A. Leu, D.P. Baker, and S.Y. Fuchs, *Pathogen recognition receptor signaling accelerates phosphorylation-dependent degradation of IFNAR1.* PLoS Pathog, 2011. **7**(6): p. e1002065.
133. Longhi, M.P., C. Trumpfheller, J. Idoyaga, M. Caskey, I. Matos, C. Kluger, A.M. Salazar, M. Colonna, and R.M. Steinman, *Dendritic cells require a systemic type I interferon response to mature and induce CD4+ Th1 immunity with poly IC as adjuvant.* J Exp Med, 2009. **206**(7): p. 1589-602.
134. Yen, J.H. and D. Ganea, *Interferon beta induces mature dendritic cell apoptosis through caspase-11/caspase-3 activation.* Blood, 2009. **114**(7): p. 1344-54.
135. Minakshi, R., K. Padhan, M. Rani, N. Khan, F. Ahmad, and S. Jameel, *The SARS Coronavirus 3a protein causes endoplasmic reticulum stress and induces ligand-independent downregulation of the type 1 interferon receptor.* PLoS One, 2009. **4**(12): p. e8342.
136. Acharya, D., G. Liu, and M.U. Gack, *Dysregulation of type I interferon responses in COVID-19.* Nat Rev Immunol, 2020. **20**(7): p. 397-398.
137. Hadjadj, J., N. Yatim, L. Barnabei, A. Corneau, J. Boussier, N. Smith, H. Pere, B. Charbit, V. Bondet, C. Chenevier-Gobeaux, P. Breillat, N. Carlier, R. Gauzit, C. Morbieu, F. Pene, N. Marin, N. Roche, T.A. Szwebel, S.H. Merkling, J.M. Treluyer, D. Veyer, L. Mouthon, C. Blanc, P.L. Tharaux, F. Rozenberg, A. Fischer, D. Duffy, F. Rieux-Laucat, S. Kerneis, and B. Terrier, *Impaired type I interferon activity and inflammatory responses in severe COVID-19 patients.* Science, 2020. **369**(6504): p. 718-724.
138. Evans, J.D., R.A. Crown, J.A. Sohn, and C. Seeger, *West Nile virus infection induces depletion of IFNAR1 protein levels.* Viral Immunol, 2011. **24**(4): p. 253-63.
139. Li, Q., R. Means, S. Lang, and J.U. Jung, *Downregulation of gamma interferon receptor 1 by Kaposi's sarcoma-associated herpesvirus K3 and K5.* J Virol, 2007. **81**(5): p. 2117-27.
140. Upton, C., K. Mossman, and G. McFadden, *Encoding of a homolog of the IFN-gamma receptor by myxoma virus.* Science, 1992. **258**(5086): p. 1369-72.

141. Alcami, A. and G.L. Smith, *Vaccinia, cowpox, and camelpox viruses encode soluble gamma interferon receptors with novel broad species specificity.* J Virol, 1995. **69**(8): p. 4633-9.
142. Colamonici, O.R., P. Domanski, S.M. Sweitzer, A. Larner, and R.M. Buller, *Vaccinia virus B18R gene encodes a type I interferon-binding protein that blocks interferon alpha transmembrane signaling.* J Biol Chem, 1995. **270**(27): p. 15974-8.
143. Alcami, A., J.A. Symons, and G.L. Smith, *The vaccinia virus soluble alpha/beta interferon (IFN) receptor binds to the cell surface and protects cells from the antiviral effects of IFN.* J Virol, 2000. **74**(23): p. 11230-9.
144. Fickenscher, H., S. Hor, H. Kupers, A. Knappe, S. Wittmann, and H. Sticht, *The interleukin-10 family of cytokines.* Trends Immunol, 2002. **23**(2): p. 89-96.
145. Kotenko, S.V., *The family of IL-10-related cytokines and their receptors: related, but to what extent?* Cytokine Growth Factor Rev, 2002. **13**(3): p. 223-40.
146. Liu, Y., R. de Waal Malefyt, F. Briere, C. Parham, J.M. Bridon, J. Banchereau, K.W. Moore, and J. Xu, *The EBV IL-10 homologue is a selective agonist with impaired binding to the IL-10 receptor.* J Immunol, 1997. **158**(2): p. 604-13.
147. Ding, Y., L. Qin, D. Zamarin, S.V. Kotenko, S. Pestka, K.W. Moore, and J.S. Bromberg, *Differential IL-10R1 expression plays a critical role in IL-10-mediated immune regulation.* J Immunol, 2001. **167**(12): p. 6884-92.
148. Stewart, J.P., F.G. Behm, J.R. Arrand, and C.M. Rooney, *Differential expression of viral and human interleukin-10 (IL-10) by primary B cell tumors and B cell lines.* Virology, 1994. **200**(2): p. 724-32.
149. Suzuki, T., H. Tahara, S. Narula, K.W. Moore, P.D. Robbins, and M.T. Lotze, *Viral interleukin 10 (IL-10), the human herpes virus 4 cellular IL-10 homologue, induces local anergy to allogeneic and syngeneic tumors.* J Exp Med, 1995. **182**(2): p. 477-86.
150. Berman, R.M., T. Suzuki, H. Tahara, P.D. Robbins, S.K. Narula, and M.T. Lotze, *Systemic administration of cellular IL-10 induces an effective, specific, and long-lived immune response against established tumors in mice.* J Immunol, 1996. **157**(1): p. 231-8.
151. Kotenko, S.V., S. Saccani, L.S. Izotova, O.V. Mirochnitchenko, and S. Pestka, *Human cytomegalovirus harbors its own unique IL-10 homolog (cmvIL-10).* Proc Natl Acad Sci U S A, 2000. **97**(4): p. 1695-700.
152. Jones, B.C., N.J. Logsdon, K. Josephson, J. Cook, P.A. Barry, and M.R. Walter, *Crystal structure of human cytomegalovirus IL-10 bound to soluble human IL-10R1.* Proc Natl Acad Sci U S A, 2002. **99**(14): p. 9404-9.
153. Ouyang, P., K. Rakus, S.J. van Beurden, A.H. Westphal, A.J. Davison, D. Gatherer, and A.F. Vanderplasschen, *IL-10 encoded by viruses: a remarkable example of independent acquisition of a cellular gene by viruses and its subsequent evolution in the viral genome.* J Gen Virol, 2014. **95**(Pt 2): p. 245-262.
154. Baker, S.J., S.G. Rane, and E.P. Reddy, *Hematopoietic cytokine receptor signaling.* Oncogene, 2007. **26**(47): p. 6724-37.
155. Gadina, M., D. Hilton, J.A. Johnston, A. Morinobu, A. Lighvani, Y.J. Zhou, R. Visconti, and J.J. O'Shea, *Signaling by type I and II cytokine receptors: ten years after.* Curr Opin Immunol, 2001. **13**(3): p. 363-73.
156. Gough, D.J., D.E. Levy, R.W. Johnstone, and C.J. Clarke, *IFNgamma signaling-does it mean JAK-STAT?* Cytokine Growth Factor Rev, 2008. **19**(5-6): p. 383-94.
157. Bromberg, J.F., C.M. Horvath, Z. Wen, R.D. Schreiber, and J.E. Darnell, Jr., *Transcriptionally active Stat1 is required for the antiproliferative effects of both interferon alpha and interferon gamma.* Proc Natl Acad Sci U S A, 1996. **93**(15): p. 7673-8.
158. Riley, J.K., K. Takeda, S. Akira, and R.D. Schreiber, *Interleukin-10 receptor signaling through the JAK-STAT pathway. Requirement for two distinct receptor-derived signals for anti-inflammatory action.* J Biol Chem, 1999. **274**(23): p. 16513-21.
159. Leonard, W.J. and J.J. O'Shea, *Jaks and STATs: biological implications.* Annu Rev Immunol, 1998. **16**: p. 293-322.

160. Kaplan, D.H., A.C. Greenlund, J.W. Tanner, A.S. Shaw, and R.D. Schreiber, *Identification of an interferon-gamma receptor alpha chain sequence required for JAK-1 binding.* J Biol Chem, 1996. **271**(1): p. 9-12.
161. Wallweber, H.J., C. Tam, Y. Franke, M.A. Starovasnik, and P.J. Lupardus, *Structural basis of recognition of interferon-alpha receptor by tyrosine kinase 2.* Nat Struct Mol Biol, 2014. **21**(5): p. 443-8.
162. Saharinen, P., K. Takaluoma, and O. Silvennoinen, *Regulation of the Jak2 tyrosine kinase by its pseudokinase domain.* Mol Cell Biol, 2000. **20**(10): p. 3387-95.
163. Ho, A.S., S.H. Wei, A.L. Mui, A. Miyajima, and K.W. Moore, *Functional regions of the mouse interleukin-10 receptor cytoplasmic domain.* Mol Cell Biol, 1995. **15**(9): p. 5043-53.
164. Kotenko, S.V., L.S. Izotova, B.P. Pollack, T.M. Mariano, R.J. Donnelly, G. Muthukumaran, J.R. Cook, G. Garotta, O. Silvennoinen, J.N. Ihle, and et al., *Interaction between the components of the interferon gamma receptor complex.* J Biol Chem, 1995. **270**(36): p. 20915-21.
165. Kotenko, S.V., L.S. Izotova, B.P. Pollack, G. Muthukumaran, K. Paukku, O. Silvennoinen, J.N. Ihle, and S. Pestka, *Other kinases can substitute for Jak2 in signal transduction by interferon-gamma.* J Biol Chem, 1996. **271**(29): p. 17174-82.
166. Rawlings, J.S., K.M. Rosler, and D.A. Harrison, *The JAK/STAT signaling pathway.* J Cell Sci, 2004. **117**(Pt 8): p. 1281-3.
167. Horvath, C.M., Z. Wen, and J.E. Darnell, Jr., *A STAT protein domain that determines DNA sequence recognition suggests a novel DNA-binding domain.* Genes Dev, 1995. **9**(8): p. 984-94.
168. Strehlow, I. and C. Schindler, *Amino-terminal signal transducer and activator of transcription (STAT) domains regulate nuclear translocation and STAT deactivation.* J Biol Chem, 1998. **273**(43): p. 28049-56.
169. Chen, X., U. Vinkemeier, Y. Zhao, D. Jeruzalmi, J.E. Darnell, Jr., and J. Kuriyan, *Crystal structure of a tyrosine phosphorylated STAT-1 dimer bound to DNA.* Cell, 1998. **93**(5): p. 827-39.
170. Greenlund, A.C., M.A. Farrar, B.L. Viviano, and R.D. Schreiber, *Ligand-induced IFN gamma receptor tyrosine phosphorylation couples the receptor to its signal transduction system (p91).* EMBO J, 1994. **13**(7): p. 1591-600.
171. Weber-Nordt, R.M., J.K. Riley, A.C. Greenlund, K.W. Moore, J.E. Darnell, and R.D. Schreiber, *Stat3 recruitment by two distinct ligand-induced, tyrosine-phosphorylated docking sites in the interleukin-10 receptor intracellular domain.* J Biol Chem, 1996. **271**(44): p. 27954-61.
172. Finbloom, D.S. and K.D. Winestock, *IL-10 induces the tyrosine phosphorylation of tyk2 and Jak1 and the differential assembly of STAT1 alpha and STAT3 complexes in human T cells and monocytes.* J Immunol, 1995. **155**(3): p. 1079-90.
173. Herrero, C., X. Hu, W.P. Li, S. Samuels, M.N. Sharif, S. Kotenko, and L.B. Ivashkiv, *Reprogramming of IL-10 activity and signaling by IFN-gamma.* J Immunol, 2003. **171**(10): p. 5034-41.
174. Sharif, M.N., I. Tassiulas, Y. Hu, I. Mecklenbrauker, A. Tarakhovsky, and L.B. Ivashkiv, *IFN-alpha priming results in a gain of proinflammatory function by IL-10: implications for systemic lupus erythematosus pathogenesis.* J Immunol, 2004. **172**(10): p. 6476-81.
175. Qing, Y. and G.R. Stark, *Alternative activation of STAT1 and STAT3 in response to interferon-gamma.* J Biol Chem, 2004. **279**(40): p. 41679-85.
176. Schindler, C., K. Shuai, V.R. Prezioso, and J.E. Darnell, Jr., *Interferon-dependent tyrosine phosphorylation of a latent cytoplasmic transcription factor.* Science, 1992. **257**(5071): p. 809-13.
177. Lohi, O. and V.P. Lehto, *STAM/EAST/Hbp adapter proteins--integrators of signalling pathways.* FEBS Lett, 2001. **508**(3): p. 287-90.
178. Wakioka, T., A. Sasaki, K. Mitsui, M. Yokouchi, A. Inoue, S. Komiya, and A. Yoshimura, *APS, an adaptor protein containing Pleckstrin homology (PH) and Src homology-2 (SH2)*

domains inhibits the JAK-STAT pathway in collaboration with c-Cbl. Leukemia, 1999. **13**(5): p. 760-7.
179. Cheng, Y., K. Chikwava, C. Wu, H. Zhang, A. Bhagat, D. Pei, J.K. Choi, and W. Tong, *LNK/SH2B3 regulates IL-7 receptor signaling in normal and malignant B-progenitors.* J Clin Invest, 2016. **126**(4): p. 1267-81.
180. Greenhalgh, C.J. and D.J. Hilton, *Negative regulation of cytokine signaling.* J Leukoc Biol, 2001. **70**(3): p. 348-56.
181. Klingmuller, U., U. Lorenz, L.C. Cantley, B.G. Neel, and H.F. Lodish, *Specific recruitment of SH-PTP1 to the erythropoietin receptor causes inactivation of JAK2 and termination of proliferative signals.* Cell, 1995. **80**(5): p. 729-38.
182. David, M., H.E. Chen, S. Goelz, A.C. Larner, and B.G. Neel, *Differential regulation of the alpha/beta interferon-stimulated Jak/Stat pathway by the SH2 domain-containing tyrosine phosphatase SHPTP1.* Mol Cell Biol, 1995. **15**(12): p. 7050-8.
183. Irie-Sasaki, J., T. Sasaki, W. Matsumoto, A. Opavsky, M. Cheng, G. Welstead, E. Griffiths, C. Krawczyk, C.D. Richardson, K. Aitken, N. Iscove, G. Koretzky, P. Johnson, P. Liu, D.M. Rothstein, and J.M. Penninger, *CD45 is a JAK phosphatase and negatively regulates cytokine receptor signalling.* Nature, 2001. **409**(6818): p. 349-54.
184. Liu, B., J. Liao, X. Rao, S.A. Kushner, C.D. Chung, D.D. Chang, and K. Shuai, *Inhibition of Stat1-mediated gene activation by PIAS1.* Proc Natl Acad Sci U S A, 1998. **95**(18): p. 10626-31.
185. Chung, C.D., J. Liao, B. Liu, X. Rao, P. Jay, P. Berta, and K. Shuai, *Specific inhibition of Stat3 signal transduction by PIAS3.* Science, 1997. **278**(5344): p. 1803-5.
186. Greenlund, A.C., R.D. Schreiber, D.V. Goeddel, and D. Pennica, *Interferon-gamma induces receptor dimerization in solution and on cells.* J Biol Chem, 1993. **268**(24): p. 18103-10.
187. Bach, E.A., J.W. Tanner, S. Marsters, A. Ashkenazi, M. Aguet, A.S. Shaw, and R.D. Schreiber, *Ligand-induced assembly and activation of the gamma interferon receptor in intact cells.* Mol Cell Biol, 1996. **16**(6): p. 3214-21.
188. Wilmes, S., M. Hafer, J. Vuorio, J.A. Tucker, H. Winkelmann, S. Lochte, T.A. Stanly, K.D. Pulgar Prieto, C. Poojari, V. Sharma, C.P. Richter, R. Kurre, S.R. Hubbard, K.C. Garcia, I. Moraga, I. Vattulainen, I.S. Hitchcock, and J. Piehler, *Mechanism of homodimeric cytokine receptor activation and dysregulation by oncogenic mutations.* Science, 2020. **367**(6478): p. 643-652.
189. Mendoza, J.L., W.M. Schneider, H.H. Hoffmann, K. Vercauteren, K.M. Jude, A. Xiong, I. Moraga, T.M. Horton, J.S. Glenn, Y.P. de Jong, C.M. Rice, and K.C. Garcia, *The IFN-lambda-IFN-lambdaR1-IL-10Rbeta Complex Reveals Structural Features Underlying Type III IFN Functional Plasticity.* Immunity, 2017. **46**(3): p. 379-392.
190. Saxton, R.A., L.T. Henneberg, M. Calafiore, L. Su, K.M. Jude, A.M. Hanash, and K.C. Garcia, *The tissue protective functions of interleukin-22 can be decoupled from pro-inflammatory actions through structure-based design.* Immunity, 2021. **54**(4): p. 660-672 e9.
191. Heldin, C.H., *Dimerization of cell surface receptors in signal transduction.* Cell, 1995. **80**(2): p. 213-23.
192. Cunningham, B.C., M. Ultsch, A.M. De Vos, M.G. Mulkerrin, K.R. Clauser, and J.A. Wells, *Dimerization of the extracellular domain of the human growth hormone receptor by a single hormone molecule.* Science, 1991. **254**(5033): p. 821-5.
193. Richter, D., I. Moraga, H. Winkelmann, O. Birkholz, S. Wilmes, M. Schulte, M. Kraich, H. Kenneweg, O. Beutel, P. Selenschik, D. Paterok, M. Gavutis, T. Schmidt, K.C. Garcia, T.D. Muller, and J. Piehler, *Ligand-induced type II interleukin-4 receptor dimers are sustained by rapid re-association within plasma membrane microcompartments.* Nat Commun, 2017. **8**: p. 15976.
194. Krause, C.D., E. Mei, J. Xie, Y. Jia, M.A. Bopp, R.M. Hochstrasser, and S. Pestka, *Seeing the light: preassembly and ligand-induced changes of the interferon gamma receptor complex in cells.* Mol Cell Proteomics, 2002. **1**(10): p. 805-15.

195. Krause, C.D., N. Lavnikova, J. Xie, E. Mei, O.V. Mirochnitchenko, Y. Jia, R.M. Hochstrasser, and S. Pestka, *Preassembly and ligand-induced restructuring of the chains of the IFN-gamma receptor complex: the roles of Jak kinases, Stat1 and the receptor chains.* Cell Res, 2006. **16**(1): p. 55-69.
196. Krause, C.D., E. Mei, O. Mirochnitchenko, N. Lavnikova, J. Xie, Y. Jia, R.M. Hochstrasser, and S. Pestka, *Interactions among the components of the interleukin-10 receptor complex.* Biochem Biophys Res Commun, 2006. **340**(2): p. 377-85.
197. Blouin, C.M., Y. Hamon, P. Gonnord, C. Boularan, J. Kagan, C. Viaris de Lesegno, R. Ruez, S. Mailfert, N. Bertaux, D. Loew, C. Wunder, L. Johannes, G. Vogt, F.X. Contreras, D. Marguet, J.L. Casanova, C. Gales, H.T. He, and C. Lamaze, *Glycosylation-Dependent IFN-gammaR Partitioning in Lipid and Actin Nanodomains Is Critical for JAK Activation.* Cell, 2016. **166**(4): p. 920-934.
198. Remy, I., I.A. Wilson, and S.W. Michnick, *Erythropoietin receptor activation by a ligand-induced conformation change.* Science, 1999. **283**(5404): p. 990-3.
199. Gent, J., P. van Kerkhof, M. Roza, G. Bu, and G.J. Strous, *Ligand-independent growth hormone receptor dimerization occurs in the endoplasmic reticulum and is required for ubiquitin system-dependent endocytosis.* Proc Natl Acad Sci U S A, 2002. **99**(15): p. 9858-63.
200. Livnah, O., E.A. Stura, S.A. Middleton, D.L. Johnson, L.K. Jolliffe, and I.A. Wilson, *Crystallographic evidence for preformed dimers of erythropoietin receptor before ligand activation.* Science, 1999. **283**(5404): p. 987-90.
201. Mandai, M., J. Hamanishi, K. Abiko, N. Matsumura, T. Baba, and I. Konishi, *Dual Faces of IFNgamma in Cancer Progression: A Role of PD-L1 Induction in the Determination of Pro- and Antitumor Immunity.* Clin Cancer Res, 2016. **22**(10): p. 2329-34.
202. Herfarth, H. and J. Scholmerich, *IL-10 therapy in Crohn's disease: at the crossroads. Treatment of Crohn's disease with the anti-inflammatory cytokine interleukin 10.* Gut, 2002. **50**(2): p. 146-7.
203. Josephson, K., R. DiGiacomo, S.R. Indelicato, A.H. Iyo, T.L. Nagabhushan, M.H. Parker, and M.R. Walter, *Design and analysis of an engineered human interleukin-10 monomer.* J Biol Chem, 2000. **275**(18): p. 13552-7.
204. Landar, A., B. Curry, M.H. Parker, R. DiGiacomo, S.R. Indelicato, T.L. Nagabhushan, G. Rizzi, and M.R. Walter, *Design, characterization, and structure of a biologically active single-chain mutant of human IFN-gamma.* J Mol Biol, 2000. **299**(1): p. 169-79.
205. Lunn, C.A., J. Fossetta, D. Dalgarno, N. Murgolo, W. Windsor, P.J. Zavodny, S.K. Narula, and D. Lundell, *A point mutation of human interferon gamma abolishes receptor recognition.* Protein Eng, 1992. **5**(3): p. 253-7.
206. Krause, C.D., C.A. Lunn, L.S. Izotova, O. Mirochnitchenko, S.V. Kotenko, D.J. Lundell, S.K. Narula, and S. Pestka, *Signaling by covalent heterodimers of interferon-gamma. Evidence for one-sided signaling in the active tetrameric receptor complex.* J Biol Chem, 2000. **275**(30): p. 22995-3004.
207. Marchetti, M., M.N. Monier, A. Fradagrada, K. Mitchell, F. Baychelier, P. Eid, L. Johannes, and C. Lamaze, *Stat-mediated signaling induced by type I and type II interferons (IFNs) is differentially controlled through lipid microdomain association and clathrin-dependent endocytosis of IFN receptors.* Mol Biol Cell, 2006. **17**(7): p. 2896-909.
208. Gandhi, H., R. Worch, K. Kurgonaite, M. Hintersteiner, P. Schwille, C. Bokel, and T. Weidemann, *Dynamics and interaction of interleukin-4 receptor subunits in living cells.* Biophys J, 2014. **107**(11): p. 2515-27.
209. Kurgonaite, K., H. Gandhi, T. Kurth, S. Pautot, P. Schwille, T. Weidemann, and C. Bokel, *Essential role of endocytosis for interleukin-4-receptor-mediated JAK/STAT signalling.* J Cell Sci, 2015. **128**(20): p. 3781-95.
210. Chmiest, D., N. Sharma, N. Zanin, C. Viaris de Lesegno, M. Shafaq-Zadah, V. Sibut, F. Dingli, P. Hupe, S. Wilmes, J. Piehler, D. Loew, L. Johannes, G. Schreiber, and C. Lamaze, *Spatiotemporal control of interferon-induced JAK/STAT signalling and gene transcription by the retromer complex.* Nat Commun, 2016. **7**: p. 13476.

211. Dorman, S.E. and S.M. Holland, *Mutation in the signal-transducing chain of the interferon-gamma receptor and susceptibility to mycobacterial infection.* J Clin Invest, 1998. **101**(11): p. 2364-9.
212. McKinstry, W.J., C.L. Li, J.E. Rasko, N.A. Nicola, G.R. Johnson, and D. Metcalf, *Cytokine receptor expression on hematopoietic stem and progenitor cells.* Blood, 1997. **89**(1): p. 65-71.
213. Patterson, G., M. Davidson, S. Manley, and J. Lippincott-Schwartz, *Superresolution imaging using single-molecule localization.* Annu Rev Phys Chem, 2010. **61**: p. 345-67.
214. Roder, F., S. Wilmes, C.P. Richter, and J. Piehler, *Rapid transfer of transmembrane proteins for single molecule dimerization assays in polymer-supported membranes.* ACS Chem Biol, 2014. **9**(11): p. 2479-84.
215. Kirchhofer, A., J. Helma, K. Schmidthals, C. Frauer, S. Cui, A. Karcher, M. Pellis, S. Muyldermans, C.S. Casas-Delucchi, M.C. Cardoso, H. Leonhardt, K.P. Hopfner, and U. Rothbauer, *Modulation of protein properties in living cells using nanobodies.* Nat Struct Mol Biol, 2010. **17**(1): p. 133-8.
216. Pestka, S., S.V. Kotenko, G. Muthukumaran, L.S. Izotova, J.R. Cook, and G. Garotta, *The interferon gamma (IFN-gamma) receptor: a paradigm for the multichain cytokine receptor.* Cytokine Growth Factor Rev, 1997. **8**(3): p. 189-206.
217. Morone, N., T. Fujiwara, K. Murase, R.S. Kasai, H. Ike, S. Yuasa, J. Usukura, and A. Kusumi, *Three-dimensional reconstruction of the membrane skeleton at the plasma membrane interface by electron tomography.* J Cell Biol, 2006. **174**(6): p. 851-62.
218. Vogelsang, J., R. Kasper, C. Steinhauer, B. Person, M. Heilemann, M. Sauer, and P. Tinnefeld, *A reducing and oxidizing system minimizes photobleaching and blinking of fluorescent dyes.* Angew Chem Int Ed Engl, 2008. **47**(29): p. 5465-9.
219. VandeVondele, S., J. Voros, and J.A. Hubbell, *RGD-grafted poly-L-lysine-graft-(polyethylene glycol) copolymers block non-specific protein adsorption while promoting cell adhesion.* Biotechnol Bioeng, 2003. **82**(7): p. 784-90.
220. Marsters, S.A., D. Pennica, E. Bach, R.D. Schreiber, and A. Ashkenazi, *Interferon gamma signals via a high-affinity multisubunit receptor complex that contains two types of polypeptide chain.* Proc Natl Acad Sci U S A, 1995. **92**(12): p. 5401-5.
221. Thiel, D.J., M.H. le Du, R.L. Walter, A. D'Arcy, C. Chene, M. Fountoulakis, G. Garotta, F.K. Winkler, and S.E. Ealick, *Observation of an unexpected third receptor molecule in the crystal structure of human interferon-gamma receptor complex.* Structure, 2000. **8**(9): p. 927-36.
222. Mikulecky, P., J. Zahradnik, P. Kolenko, J. Cerny, T. Charnavets, L. Kolarova, I. Necasova, P.N. Pham, and B. Schneider, *Crystal structure of human interferon-gamma receptor 2 reveals the structural basis for receptor specificity.* Acta Crystallogr D Struct Biol, 2016. **72**(Pt 9): p. 1017-25.
223. Lundell, D., C.A. Lunn, M.M. Senior, P.J. Zavodny, and S.K. Narula, *Importance of the loop connecting A and B helices of human interferon-gamma in recognition by interferon-gamma receptor.* J Biol Chem, 1994. **269**(23): p. 16159-62.
224. Bustamante, J., C. Picard, C. Fieschi, O. Filipe-Santos, J. Feinberg, C. Perronne, A. Chapgier, L. de Beaucoudrey, G. Vogt, D. Sanlaville, A. Lemainque, J.F. Emile, L. Abel, and J.L. Casanova, *A novel X-linked recessive form of Mendelian susceptibility to mycobaterial disease.* J Med Genet, 2007. **44**(2): p. e65.
225. Vogt, G., A. Chapgier, K. Yang, N. Chuzhanova, J. Feinberg, C. Fieschi, S. Boisson-Dupuis, A. Alcais, O. Filipe-Santos, J. Bustamante, L. de Beaucoudrey, I. Al-Mohsen, S. Al-Hajjar, A. Al-Ghonaium, P. Adimi, M. Mirsaeidi, S. Khalilzadeh, S. Rosenzweig, O. de la Calle Martin, T.R. Bauer, J.M. Puck, H.D. Ochs, D. Furthner, C. Engelhorn, B. Belohradsky, D. Mansouri, S.M. Holland, R.D. Schreiber, L. Abel, D.N. Cooper, C. Soudais, and J.L. Casanova, *Gains of glycosylation comprise an unexpectedly large group of pathogenic mutations.* Nat Genet, 2005. **37**(7): p. 692-700.
226. Ku, C.L., C.Y. Chi, H. von Bernuth, and R. Doffinger, *Autoantibodies against cytokines: phenocopies of primary immunodeficiencies?* Hum Genet, 2020. **139**(6-7): p. 783-794.

227. Gavel, Y. and G. von Heijne, *Sequence differences between glycosylated and non-glycosylated Asn-X-Thr/Ser acceptor sites: implications for protein engineering.* Protein Eng, 1990. **3**(5): p. 433-42.
228. Ku, C.L., C.H. Lin, S.W. Chang, C.C. Chu, J.F. Chan, X.F. Kong, C.H. Lee, E.A. Rosen, J.Y. Ding, W.I. Lee, J. Bustamante, T. Witte, H.P. Shih, C.Y. Kuo, P. Chetchotisakd, S. Kiertiburanakul, Y. Suputtamongkol, K.Y. Yuen, J.L. Casanova, S.M. Holland, R. Doffinger, S.K. Browne, and C.Y. Chi, *Anti-IFN-gamma autoantibodies are strongly associated with HLA-DR*15:02/16:02 and HLA-DQ*05:01/05:02 across Southeast Asia.* J Allergy Clin Immunol, 2016. **137**(3): p. 945-8 e8.
229. Chi, C.Y., C.H. Lin, M.W. Ho, J.Y. Ding, W.C. Huang, H.P. Shih, C.F. Yeh, C.P. Fung, H.Y. Sun, C.T. Huang, T.S. Wu, C.Y. Chang, Y.M. Liu, J.Y. Feng, W.K. Wu, L.S. Wang, C.H. Tsai, C.M. Ho, H.S. Lin, H.J. Chen, P.C. Lin, W.C. Liao, W.T. Chen, C.C. Lo, S.Y. Wang, C.Y. Kuo, C.H. Lee, and C.L. Ku, *Clinical manifestations, course, and outcome of patients with neutralizing anti-interferon-gamma autoantibodies and disseminated nontuberculous mycobacterial infections.* Medicine (Baltimore), 2016. **95**(25): p. e3927.
230. Tham, E.H., C.H. Huang, J.Y. Soh, M. Thayalasingam, A.J. Lee, L.H. Lum, L.M. Poon, D.C. Lye, L.Y. Chai, P.A. Tambyah, B.W. Lee, and L.P. Shek, *Neutralizing Anti-Interferon-Gamma Autoantibody Levels May Not Correlate With Clinical Course of Disease.* Clin Infect Dis, 2016. **63**(4): p. 572-3.
231. Logsdon, N.J., B.C. Jones, K. Josephson, J. Cook, and M.R. Walter, *Comparison of interleukin-22 and interleukin-10 soluble receptor complexes.* J Interferon Cytokine Res, 2002. **22**(11): p. 1099-112.
232. Suzuki, K.G., T.K. Fujiwara, F. Sanematsu, R. Iino, M. Edidin, and A. Kusumi, *GPI-anchored receptor clusters transiently recruit Lyn and G alpha for temporary cluster immobilization and Lyn activation: single-molecule tracking study 1.* J Cell Biol, 2007. **177**(4): p. 717-30.
233. Donnelly, R.P., F. Sheikh, S.V. Kotenko, and H. Dickensheets, *The expanded family of class II cytokines that share the IL-10 receptor-2 (IL-10R2) chain.* J Leukoc Biol, 2004. **76**(2): p. 314-21.
234. Suzuki, K.G., T.K. Fujiwara, M. Edidin, and A. Kusumi, *Dynamic recruitment of phospholipase C gamma at transiently immobilized GPI-anchored receptor clusters induces IP3-Ca2+ signaling: single-molecule tracking study 2.* J Cell Biol, 2007. **177**(4): p. 731-42.
235. Bijlmakers, M.J., *Protein acylation and localization in T cell signaling (Review).* Mol Membr Biol, 2009. **26**(1): p. 93-103.
236. Chum, T., D. Glatzova, Z. Kvicalova, J. Malinsky, T. Brdicka, and M. Cebecauer, *The role of palmitoylation and transmembrane domain in sorting of transmembrane adaptor proteins.* J Cell Sci, 2016. **129**(15): p. 3053.
237. Levental, I., D. Lingwood, M. Grzybek, U. Coskun, and K. Simons, *Palmitoylation regulates raft affinity for the majority of integral raft proteins.* Proc Natl Acad Sci U S A, 2010. **107**(51): p. 22050-4.
238. Sharpe, H.J., T.J. Stevens, and S. Munro, *A comprehensive comparison of transmembrane domains reveals organelle-specific properties.* Cell, 2010. **142**(1): p. 158-69.
239. Fiorentino, D.F., A. Zlotnik, P. Vieira, T.R. Mosmann, M. Howard, K.W. Moore, and A. O'Garra, *IL-10 acts on the antigen-presenting cell to inhibit cytokine production by Th1 cells.* J Immunol, 1991. **146**(10): p. 3444-51.
240. Oft, M., *Immune regulation and cytotoxic T cell activation of IL-10 agonists - Preclinical and clinical experience.* Semin Immunol, 2019. **44**: p. 101325.
241. Correa, I., M. Veny, M. Esteller, J.M. Pique, J. Yague, J. Panes, and A. Salas, *Defective IL-10 production in severe phenotypes of Crohn's disease.* J Leukoc Biol, 2009. **85**(5): p. 896-903.
242. Zhu, L., T. Shi, C. Zhong, Y. Wang, M. Chang, and X. Liu, *IL-10 and IL-10 Receptor Mutations in Very Early Onset Inflammatory Bowel Disease.* Gastroenterology Res, 2017. **10**(2): p. 65-69.

243. Yoon, S.I., B.C. Jones, N.J. Logsdon, and M.R. Walter, *Same structure, different function crystal structure of the Epstein-Barr virus IL-10 bound to the soluble IL-10R1 chain.* Structure, 2005. **13**(4): p. 551-64.
244. Yoon, S.I., B.C. Jones, N.J. Logsdon, B.D. Harris, S. Kuruganti, and M.R. Walter, *Epstein-Barr virus IL-10 engages IL-10R1 by a two-step mechanism leading to altered signaling properties.* J Biol Chem, 2012. **287**(32): p. 26586-95.
245. Ding, Y., L. Qin, S.V. Kotenko, S. Pestka, and J.S. Bromberg, *A single amino acid determines the immunostimulatory activity of interleukin 10.* J Exp Med, 2000. **191**(2): p. 213-24.
246. Colombel, J.F., P. Rutgeerts, H. Malchow, M. Jacyna, O.H. Nielsen, J. Rask-Madsen, S. Van Deventer, A. Ferguson, P. Desreumaux, A. Forbes, K. Geboes, L. Melani, and M. Cohard, *Interleukin 10 (Tenovil) in the prevention of postoperative recurrence of Crohn's disease.* Gut, 2001. **49**(1): p. 42-6.
247. Buruiana, F.E., I. Sola, and P. Alonso-Coello, *Recombinant human interleukin 10 for induction of remission in Crohn's disease.* Cochrane Database Syst Rev, 2010(11): p. CD005109.
248. Saraiva, M., P. Vieira, and A. O'Garra, *Biology and therapeutic potential of interleukin-10.* J Exp Med, 2020. **217**(1).
249. Chao, G., W.L. Lau, B.J. Hackel, S.L. Sazinsky, S.M. Lippow, and K.D. Wittrup, *Isolating and engineering human antibodies using yeast surface display.* Nat Protoc, 2006. **1**(2): p. 755-68.
250. Wehinger, J., F. Gouilleux, B. Groner, J. Finke, R. Mertelsmann, and R.M. Weber-Nordt, *IL-10 induces DNA binding activity of three STAT proteins (Stat1, Stat3, and Stat5) and their distinct combinatorial assembly in the promoters of selected genes.* FEBS Lett, 1996. **394**(3): p. 365-70.
251. Martinez-Fabregas, J., S. Wilmes, L. Wang, M. Hafer, E. Pohler, J. Lokau, C. Garbers, A. Cozzani, P.K. Fyfe, J. Piehler, M. Kazemian, S. Mitra, and I. Moraga, *Kinetics of cytokine receptor trafficking determine signaling and functional selectivity.* Elife, 2019. **8**.
252. Mittal, S.K. and P.A. Roche, *Suppression of antigen presentation by IL-10.* Curr Opin Immunol, 2015. **34**: p. 22-7.
253. Gorby, C., J. Sotolongo Bellon, S. Wilmes, W. Warda, E. Pohler, P.K. Fyfe, A. Cozzani, C. Ferrand, M.R. Walter, S. Mitra, J. Piehler, and I. Moraga, *Engineered IL-10 variants elicit potent immunomodulatory effects at low ligand doses.* Sci Signal, 2020. **13**(649).
254. Oft, M., *IL-10: master switch from tumor-promoting inflammation to antitumor immunity.* Cancer Immunol Res, 2014. **2**(3): p. 194-9.
255. Naing, A., J.R. Infante, K.P. Papadopoulos, I.H. Chan, C. Shen, N.P. Ratti, B. Rojo, K.A. Autio, D.J. Wong, M.R. Patel, P.A. Ott, G.S. Falchook, S. Pant, A. Hung, K.L. Pekarek, V. Wu, M. Adamow, S. McCauley, J.B. Mumm, P. Wong, P. Van Vlasselaer, J. Leveque, N.M. Tannir, and M. Oft, *PEGylated IL-10 (Pegilodecakin) Induces Systemic Immune Activation, CD8(+) T Cell Invigoration and Polyclonal T Cell Expansion in Cancer Patients.* Cancer Cell, 2018. **34**(5): p. 775-791 e3.
256. Rollings, C.M., L.V. Sinclair, H.J.M. Brady, D.A. Cantrell, and S.H. Ross, *Interleukin-2 shapes the cytotoxic T cell proteome and immune environment-sensing programs.* Sci Signal, 2018. **11**(526).
257. Moraga, I., G. Wernig, S. Wilmes, V. Gryshkova, C.P. Richter, W.J. Hong, R. Sinha, F. Guo, H. Fabionar, T.S. Wehrman, P. Krutzik, S. Demharter, I. Plo, I.L. Weissman, P. Minary, R. Majeti, S.N. Constantinescu, J. Piehler, and K.C. Garcia, *Tuning cytokine receptor signaling by re-orienting dimer geometry with surrogate ligands.* Cell, 2015. **160**(6): p. 1196-208.
258. Kalay, Z., T.K. Fujiwara, and A. Kusumi, *Confining domains lead to reaction bursts: reaction kinetics in the plasma membrane.* PLoS One, 2012. **7**(3): p. e32948.
259. Kusumi, A., C. Nakada, K. Ritchie, K. Murase, K. Suzuki, H. Murakoshi, R.S. Kasai, J. Kondo, and T. Fujiwara, *Paradigm shift of the plasma membrane concept from the two-dimensional continuum fluid to the partitioned fluid: high-speed single-molecule tracking of membrane molecules.* Annu Rev Biophys Biomol Struct, 2005. **34**: p. 351-78.

260. D'Agostino, Y. and S. D'Aniello, *Molecular basis, applications and challenges of CRISPR/Cas9: a continuously evolving tool for genome editing.* Brief Funct Genomics, 2017. **16**(4): p. 211-216.
261. Landar, A., B. Curry, M.H. Parker, R. DiGiacomo, S.R. Indelicato, T.L. Nagabhushan, G. Rizzi, and M.R. Walter, *Design, characterization, and structure of a biologically active single- chain mutant of human IFN-gamma.* J Mol Biol, 2000. **299**(1): p. 169-79.
262. Serge, A., N. Bertaux, H. Rigneault, and D. Marguet, *Dynamic multiple-target tracing to probe spatiotemporal cartography of cell membranes.* Nat Methods, 2008. **5**(8): p. 687-94.
263. Sander, J., M. Ester, H.P. Kriegel, and X.W. Xu, *Density-based clustering in spatial databases: The algorithm GDBSCAN and its applications.* Data Mining and Knowledge Discovery, 1998. **2**(2): p. 169-194.
264. Niewidok, B., M. Igaev, A. Pereira da Graca, A. Strassner, C. Lenzen, C.P. Richter, J. Piehler, R. Kurre, and R. Brandt, *Single-molecule imaging reveals dynamic biphasic partition of RNA-binding proteins in stress granules.* J Cell Biol, 2018. **217**(4): p. 1303-1318.
265. Rieger, B. and S. Stallinga, *The lateral and axial localization uncertainty in super-resolution light microscopy.* Chemphyschem, 2014. **15**(4): p. 664-70.
266. Jaqaman, K., D. Loerke, M. Mettlen, H. Kuwata, S. Grinstein, S.L. Schmid, and G. Danuser, *Robust single-particle tracking in live-cell time-lapse sequences.* Nat Methods, 2008. **5**(8): p. 695-702.
267. Michalet, X., *Mean square displacement analysis of single-particle trajectories with localization error: Brownian motion in an isotropic medium.* Phys Rev E Stat Nonlin Soft Matter Phys, 2010. **82**(4 Pt 1): p. 041914.
268. Rousseeuw, P.J. and A.M. Leroy, *Outlier Diagnostics*, in *Robust Regression and Outlier Detection*, P.J. Rousseeuw and A.M. Leroy, Editors. 1987, Wiley. p. 216-247.

8 List of Abbreviations

AIGA	Anti-IFNγ Autoantibody	**ICD**	intracellular domain
APC	antigen presenting cell	**IFN**	Interferon
BLI	Bio-layer interferometry	**IFNAR**	Interferon α/β receptor
CD	Cluster of Differentiation	**IFNGR**	Interferon gamma receptor
CFP	cyan fluorescent protein	**IFNLR**	Interferon lambda receptor
CME	Clathrin-mediated Endocytosis	**IgSF**	Immunoglobulin superfamily
CMV	Cytomegalovirus	**IL**	Interleukin
CSF1	colony-stimulatory factor 1	**ILC**	innate lymphoid cells
DOL	degree of labeling	**IRF9**	Interferon Response Factor 9
EBV	Epstein-Barr virus	**ISRE**	Interferon-Stimulated Response Elements
ECD	extracellular domain	**JAK**	Janus kinase
ELISA	enzyme-linked immunosorbent assay	**mAb**	monoclonal Antibody
EN	Enhancer, anti-GFP nanobody	**mEGFP/ mECFP**	monomeric enhanced GFP/ CFP
FRET	Förster Resonance Energy Transfer	**MHC**	major histocompatibility complex
GAS	Interferon-Gamma Activated Sequence	**MI**	Minimizer, anti-GFP nanobody
GFP	green fluorescent protein	**mIFNγ**	monomeric IFNγ
GIFN1-4	engineered partial agonist of IFNGR	**mIL-10**	monomeric IL-10
GPCR	G protein-coupled receptor	**MSD analysis**	mean square displacement analysis
GPCR	G protein-coupled receptor	**MSMD**	Mendelian Susceptibility to Mycobacterial Disease syndrome
HTC	hematopoietic stem cell		

mXFPe	mutated non-fluorescent mEGFP (Y66F, N198D, Y200F)
mXFPm	mutated non-fluorescent mECFP (W66F, E142K, H164N)
NB	nanobody
NF-kB	Nuclear factor kappa B
NK cell	natural killer cell
PIAS	protein inhibitors of STATs
PNGaseF	Peptide:N-Glycosidase F
pSTAT	phosphorylated STAT molecule
PTP	Protein Tyrosine Phosphatases
SD	square displacement
SMFM	Single molecule fluorescence microscopy
smFRET	single molecule FRET
SMLM	Single molecule localization microscopy
SNR	signal-to-noise ratio
SOCS	Suppressor of cytokine signaling
SPR	surface plasmon resonance
STALL	stimulation-induced temporary arrest of lateral diffusion
STAM	Signal-Transducing adapter molecules
STAT	Signal Transducer and Activator of Transcription
TGF-b	transforming growth factor beta
TIRF	Total internal reflection fluorescence microscopy
TMD	transmembrane domain
TNF	Tumor necrosis factor
TNFRSF	tumor necrosis factor receptor superfamily
TYK	non receptor tyrosine kinase

9 Acknowledgements

Zuerst möchte ich Prof. Dr. Jacob Piehler danken, für die Möglichkeit und das Vertrauen an so einem interessanten Thema forschen zu dürfen, sowieso für alles was ich jenseits von der Wissenschaft lernen konnte. Außerdem möchte ich mich bei Prof. Dr. Christian Ungermann bedanken, für das Übernehmen der Rolle des Zweitgutachters. Ich möchte mich auch bei allen anderen bedanken, die in irgendeiner Art und Weise zu dieser Arbeit beigetragen haben, sei es durch die ertragreiche Zusammenarbeit und die endlosen Diskussionen, als auch durch das kritische Lesen dieser Arbeit.

Des Weiteren möchte ich mich bei all meinen Kollegen aus der Abteilung Biophysik für die schöne Zeit bedanken. Unsere unzähligen Grillabende und Doppelkopfrunden haben mir immer eine besondere Freude gemacht, insbesondere wenn es mal im Labor nicht rund lief. Mein besonderer Dank gilt Teff, der mich damals in das spannende Thema der Zytokine eingeführt hat und auf dessen Unterstützung ich bis zum Ende zählen konnte. Ebenso möchte ich mich bei Rainer bedanken, für seine unermüdliche Unterstützung an den Mikroskopen. Christian möchte ich danken, für die stetige Weiterentwicklung der Auswertung, sowie für seinen Rat, der häufig meine Aufmerksamkeit auf wichtige Details gelenkt hat. Zusätzlich möchte ich mich herzlich bei Gabi und Hella bedanken, für ihre praktische Unterstützung mit Klonierungsarbeiten und Proteinreinigungen, aber auch ihren unendlichen Wissensschatz, den sie bei Bedarf immer bereitwillig mit mir geteilt haben.

Außerdem möchte ich mich bei allen meinen ehemaligen sowie aktuellen Sitznachbarn im Doktorandenbüro bedanken, die mich auf dieser Reise begleitet haben und stets einen Spruch auf Lager hatten, um jede Situation lustig und denkwürdig zu gestalten. Einen speziellen Dank möchte ich nochmal an Christian und Tim richten, für die Freundschaft, die aus dieser Zeit hervorgegangen ist. Möge sie noch ewig andauern!

Zum Schluss möchte ich mich bei meiner gesamten Familie bedanken, die, obwohl sie zum Teil sehr weit weg ist, mir stets Mut gemacht hat weiterzumachen und meinen Traum zu verfolgen. Ganz besonders möchte ich meiner Verlobten und Liebe meines Lebens danken, die mir in dieser Zeit nichts außer Liebe und Unterstützung entgegengebracht hat.

10 Declaration

I hereby declare that the presented thesis ‘Spatiotemporal Dynamics of Assembly and Activation of Class II Cytokine Receptors’ was prepared entirely on my own and I have not used outside sources without declaration in the text. Any concepts or quotations applicable to these sources are clearly attributed to them. The following people attributed to this work as collaboration partner:

1. Christian P. Richter developed and provided the analysis software “SLIMfast”
2. Gabriele Hikade supported me in molecule biology work
3. Hella Kenneweg supported me in protein purification and labeling

I have not attempted a promotion before.

Junel Sotolongo Bellón

Osnabrück, 22.02.2022